Polycrystalline Silicon Thin Films with Improved Crystallographic and Electronic Properties for Photovoltaic Applications

(太陽電池素子応用を目指した高品質薄膜多結晶シリコンに関する研究)

Akiyoshi Ogane

大鐘　章義

Supervised by Professor Takashi Fuyuki

March 2009

Nara Institute of Science and Technology

Graduate School of Materials Science

Microelectronic Device Science laboratory

Abstract

Polycrystalline silicon (poly-Si) thin film is expected as one of the most promising materials for the next generation solar cell with the advantages of low-cost and stable high efficiency. The performance of poly-Si thin film solar cells can be influenced and limited by the crystalline defects including grain boundaries because they act as recombination centers of photo-generated carriers, therefore it is indispensable to reduce such defects in poly-Si thin films to improve the photovoltaic properties. In this study, the deposition and treatment techniques of poly-Si thin films on foreign alumina substrate were developed in order to obtain poly-Si thin films with less crystalline defects and high electronic properties heading for the solar cell application. For the improvement of poly-Si thin film properties, mainly two methods were applied; grain size enlargement during the deposition of poly-Si thin films and passivation by high-pressure water vapor heat treatment (HWT). These poly-Si thin films were investigated from the points of view of the crystallinity, i.e., the amount of crystalline disorder, and macro- and microscopic electronic properties. And related cell fabrication processes were also developed with the final goal of development of poly-Si thin film solar cells on foreign substrates with high photovoltaic performances.

In Chapter 2, poly-Si thin films with thickness of 10 μm were deposited on alumina substrates and reference silicon substrates by atmospheric pressure thermal chemical vapor deposition method at approximately 1100 °C. In order to decrease the influence of crystallographic defects, especially grain boundaries, the larger grain size is desirable. In order to control the grain size of poly-Si thin film directly in deposition time, 2-step deposition with the intermittent source gas supplying was applied. By changing the intermittent ratio, the grain size of poly-Si thin films on alumina was controlled in the range of a few µm to over 10 µm, with the same tendency as the case of deposition on silicon substrate.

The defect passivation treatment after the deposition is also important. As the less complicated passivation method, HWT was applied to both poly-Si thin films and bulk silicon solar cells in Chapter 4. This method has advantages such as very easy to be performed and free from the large-scale apparatus and dangerous chemical gases are suitable to low-cost solar cell production.

In Chapter 3 and 4, the crystallographic properties of poly-Si thin films were investigated by Raman scattering, X-ray diffraction, and Photoluminescence measurement. The full-width at half maximum and peak position of Raman peak (at 520 cm^{-1}) showed that poly-Si thin films with small grains on alumina substrates gave very large shift from crystalline silicon's value. These shifts from crystalline silicon indicate the large internal compressive stress and large amount of disorders in poly-Si thin films on alumina, caused by the difference of thermal expansion coefficient between silicon film and alumina substrate. However, these values became closer to crystalline silicon by grain size enlargement and HWT. Grain size enlargement and HWT can be effective to internal stress relaxation, resulting in crystallinity improvement. The other measurements showed the same tendency. For the analysis of macro- and microscopic electronic properties of poly-Si thin films, Hall effect measurement and Kelvin force microscopy were performed, and they suggested that grain size enlargement and HWT caused the decrease of potential barrier height at grain boundaries, indicating the reduction of crystallographic defects.

In Chapter 5, the interdigitated-type poly-Si thin film solar cells on alumina substrates were fabricated by the way of trial. In fabrication process of poly-Si thin film solar cells, p-n junction formation is one important thing to be considered. As a new impurity doping process, laser doping technique was introduced and developed in poly-Si thin film solar cell process as well as bulk crystalline silicon solar cell process. The precise controlling of doping conditions, especially doping depth, was achieved by changing laser output power. The fabricated interdigitated-type poly-Si thin film solar cells on alumina substrates using laser doping method certainly showed the photovoltaic performance and the improvements by grain size enlargement and HWT were confirmed.

Acknowledgements

This work has been done at the Microelectronic Device Science Laboratory, Graduate School of Materials Science, Nara Institute of Science and Technology (NAIST), under the direction of Professor Takashi Fuyuki. This work was partially supported by Foundation for Nara Institute of Science and Technology, Kansai Research Foundation for Technology Promotion, The Murata Science Foundation, Graduate school GP program, and New Energy and Industrial Technology Development Organization (NEDO) as part of the Innovative Solar Cells R&D Program.

The author would like to express his deepest appreciation and gratitude to his main supervisor, Professor Takashi Fuyuki for his kind advices, continuous supporting, valuable suggestions and encouragements through the course of this work as well as critical reading of this thesis. The author is also grateful to his supervisors at NAIST; Associate Professor Kiyoshi Uchiyama, Professor Hisao Yanagi, Associate Professor Yukiharu Uraoka, and Professor Tadashi Shiosaki for their valuable discussions and critical reading of this thesis.

The author sincerely acknowledges to Dr. Antonín Fejfar at the Department of Thin Films, Institute of Physics, Academy of Sciences of the Czech Republic, v. v. i. for his international supervision, the collaboration work and giving the author the chance of oversea study at his laboratory. The author also acknowledges to Dr. Jan Kočka, the head of the Department of Thin Films, and all members in his laboratory for the acceptance and guidance for author’s short stay with useful discussions. In particular, the author would like to express sincere thanks to his co-worker, Dr. Shinya Honda (now at SHARP Corporation) for the

excellent collaborations and valuable discussions.

The author also wishes express his thanks to Associate Professor Noritaka Usami and Dr. Kentaro Kustukake at Tohoku University, Associate Professor Takuji Takahashi and Mr. Masaki Takihara at University of Tokyo, Associate Professor Koji Arafune at University of Hyogo, Dr. Takashi Minemoto at Ritsumeikan University, Dr. Keisuke Ohdaira at Japan Advanced Institute of Science and Technology, Dr. Dhamrin Marwan at Tokyo University of Agriculture and Technology, and Dr. Yuji Komatsu at Energy research Centre of the Netherland for their fruitful advices and discussions.

The author is grateful to Professor Syuichi Nonomura, Dr. Hironori Natsuhara, and Dr. Syunsuke Ogawa at Gihu University for their kind advices and discussions about AFM measurement.

The author would like to thank those who related to collaboration works between the Microelectronic Device Science Laboratory and companies; Dr. Makoto Tanaka, Dr. Eiji Maruyama, Dr. Mikio Taguchi, Mr. Takashi Nakashima, and Dr. Toshie Kunii at SANYO Electronic Co., Ltd., Mr. Katsuhiko Shirasawa, Mr. Koichiro Niira, Mr. Kazuaki Iwameji, and Dr. Hiroshi Hashigami at KYOCERA Corporation, and Mr. Kazuo Murakami and Mr. Hiroshi Ueno at OYO Electronic Co., Ltd. for useful discussions.

The author is indebted to the staffs and researchers in the Microelectronic Device Science Laboratory; Dr. Tomoaki Hatayama, Dr. Hiroshi Yano, Dr. Atsushi Miura, Ms. Ayumi Tani, Ms. Kumiko Sato, Ms. Yuko Tanaka, and Ms. Kumi Hora for their experimental and clerical helps, useful advices and heartfelt encouragements.

The author sincerely acknowledges to those who belonged or belongs to PV group in the Microelectronic Device Science Laboratory; Dr. Yasuaki Ishikawa (now at SHARP Corporation), Dr. Yukie Hamamoto, Dr. Toshiki Yagi (now at SHARP Corporation),

Dr. Kensuke Nishioka (now Associate Professor at University of Miyazaki), Dr. Tsutomu Yamazaki (now at SHARP Corporation), Mr. Nobuhiro Sakitani (now at SANYO Electronic Co., Ltd.), Dr. Yu Takahashi (now at SHARP Corporation), Mr. Yoshiaki Matsumura (now at TOYOTA Motor Corporation), Mr. Hayato Kondo (now at Hoshiden Corporation), Ms. Yasue Kaji (now at DENSO Corporation), Mr. Jin Nigo (now at Canon Inc.), Mr. Yoshiyuki Nishihara (now at Murata Manufacturing Co., Ltd.), Ms. Yuki Kishiyama (now at Daihatsu Motor Co., Ltd.), Mr. Koyo Horiuchi (now at Panasonic Corporation), Mr. Kenji Hirata, Ms. Mami Fujii, Mr. Takashi Saitoh, Ms. Emi Sugimura, and Mr. Masakazu Nakatani for their valuable discussions, continuous encouragements, kind helps and excellent time of working together. The author also wishes to thank Dr. Athapol Kitiyanan, the Ph. D. researcher in PV group, Dr. Karsten Bothe, the short-stayed researcher from Institut fu̇r Solarenergieforsdhung Hameln (ISFH, Gernamy), and Ms. Marie Buffière, the exchanged student from Universite de Poitiers (France) for having useful discussions and good days.

The author wishes to thank all other members in the Microelectronic Device Science Laboratory for sharing good time in not only research work but daily life.

Finally, the author really thank his family for their understanding and continuous support.

March, 2009

Akiyoshi Ogane

Contents

Abstract i

Acknowledgements iv

Contents vii

List of abbreviations and symbols xi

Chapter 1 Introduction 1

1.1. Background and introduction of poly-Si thin films 1

1.1.1. Background 1

1.1.2. Poly-Si thin film solar cells 4

1.2. Purpose and outline of this thesis 7

1.3. Economical aspects of poly-Si thin film solar cells 12

1.3.1. Substrate selection 12

1.3.2. Deposition cost 13

1.3.3. Comparison with conventional multicrystalline silicon solar cells 13

References of Chapter 1 17

Chapter 2 Deposition of poly-Si thin films on foreign substrates with in-situ grain size controlling 21

2.1. Introduction 21

2.2. Deposition technique 22

2.2.1. Thermal-APCVD 22

2.2.2. 2-step deposition with intermittent source gas supplying 24

2.2.3. Substrate preparation 25

2.3. Grain size controlling 33

2.3.1. Nucleation density and grain size controlling 33

2.3.2. Discussion of grain size controlling mechanism 37

2.4. Substrate type dependency 39

2.4.1. Intermediated layer dependency 39

2.4.2. Deposition on alumina substrate 45

2.5. Summary 49

References of Chapter 2 50

Chapter 3 Crystallographic and electronic properties of grain size-controlled poly- Si thin films 52

3.1. Introduction 52

3.2. Role of deposition temperature in APCVD 53

3.3. Crystalline quality of poly- Si thin films with different grain size 56

3.3.1. Results of measurements 57

3.3.2. Discussion 60

3.4. Electronic property of poly- Si thin films with different grain size 64

3.4.1. Macroscopic analysis (Hall effect measurement) 64

3.4.2. Microscopic analysis (KFM measurement) 66

3.5. Summary 72

References of Chapter 3 74

Chapter 4 Defect passivation by high-pressure water vapor heat treatment 76

4.1. Introduction 76

4.2. HWT experimental method 77

4.3. Applying to bulk crystalline silicon solar cells 79

4.3.1 Experimental 79

4.3.2 Lifetime properties 80

4.3.3 Solar cell properties 82

4.3.4 Discussion of HWT mechanism 86

4.4. Applying to poly-Si thin films 88

4.4.1 Crystallographic properties 89

4.4.2 Electronic properties 89

4.4.3 Discussion of HWT mechanism in poly-Si thin film passivation 94

4.5. Summary 97

References of Chapter 4 100

Chapter 5 Development of poly-Si thin film solar cells fabricated on alumina substrates 103

5.1 Introduction 103

5.2 Development of laser doping technique in c-Si solar cells 104

5.3 Introduction of this section 104

5.3.1 Experimental 105

5.3.2 Doping conditions 108

5.3.3 Solar cell properties with laser-doped emitter 113

5.3.4 Back Surface Field formation 118

5.3.5 Laser doping for multicrystalline silicon solar cells 118

5.4 Development of poly-Si thin film solar cells fabricated on alumina substrates 121

5.4.1 Device structure of poly-Si thin film solar cells 123

5.4.2 Fabrication of poly-Si thin film solar cells 123

5.4.3 Poly-Si thin film solar cell properties 129

5.5 Summary 132

References of Chapter 5 133

Chapter 6 Conclusions 136

6.1. Summary 136

6.2. Outlooks 139

Appendix: Summary of characterization methods 141

List of publications 157

About the author 174

List of abbreviations and symbols

Experimental techniques

APCVD	Atmospheric Pressure Chemical Vapor Deposition
PECVD	Plasma Enhanced Chemical Vapor Deposition
LPCVD	Low Pressure Chemical Vapor Deposition
SPC	Solid Phase Crystallization
AIC	Aluminum Induced Crystallization
LLC	Layered Laser Crystallization
ZMR	Zone Melting Re-crystallization
RTA	Rapid Thermal Annealing
HWT	High-pressure Water vapor heat Treatment
ARC	Anti-Reflection Coating
BSF	Back Surface Field
BSR	Back Surface Reflector
LD	Laser Doping
TD	Thermal Diffusion
SC	Standard Clean in RCA cleaning
SPM	Sulfuric acid / hydrogen Peroxide Mixture clean in RCA cleaning
D/T	Intermittent ratio
slm	Standard liters per minute
sccm	Standard cubic centimeter per minute
ppm	Parts per million

Materials

(c-) Si	(Monocrystalline) silicon

mc-Si	Multicrystalline silicon
poly-Si	Polycrystalline silicon
μc-Si (:H)	(Hydrogenated) micro-crystalline silicon
a-Si (:H)	(Hydrogenated) amorphous silicon
$SiO_{(2)}$	Silicon (di-) oxide
SiN(:H)	(Hydrogenated) silicon nitride
SiC	Silicon carbide
FZ	Float Zone
SOG-Si	Solar grade silicon
Al_2O_3	Aluminum oxide (Alumina)
GB	Grain boundary
DCS	Dichlorosilane (SiH_2Cl_2)
TEOS	Tetra eth-oxy silane
BSG	Boron silicate glass
PSG	Phosphorus silicate glass
Ag	Silver
Al	Aluminum
B	Boron
Fe	Iron
Ge	Germanium
P	Phosphorus
Pt(Ir)	(Iridium containing) Platinum
Ti	Titanium

Measurements

AFM	Atomic Force Microscopy
C-AFM	Combined and/or Conductive Atomic Force Microscopy
KFM	Kelvin Force Microscopy
EL	Electroluminescence
EQE	External Quantum Efficiency
FT-IR	Fourier-Transform Infra-Red spectrometry

IQE	Internal Quantum Efficiency
µ-PCD	Microwave Photo-Conductivity Decay
PL	Photoluminescence
SEM	Scanning Electron Microscopy
SIMS	Secondary Ion Mass Spectroscopy
SP	Spectral Responce
XRD	X-Ray Diffraction
FWHM	Full Width at Half Maximum
BE	Bound Excitons
TA	Transverse Acoustic mode
TO	Transverse Optical mode
LO	Longitudinal Optical mode
D1	Dislocation 1
RMS	Root Mean Square
SRV	Surface Recombination Velocity
a.u.	Arbitrary unit

Symbols

A	Cross-sectional area of diode
AC_k	Total cost of PV components per year
AM	Air Mass
B	Magnetic filed
C	Capacitance
CP	Contact potential
c	Light speed
D	Time of DCS supply
D/T	Intermittent ratio
D_n	Electron diffusion coefficient
D_p	Hole diffusion coefficient
D_x	Diffusion coefficient of factor x
d_{exp}	Lattice spacing

E	Young's modulus
E_c	Energy level of the edge of the conduction band
E_f	Fermi energy level
E_v	Energy level of the edge of the valence band
E_t	Energy level of a trap in the bandgap
Eff.	Conversion efficiency
F_{es}	Oscillatory electrostatic force
F_ω	Spectral component at the frequency
F.F.	Fill factor
G_{av}	Average generation rate
G_{bulk}	Generation rate in the bulk
gc_{PV}	Power generation cost of photovoltaic system
h	Plunk constant
I	Current
I_{sc}	Short circuit current
J_0	Saturation current density
J_d	Diode current density
J_L	Photo-generated current density
J_{max}	Current density at maximum power point
J_n	Electron current density
J_{sc}	Short circuit current density
k	Boltzmann constant
L_{eff}	Effective diffusion length
L_g	Average grain size
L_n	Electron diffusion length
L_p	Hole diffusion length
N	Total number of minority carrier
N_A	Doping level in a p-doped material (Acceptor concentration)
N_A	Doping level in a n-doped material (Donner concentration)
N_d	Nucleation density
N_t	Interface (trap) density at grain boundaries
n	Electron density, or ideality factor

Δn	Excess carrier (electron) density
Δn_{av}	Average excess carrier (electron) density
n_i	Intrinsic electron density
n_{peak}	Peak concentration of doping
$n_{p(\mathrm{x})}$	Electron density in p-type material at x
n_s	Sheet electron density
P_{in}	Power of illuminated light
P_{max}	Maximum output power
p	Hole concentration
$p_{n(\mathrm{x})}$	Hole density in n-type material at x
p_{ef}	Total power generation per year
q	Elementary electric charge
R	reflectance
R_s	Series resistance
R_{sh}	Shunt resistance
R_{sq}	Sheet resistance
S	Surface recombination velocity
S_{eff}	Effective surface recombination velocity
T	Time of period of one cycle in a intermittent source gas supply method, or Temperature
t	time
U_{eff}	Effective recombination rate
U_{bulk}	Generation rate in the bulk
V	Applied voltage
V_{AC}	Amplitude of alternate current voltage
V_{DC}	Direct current voltage
V_{bi}	Built-in potential
V_H	Hall voltage
V_{max}	Voltage at maximum power point
V_{oc}	Open circuit voltage
W	thickness

x_{GB}	Depth of p-n junction at grain boundary
α	Absorption coefficient
α_x	Thermal expansion coefficient of material x
ε	Permittivity
η	Conversion efficiency
λ	wavelength
μ_H	Hall mobility
μ_n	electron mobility
μ_p	Hole mobility
v	Poisson's ratio
v_{th}	Thermal velocity in silicon
$\sigma_1+\sigma_2$	Two main stress tensor components
σ_{in}	Internal stress
σ_n	Capture cross section
σ_{th}	Theoretical thermal stress
$\Delta\sigma$	Time dependence of excess photo-conductance
τ	minority carrier lifetime
τ_{bulk}	bulk minority carrier lifetime
τ_{eff}	Effective minority carrier lifetime
τ_g	minority carrier lifetime inside grain
Δ	Shift value of Raman peak
ϕ_b	Potential barrier height at grain boundary
Ω	ohm

Chapter 1

Introduction

1.1. Background and introduction of poly-Si thin film

1.1.1. Background

Securing the supply of reliable and sustainable energy is one of the biggest issues in the future of human prosperity. The world primary energy demand is predicted to grow by 1.6% per year on average during 2006-2030, from 11 billion toe (tonne oil equivalent) to over 17 billion toe [1.1]. However, fossil fuels, especially oil, which are the world's vital energy sources today, have two risks; a lack of resources and uncertain price depended on investments. In addition, gases like CO_2, NO_x, or SO_x emitted by the consumption of fossil fuels are said to cause the acid rain, air pollution, and climate change followed by the secondary problems such as sea-level rise, vegetation disturbance, and desertification. In concrete terms, the CO_2 concentration in the atmosphere has increased to over 380 ppm from 280 ppm before the industrial revolution, and average temperature and sea-level have been risen 0.3-0.6 °C and 10-20 cm, respectively [1.2]. In order to meet future's energy demand reliably without stressing the global environment, the role of renewable and clean energy production will become more important.

The most important forms of renewable energy are hydropower, biomass, wind power and solar energy. “New” renewable energies (wind, “new” biomass, and solar energy) account at the moment for about 8% of primary energy production in Japan [1.3], and all scenarios predict that this share is going to increase. Among them, photovoltaic conversion (PV, in other words: Solar Cell) is especially expected to play one of the most important roles because of its attractive advantages. The solar energy soured to the earth is virtually unlimited and quite huge (1.8×10^{14} kW), and distributed to over the globe. In addition, solar cell is a converter, which can transform the sunlight to the electric power directly by the photovoltaic effect, without any pollutions, noises, and vibrations. This feature brings other advantages; easy to be maintained, set locally, operated without manpower.

Recently, solar cell production and installation has been dramatically increasing all over the world. The total production of solar cells has grown at the annual rate of over 45% in the last five years, and in 2007 it exceeded 3.5 GW [1.4]. The growth is predicted to continue by 27% till 2012 [1.5]. The conversion efficiency of modules of wafer-based multicrystalline silicon solar cell, today’s dominant type of solar cell, has improved by about 15% and the power generating cost has reduced to around 45 yen/kWh [1.6]. However, in spite of the progress, this power generating cost is still much higher than other conventional electricity cost as shown in Table 1.1 [1.7], and the present contribution of the solar cells to the primary energy production is very small. For the goal that photovoltaic conversion covers 10% of electricity by 2030, which was raised in “PV Roadmap 2030 (PV2030)” by New Energy and Industrial Development Organization (NEDO), the comparable power generation cost of 5-10 yen/kWh has to be accomplished [1.6]. Of course, large investment and mass-production lead to the reduction of the power generation cost, however, some technological developments are necessary for the drastic progress.

Table 1.1: Power generation cost and CO_2 emission amount of different energy source [1.7].

Energy source	Power generation cost (yen/kWh)	CO_2 emission amount (g-CO_2/kWh)
oil	10.0-17.3	742
coal	5.0-6.5	975
LNG	5.8-7.1	519-608
water	8.2-13.3	11
atomic	4.8-6.2	22-25
solar	45	53
wind	10-14	29

1.1.2. Poly-Si thin film solar cells

Today's solar cell market is largely based on the bulk crystalline silicon technology, with a share of more than 95% (monocrystalline silicon cells; 36%, multicrystalline silicon cells; 58%) [1.4]. Bulk silicon cells combine an impressive number of advantages such as high performance, stability, abundance and no toxicity, therefore they will keep playing the most important roles even other materials will be proposed and developed. To reduce the power generation cost of conventional (c-Si) solar cell, material cost reduction by means of material volume reducing is one promising strategy. In conventional fabrication of 250-μm-thick multicrystalline silicon solar modules, approximately a half of the fabrication cost consists of the cost of silicon substrates [1.8]. Hence, reduction of silicon materials is effective for low cost fabrication of solar modules. Additionally, there's an issue of limitation of silicon feed stock for solar cells. Certainly, it is very important to develop the thinner (50-100 μm) silicon solar cells with high efficiency, however, the wafer-based technology includes the costly silicon ingot fabrication and kerf-loss in slicing step. Then, the impact to power generation cost reduction is not so large (mentioned in detail at later section).

Here, crystalline silicon, especially polycrystalline silicon (poly-Si), thin films solar cells based on direct deposition technology are one of the promising future directions, which have the potential of low-cost and relatively high and stable performance. By fabricating the thin film silicon with 5 to 50 μm thickness directly on foreign cheap substrates without any kerf-loss, the impact to power generation cost reduction is quite big. And it is crystalline phase silicon, therefore there's no light degradation observed in amorphous silicon (a-Si) solar cell (Stabler-Wronski effect [1.9]), and can apply the well-established cell fabrication techniques for bulk crystalline silicon with a little change. The potential of crystalline silicon thin film solar cells has been proved theoretically and the expected performance of poly-Si thin film solar cell has been calculated [1.10-1.14].

There are several techniques to create poly-Si thin films on foreign substrates heading for photovoltaic applications. Direct deposition at low temperature (below 700 °C) using low pressure chemical vapor deposition (LPCVD), plasma enhanced chemical vapor deposition (PECVD), or hot-wire CVD typically creates poly-Si thin films with grain size of sub-micron or less (complicated-mixed phase with a-Si [1.15]). Yamamoto *et al.* reported a best conversion efficiency of 10.1% using PECVD method [1.16], but these techniques have the problem of low process speed. Other low temperature approaches consist of deposition of a-Si layer by LPCVD, PECVD, hot-wire CVD, sputtering, or evaporation followed by the crystallization step like solid phase crystallization (SPC) [1.17-1.19], aluminum induced crystallization (AIC) [1.20, 1.21], layered laser crystallization (LLC) [1.22], or flash lamp annealing [1.23]. Recently CSG Solar Corporation started production of silicon thin films prepared by SPC on glass followed by rapid thermal annealing (RTA), for which the solar cell efficiency achieved around 10% [1.17]. Another approach to obtain poly-Si thin films is a high temperature process over 700 °C using thermal CVD [1.24, 1.25], AIC [1.26, 1.27], or zone melting re-crystallization (ZMR) [1.28-1.31]. Some of these researches are arranged in Table 1.2 and Fig. 1.1 which shows the relationship between grain size and open circuit voltage [1.32].

Among them, thermal CVD method seems most suitable for thin film poly-Si solar cells for following reasons. First, high deposition rates (several microns per minute) are possible and routinely achieved. Second, if carried out in the right conditions, it yields the relatively high quality poly-Si layers reproducing the underlying crystallographic structure, without any re-crystallization step which needs long time. And poly-Si thin films deposited directly on foreign substrates by the higher temperature CVD have the columnar structure and

Table 1.2: Techniques to fabricate poly-Si thin film and its cell properties [1.32].

Institute/ Company	Substrate	Technique	V_{oc} (mV)	*Eff.* (%)
CGS Solar [1.17]	Borosilicate glass	SPC + RTA	497	10.0
Sanyo [1.18]	Metal	SPC	553	9.2
UNSW [1.19]	Borosilicate glass	SPC + RTA	517	1.5
UNSW [1.20]	Borosilicate glass	AIC + epi.	441	3.0
HMI [1.21]	Borosilicate glass	AIC + CVD	378	1.3
IPHT [1.22]	Borosilicate glass	LLC	510	3.6
IMEC [1.26]	Ceramic	AIC + CVD	533	8.0
InESS [1.27]	Ceramic	(AIC) + CVD	410	~ 3

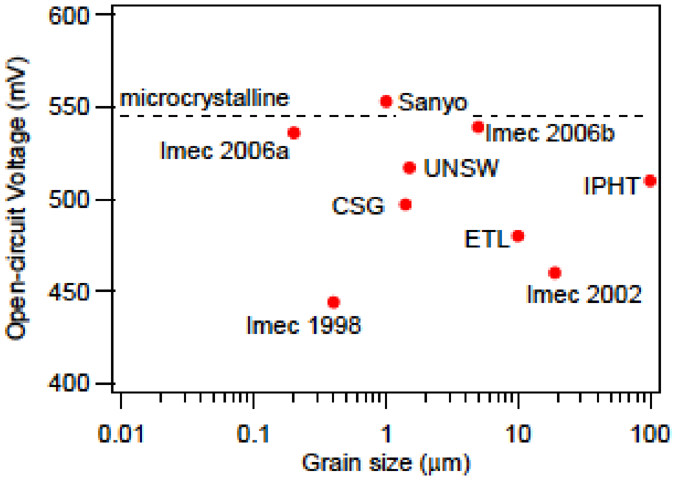

Fig. 1.1: Comparison of the best open-circuit values of fabricated poly-Si thin film solar cells, plotted as a function of the grain size [1.32].

preferential orientation of the grains, which is suitable for solar cell application [1.24]. However, hydrogen can easily diffuse out of the film during the deposition and therefore it is not possible to deposit poly-Si films with enough hydrogen for passivation of the defects and grain boundaries (GBs). This is the main disadvantage in comparison with the low temperature processes. Given all these features, high temperature thermal CVD technique was applied to deposit poly-Si thin films on foreign substrates in this study.

1.2. Purpose and outline of this thesis

It was proved that poly-Si thin films directly deposited on cheap foreign substrates by thermal CVD could achieve 15-18% solar cell efficiency by effective light trapping and passivation of defects [1.33]. And it is revealed that the power generation cost could be improved by 50% even with conversion efficiency of 10%, as mentioned in next section. However, still there is no report of directly-deposited poly-Si thin film solar cells which reached these efficiencies [1.24, 1.25]. Improvement of poly-Si thin films solar cell's efficiency is strongly required.

The final goal of this kind of research is of course to achieve the poly-Si thin film solar cells with enough conversion efficiency, but this thesis concentrates on the improvement of poly-Si thin films' crystallographic and electronic properties for solar cell applications. And the collateral development of techniques related to the poly-Si solar cell fabrication is also described.

To reduce the crystalline disorders in poly-Si thin film is essential for the improvement of poly-Si thin film solar cell. Poly-Si thin film includes certain numbers of crystalline defects, especially at GBs. These defects influence the charge carrier transport properties, acting as recombination centers for the photo-generated minority carriers. The target values related to crystallographic properties are set with roughly assumptions as follows, referring the work by Yamazaki using 2-demantional simulation [1.34]. The simulation model and results are shown in Fig.1.2 and Fig. 1.3, respectively. It has been revealed that in order to achieve the conversion efficiency of over 10%, effective and conceivable value in poly-Si thin film solar cells with thickness of 10 μm, the factor $L_g/2S_{GB}$ (L_g: grain size, S_{GB}: surface recombination velocity at GBs) should be higher than 5×10^{-8} s with the assumption of minority carrier life time within grain of 0.3 μs.

In order to obtain enough small number of crystalline defects that meet the values mentioned above, mainly two points are focused for investigation; the grain size enlargement and the defect passivation. The enlargement of the grains, which can reduce GBs, is demonstrated directly-during the deposition step on cheap alumina substrate and reference silicon wafer using an intermittent source gas supply method. For the defects passivation, high-pressure H_2O vapor heat treatment (HWT) as a new simple and low-cost defect passivation is proposed and demonstrated on poly-Si thin films. The roles of grain size enlargement and HWT in poly-Si thin films are investigated in detail from the view points of crystallographic properties in relation to electronic properties.

Following the general introduction and purpose describing in Chapter 1, experimental results are reported in Chapters 2-5. The Chapters correspond to thematic blocks, so each of them contains a short introduction and a summary in order to make them self-contained.

In Chapter 1, it is also briefly simulated the cost performance of poly-Si thin film solar cells, emphasizing the utility of poly-Si thin film solar cells.

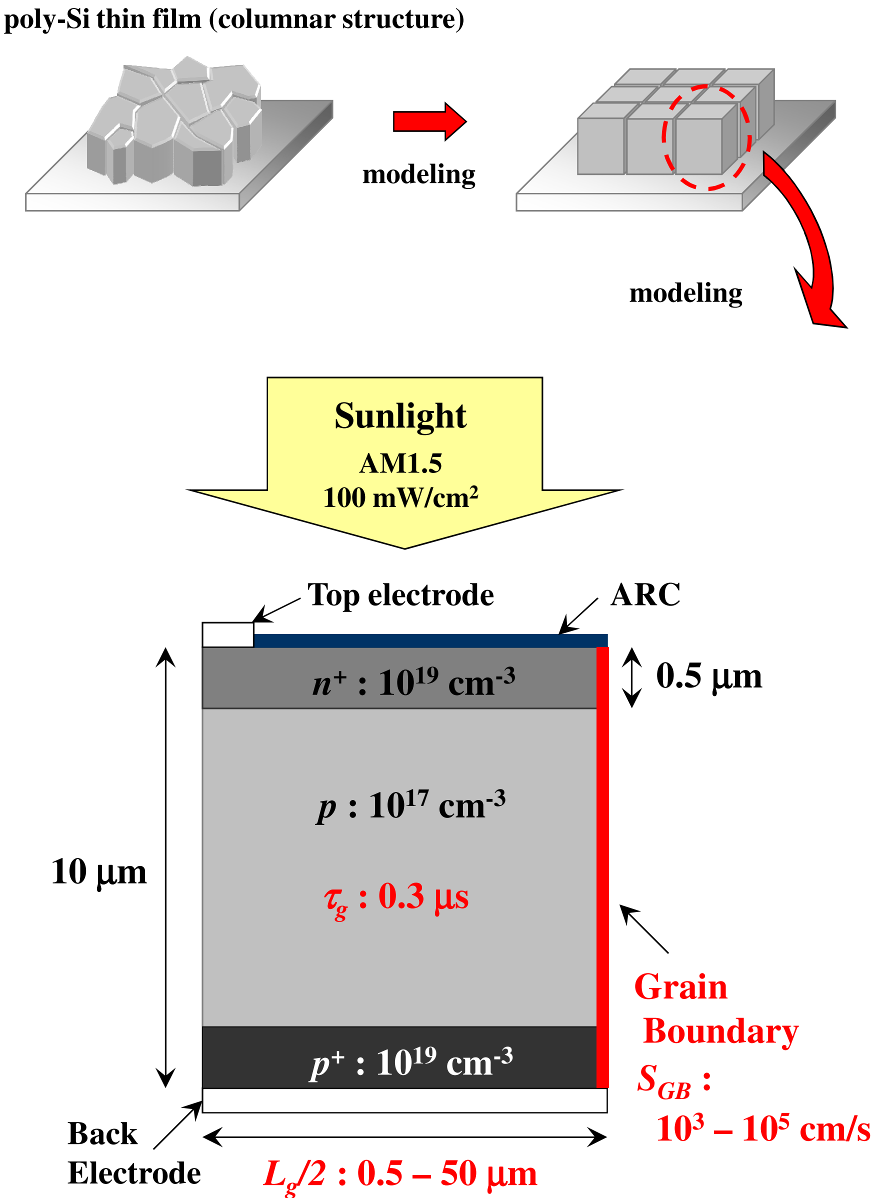

Fig. 1.2: Structure of 2-D simulation model of poly-Si thin film solar cell [1.34].

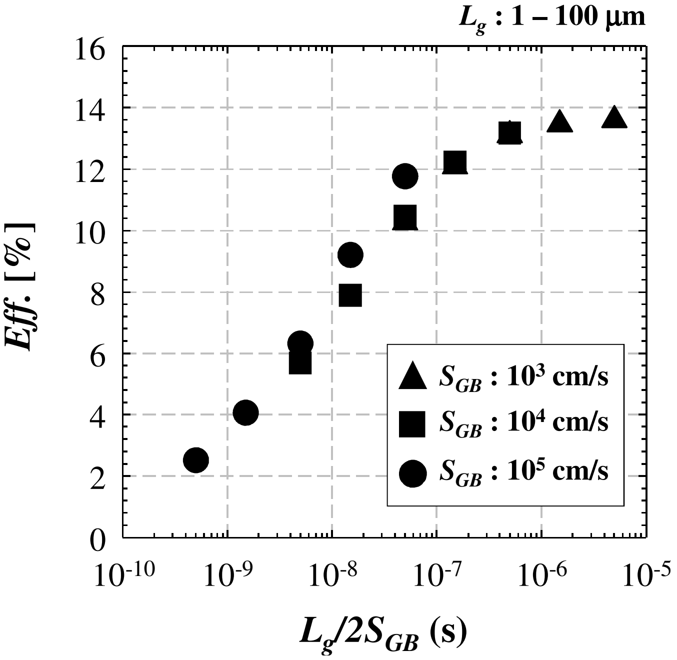

Fig. 1.3: Simulated photovoltaic performance for various combinations of S_{GB} and L_g as a function of $L_g/2S_{GB}$ [1.34].

In Chapter 2, to fabricate high-quality poly-Si thin films with high deposition rate, thermal CVD in atmospheric pressure (thermal-APCVD) method is employed for poly-Si thin films deposition on foreign alumina substrates as well as on reference silicon wafers. And in order to enlarge the grain size directly in deposition process, an intermittent source gas supply method is applied. After the introduction of deposition technique, the condition of poly-Si thin films' grain size is investigated, concentrating on the source gas supplying condition and substrate type.

In Chapter 3, the crystallographic and electronic properties of grain size-controlled poly-Si thin films is characterized by means of Raman scattering measurement, X-ray diffraction measurement, photoluminescence measurement, Hall effect measurement and atomic force microscopy measurement. The dependency of these results on grain size and substrate type is discussed, concerning the internal stress involved in poly-Si thin films and defect densities.

In Chapter 4, the effect of HWT as a new and simple defect passivation method for poly-Si thin films is investigated as well as applying to bulk crystalline silicon solar cells. For poly-Si thin films, the crystallographic and electronic characterization is applied in the same way as Chapter 3, and bulk crystalline silicon solar cells are evaluated by means of photovoltaic performance and related properties, revealing the effect of HWT.

In Chapter 5, it is described about the trail fabrication of poly-Si thin film solar cells on alumina substrates. And as a new and suitable technique for the p-n junction formation in poly-Si thin film solar cell fabrication, laser doping method, which can from the shallow emitter, is introduced and developed as well as in bulk crystalline silicon solar cell fabrication, investigating the doping conditions and photovoltaic properties.

Finally, conclusions and outlooks of this research are summarized in Chapter 6.

1.3. Economical aspects of poly-Si thin film solar cells

In order to clarify the impact of poly-Si thin film solar cells on economic aspects, some calculations which leads to the power generation cost of poly-Si thin film solar cells fabricated on cheap foreign substrates are arranged with some assumptions in this section. The power generation cost of conventional multicrystalline silicon solar cells are also discussed with the comparison with poly-Si thin film solar cells.

1.3.1. Substrate selection

The choice of the substrate is one of the most important issues in poly-Si thin film solar cell for not only technological reasons but also economic reasons. Simple production methods and cheap source materials are essential. In high temperature deposition process (from 800 °C to 1200 °C), choice of substrate material is limited, which is too high for most standard glasses. Substrates should fulfill a number of other requirements. To avoid excessive stress from the differential contraction due to cooling down after the deposition, thermal expansion coefficient of the substrate material should be matched to the value of silicon (4.2×10^{-6} K^{-1}). Also substrate should contain as little impurities as possible in order to eliminate contamination of the silicon thin films [1.35]. Conceivable candidates are arranged and compared with each other in Table 1.3 [1.36].

Alumina is a ceramic material consisting of small grains of aluminum oxide Al_2O_3. It is widely used in the electronic packaging industry and is produced on an industrial scale with the tape casting process, and its high reflectance is expected to have Back Surface Reflectance effect [1.37, 1.38]. Mullite is a related ceramic material, which is formed as a solid state solution of Al_2O_3 and SiO_2 within a certain concentration ratio. Graphite is a common material consisting of parallel planes of C-atoms arranged in a hexagonal form which leads to its use in electrical equipment. Silicon carbide (SiC) is a refractory polycrystalline material produced mainly by sintering and reaction bonding of SiC powders. Among them, mullite seems to be most suitable with both physical and economical reasons, but unfortunately it is much less widespread than alumina, and today produced by very few companies. Therefore, alumina substrate was applied as foreign substrates in this cost calculation and the research of whole this thesis.

1.3.2. Deposition cost

In this cost evaluation, two options; with or without re-crystallization step, are discussed and compared with each other [1.36]. Process without re-crystallization consist just two steps; substrate preparation and active layer deposition. If alumina is used as a substrate, both substrate cost and deposition cost share total cost approximately half and half. On the other hand, process with re-crystallization needs ever so six steps; substrate preparation, seeding layer deposition, capping layer deposition, re-crystallization, stripping of capping layer, and active layer deposition. Re-crystallization cost is almost equal to deposition cost, so total cost of with re-crystallization case is approximately twice as without re-crystallization case because there are two times of deposition. This suggests how favorable avoiding the re-crystallization is.

1.3.3. Comparison with conventional multicrystalline silicon solar cells

The power generation cost of photovoltaic system (gc_{PV}) can be calculated using the equation,

$$gc_{PV} = \frac{\sum_k AC_k}{p_{ef}}, \qquad (1.1)$$

where p_{ef} is total power genetation per year determined by module efficiency and total amount of solar radiation per year, and AC_k is total cost of each component per year given from production scale, durable years, module capacity, initial cost, installation cost, maintenance cost, money interest, shipping price coefficient, and so on [1.8]. Assuming the case of conventional multicrystalline silicon solar modules with annual production scale of 1 GW, module capacity of 3.5 kW, module efficiency of 15%, durable years of 20 years, and other parameters of typical values, the power generation cost is calculated as 44.6 yen/kWh. In this case, approximately 70% of power generation cost, around 30 yen/kWh, is module fabrication cost. And in module fabrication, Solar Grade Silicon (SOG-Si) purification, silicon wafer fabrication, cell processing, and module assembling account 15-20%, 20-25%, 15-25%, and 25-50% in total module fabrication cost, respectively [1.8]. Therefore, it can be confirmed that technological developments which reduce silicon material cost are essential for power generation cost as well as mass-producing by large investment. However, the simple thinning of silicon wafer doesn't have a drastic impact to total cost reduction because it cannot avoid the costly silicon ingot fabrication and kerf-loss in slicing step; only less than 5 yen/kWh could be reduced if silicon thickness would be 100 µm from 250 µm, assuming the kerf-loss of 300 µm (typical value today) and the same value of other parameters [1.8].

Poly-Si thin film with thickness of 10 µm directly deposited on foreign cheap substrate has the dramatic advantage to cost reduction by means of not only silicon volume reduction but also avoiding the costly silicon ingot fabrication and kerf-loss. The comparison of power generation cost between multicrystalline silicon solar cell and poly-Si thin film solar cell is arranged in Table 1.4 [1.36], with the same fabrication and installation condition except for silicon material preparation. Although the smaller conversion efficiency is expected in poly-Si case because of lower material quality and decreased length of light path in active layer, the comparable or improved power generation cost could be obtained even with conversion efficiency of less than 8%. When conversion efficiency gets higher than 10%, more than 50% of power generation cost reduction would be expected. Further technological progresses which achieve the poly-Si thin film solar cells with over 20% efficiency will bring in the generation cost of less than 15 yen/kWh which can be competitive in commonly-used electricity generation.

Table 1.3: Relevant properties of the main candidate materials for the substrate of poly-Si thin film deposition [1.36].

Material	Relative price of raw material (99.9% purity)	Heat resistant up to 1400 °C	Thermal expansion coefficient (K^{-1})	Conductive
Alumina	1	yes	8×10^{-6}	no
Mullite	1-2	yes	5×10^{-6}	no
Graphite	1-5	yes	4.5×10^{-6}	yes
SiC	2-7	yes	4×10^{-6}	yes/no

Table 1.4: Comparison between the material cost per unit electrical power for a bulk multicrystalline silicon cell and poly-Si thin film cell on foreign substrate.

Cell type	Conventional mc-Si		Poly-Si thin film		
sketch	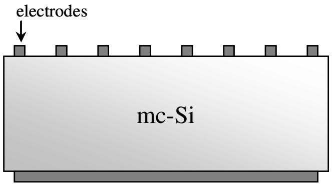		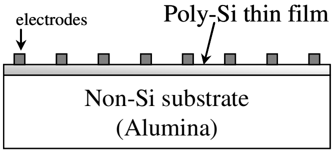		
Silicon thickness	250	100	10		
Relative cost for material	1	0.87	0.38		
Assumed efficiency (%)	15	15	8	10	20
Relative power generation cost	1	0.88-0.95	0.71	0.56	0.36

References of Chapter 1

[1.1] International Energy Agency (IEA): “World Energy Outlook 2008, Executive Summary”, IEA books (2008) p.4.

[1.2] Intergovernmental Panel on Climate Change (IPCC): “IPCC Fourth Assessment Report: Climate Change 2007, The Physical Science Basic”, World Meteorological Organization/ United Nations Environment Program (2007) p.95.

[1.3] Agency for Natural Resources and Energy (ANRE): “Energy balance sheet 2007”, , Japanese Ministry of Economy, Trade and Industry (2008).

[1.4] RTS Corporation: “Information of Solar Power Generation, Inter- and intra-national current about solar power generation”, Vol. **18**, No. 4 (2008) p.4, in Japanese.

[1.5] Fuji-Keizai Inc.: “Actual states and prospects of technology and market related to solar cells” (2008), in Japanese.

[1.6] New Energy and Industrial Development Organization (NEDO): “Overview of “PV Roadmap 2030 (PV2030)”” (2004).

[1.7] Agency for Natural Resources and Energy (ANRE): “Annual report about Energy, 2007”, Japanese Ministry of Economy, Trade and Industry (2007) p.16, in Japanese.

[1.8] Koich Yamada, and Hiroshi Komiyama: “Photovoltaic Engineering”, Nikkei Business Publications, Inc. (2002) in chapter 4-6, in Japanese.

[1.9] D. L. Staebler, and C. R. Wronski: J. Appl. Phys., **51** (1980) p.3262.

[1.10] T. Tiedje, E. Yablonovitch, G. D. Cody, and B. G. Brooks: IEEE transactions on electron devices ED-31 (1984) p.711.

[1.11] J. A. Rand, R. B. Hall, and A. M. Barnett: Proc. of 21st IEEE Photovoltaic Specialist Conference (1990) p.263.

[1.12] A. W. Blakers, J. H. Werner, E. Bauser, and H. J. Queisser: Appl. Phys. Lett., **60** (1992) p.2752.

[1.13] M. Imaizumi, T. Ito, M. Yamaguchi, and K. Kaneko: J. Appl. Phys., **81** (1997) p.7635.

[1.14] R. Brendel, R. B. Bergmann, P. Lölgen, M. Wolf, and J. H. Werner: Appl. Phis. Lett., **70** (1997) p.390.

[1.15] J. Kočka, T. Mates, H. Stuchlíková, J. Stuchlík, and A. Fejfar: Thin Solid Films, **501** (2006) p.107.

[1.16] K. Yamamoto, M. Yoshimi, T. Suzuki, Y. Tawada, Y. Okamoto, and A. Nakajima: IEEE Trans. Elect. Devices, **46** (1999) p.2014.

[1.17] M. J. Keevers, A. Turner, U. Schubert, P. A. Basore, and M. A. Green: Proc. of 20th European Photovoltaic Solar Energy Conference (2005) p.1305.

[1.18] T. Baba, M. Shima, T. Matsuyama, S. Tsuge, K. Wakisaka, and S. Tsuda: Proc. of 13th European Photovoltaic Solar Energy Conference (1995) p.1708.

[1.19] A. G. Aberle: Proc. of 20th European Photovoltaic Solar Energy Conference (2005) p.1108.

[1.20] A. G. Aberle: Proc. of 4th World Conference on Photovoltaic Energy Conversion (2006) p.1418.

[1.21] B. Rau, J. Schneider, E. Conrad, S. Gall, and W. Fuhs: Tech. Dig. of 15th Int'l Photovoltaic Science and Engineering Conference (2005) p.778.

[1.22] G. Andrä, J. Bergmann, F. Falk, E. Ose: Proc. of 19th European Photovoltaic Solar Energy Conference (2004) p.872.

[1.23] K. Ohdaira, T. Fujiwara, Y. Endo, S. Nishizaki, and H. Matsumura: Jpn. J. Appl. Phys., Vol. **47**, No. 11 (2008) p.8239.

[1.24] G. Beaucarne, S. Bourdais, A. Slaoui, and J. Poortmans: Thin Solid Films, **403-404** (2002) p.229.

[1.25] T. Yamazaki, Y. Uraoka, and T. Fuyuki: Thin Solid Films, **487** (2005) p.26.

[1.26] I. Gordon, L. Carnel, D. Van Gestel, G. Beaucarne, and J. Poortmans: Thin Solid Films, Vol. **516**, Issue 20 (2008) p.6984.

[1.27] A. Slaoui, E. Pihan, and A. Focsa: Solar Energy Materials and Solar Cells, **90** (2006) p.1542.

[1.28] A. Takami, S. Arimoto, H. Morikawa, S. Hamamoto, T. Ishihara, H. Kumabe, and T. Murotani: Proc. of 12th European Photovoltaic Solar Energy Conference (1994) p.59.

[1.29] R. Auer, J. Zettner, J. Krinke, G. Polisski, T. Hierl, R. Hezel, M. Schulz, H. P. Strunk, F. Koch, D. Nikl, and H. V. Campe: Proc. of 26th IEEE Photovoltaic Specialists Conference (1997) p.739.

[1.30] C. Hebling, S. W. Glunz, J. O. Schumacher, and J. Knobloch: Proc. of 14th European Photovoltaic Solar Energy Conference (1997) p.2318.

[1.31] H. Morikawa, Y. Kuwama, Y. Matsuno, S. Hamamoto, K. Imada, T. Ishihara, K. Kojima, and T. Ogama: Tech. Dig. of 11th Int'l Photovoltaic Solar Energy Conference (1999) p.543.

[1.32] G. Beaucarne, and A. Slaoui: "Thin-film Solar Cells: Fabrication, Characterization and Applications" edited by J. Poortmans, and V. Arkhipov, Wiley (2006) p.114.

[1.33] Y. Ishikawa, Y. Tamamoto, T. Hatayama, Y. Uraoka, and T. Fuyuki: Jpn. J. Appl. Phys., **40** (2001) p.6783.

[1.34] T. Yamazaki: Ph. D. Thesis, Graduate School of Materials Science, Nara Institute of Science and Technology (2005) p.10.

[1.35] T. L. Chu: Journal of Crystal Growth, **39** (1977) p.45.

[1.36] G. Beauarne: Ph. D. Thesis, IMEC (2000) p.13.

[1.37] A. M. Barnett, J. A. Rand, R. B. Hall, J. C. Bisaillon, E. J. Delledonne, B. W. Feyock, D. H. Ford, A. E. Ingram, M. G. Mauk, J. P. Yaskoff, and P. E. Sims: Solar Energy Materials and Solar Cells, **66** (2001) p.45.

[1.38] A. Slaoui, S. Bourdais, G. Beaucarne, J. Poortmans, and S. Reber: Solar Energy Materials and Solar Cells, **71** (2002) p.245.

Chapter 2

Deposition of poly-Si thin films on foreign substrates with in-situ grain size controlling

2.1. Introduction

Polycrystalline silicon (poly-Si) thin film includes certain number of grain boundaries (GBs) which influence the charge carrier transport properties. GBs act as potential barriers for majority carrier transportation, and act as recombination centers for minority carrier. Particularly, in solar cell devices, less GBs are desirable to obtain the higher photovoltaic performance. In order to decrease the influence of GBs, it is necessary to enlarge grains as well as passivate the defects at GBs. In order to enlarge and control grain size of poly-Si thin films, several methods were proposed such as zone melting re-crystallization [2.1-2.4] or aluminum induced crystallization [2.5-2.8]. However, these methods present a disadvantage for solar cell production as an additional time-consuming step, as described in Chapter 1. If the grain size could be enlarged during a deposition, it might be possible to achieve high efficiency poly-Si thin films solar cells without any additional processes. To enlarge grain size during deposition, an intermittent gas supply in APCVD [2.9, 2.10] was employed in this thesis.

In this Chapter, high temperature process of poly-Si thin films by thermal chemical vapor deposition in atmospheric pressure (thermal-APCVD) with direct grain size control in the deposition process is described. The possibility to fabricate poly-Si thin films with size-controlled grain on alumina substrates is discussed and compared with reference substrates of oxidized silicon wafers.

2.2. Deposition technique

2.2.1. Thermal-APCVD

A thermal-APCVD system was employed to deposit poly-Si thin films [2.9, 2.10]. Figure 2.1 shows the photograph and schematic image of cold-wall APCVD apparatus used in this thesis. The reactor was a quartz tube whose inner diameter was 71.5 mm. Temperature was controlled by as induction heating coil with the feedback of measured temperature by infrared thermo-camera. Dichlorosilane (SiH_2Cl_2: DCS), BCl_3/Ar (99.7 ppm) and H_2 were used as a silicon source gas, doping gas and carrier/reduction gas, respectively. DCS was used as a source gas instead of the more popular silane (SiH_4) because of easier gas handling and lower gas cost. Another advantage of DCS is the decrease of the defect density in silicon due to etching by chlorine during decomposition of source gas [2.11]. Mass flow controller was used to regulate the silicon source gas supply. H_2 gas was flowed through a purifier to avoid contamination. The samples were set on a SiC-coated graphite susceptor and installed into the furnace.

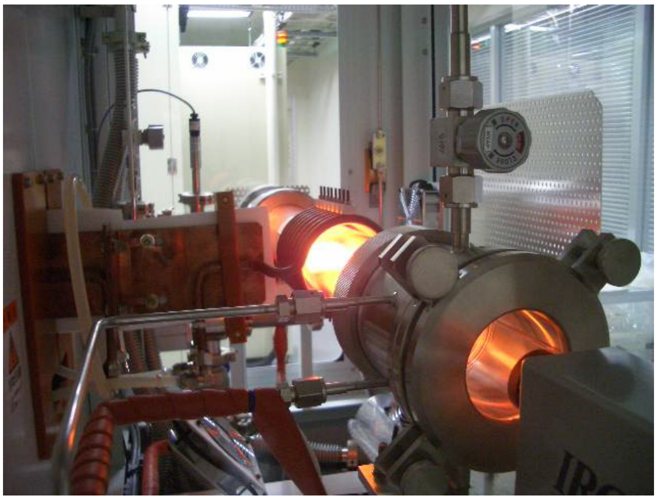

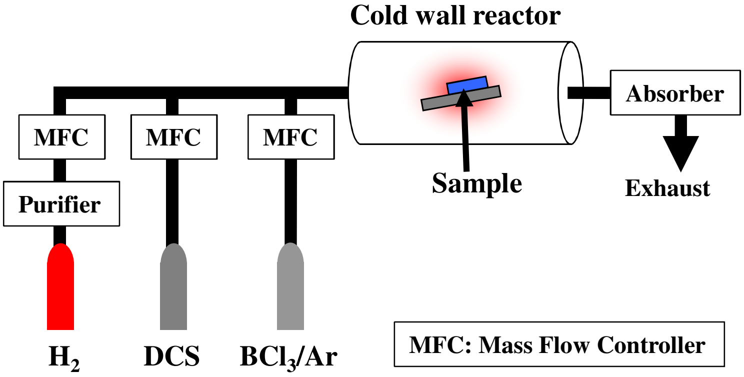

Fig. 2.1: Thermal-APCVD apparatus used in this study (upper: photograph of overview, down: schematic diagram).

The decomposition process of DCS is given by [2.12],

SiH_2Cl_2 (gas) → $SiCl_2$ (gas) + H_2 (gas), (2-1)

$SiCl_2$ (gas) → $SiCl_2$ (site), (2-2)

$SiCl_2$ (site) + H_2 (gas) → Si (site) + 2HCl (gas), (2-3)

where the first equation describes the thermal decomposition of the DCS, the second equation means the adhesion on an active site on the substrate and the third equation shows that the gaseous HCl is released. The schematic sketch of the deposition process discussed above is shown as Fig. 2.2. The surface- and cross-sectional-image of scanning electron microscope (SEM) of a typical poly-Si thin film fabricated by thermal-APCVD with thickness of around 10 µm are shown in Fig. 2.3.

2.2.2. 2-step deposition with intermittent source gas supplying

In order to enlarge and control grain size of poly-Si thin films during a deposition time, controlling the density of silicon nuclei formed at the initial stage of the deposition period is very important.

To control the nucleation density at the initial stage of deposition, a 2-step deposition method with intermittent source gas supply was employed in thermal-APCVD. In this deposition technique, two kinds of deposition temperature were introduced; the first step for silicon nucleation at 950-1000 °C and the second step for film growth with high deposition rate (0.6-0.7 µm/min) at 1000-1150 °C, as shown in Fig. 2.4. In this Chapter, CVD temperatures were decided as 950 °C in first step and 1050 °C in second step. In order to control the silicon nucleation density, the intermittent source gas supply method was introduced in the first step. Figure 2.5 shows schematic illustrations of 2-step deposition technique with the flow sequence of DCS and H_2 in the first step where DCS was supplied intermittently while H_2 flowed continuously. The period of one cycle is denoted as *T* and the flowing time of DCS in one cycle is denoted as *D*. The intermittence ratio *D/T* was varied from 100% (continuous flow of DCS) to 10% by changing *D* from 10 s to 1 s while *T* was fixed. The total time of *D* was adjusted to 3 min by changing the number of cycles. The source gas density (DSC/H_2) was fixed to 0.1 %. After the first step, the high-rate growth (0.6-0.7 μm/min) of poly-Si thin films was performed on the nucleation-controlled substrates, supplying DCS continuously with DSC/H_2=0.3% in the second step. The obtained film thickness was adjusted to approximately 10 μm. The poly-Si thin films were simultaneously doped into p-type in the second step thanks to boron incorporation from BCl_3, and the carrier (hole) concentration was adjusted to around 10^{17} cm^{-3}. Also, direct deposition of poly-Si thin films with the same condition as that of second step mentioned above without the first step was performed (denoted as 1-step). These CVD conditions of poly-Si deposition are summarized in Table 2.1.

2.2.3. Substrate preparation

A choice of the substrate is one of the most important material issues in the poly-Si thin film solar cell research and conceivable candidates are discussed in Chapter 1. In the course of this research, commercially available alumina substrates with features shown in Table 2.2 were applied as true ‘foreign’ substrates for the deposition of poly-Si thin films. Alumina is widely used in the electronic packaging industry and is produced on an industrial scale with the tape casting process. Alumina substrates have an additional advantage of a large reflection, serving for light trapping as a back surface reflector (BSR). Poly-Si thin film solar

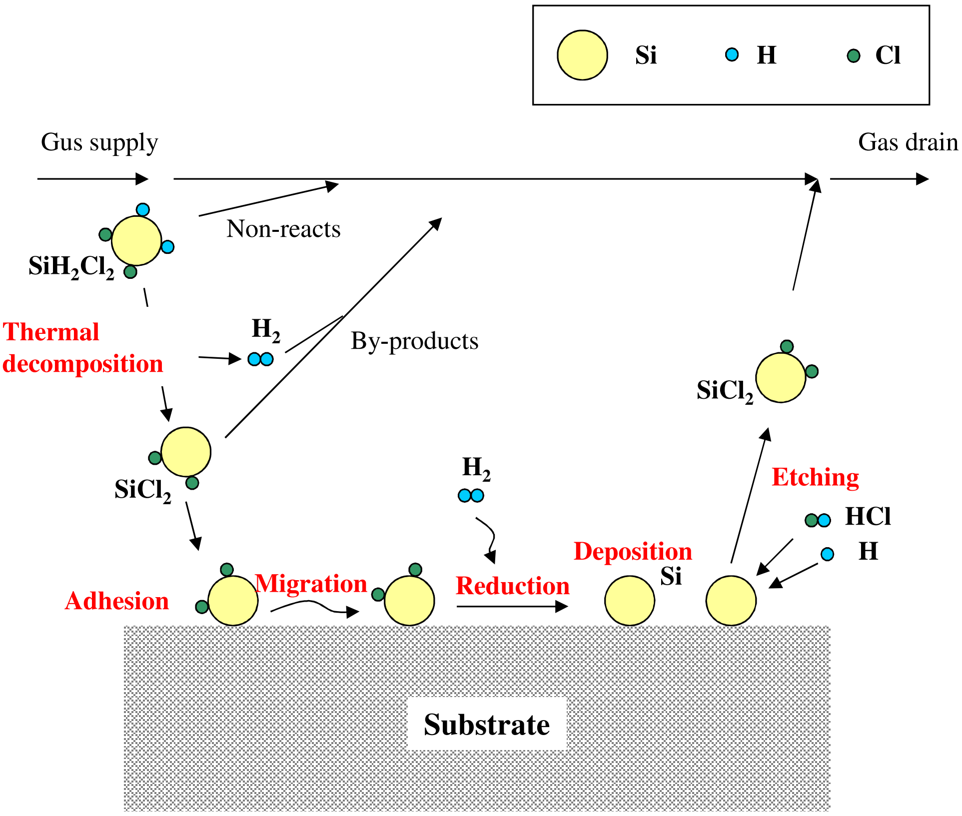

Fig. 2.2: Schematic diagram of the decomposed $SiCl_2$ activity.

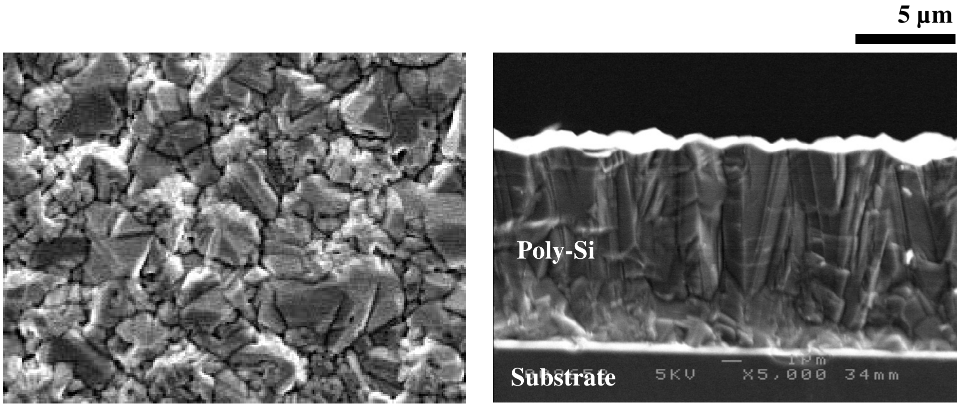

Fig. 2.3: Surface- and cross-SEM images of a typical poly-Si thin film fabricated by 1-step thermal-APCVD.

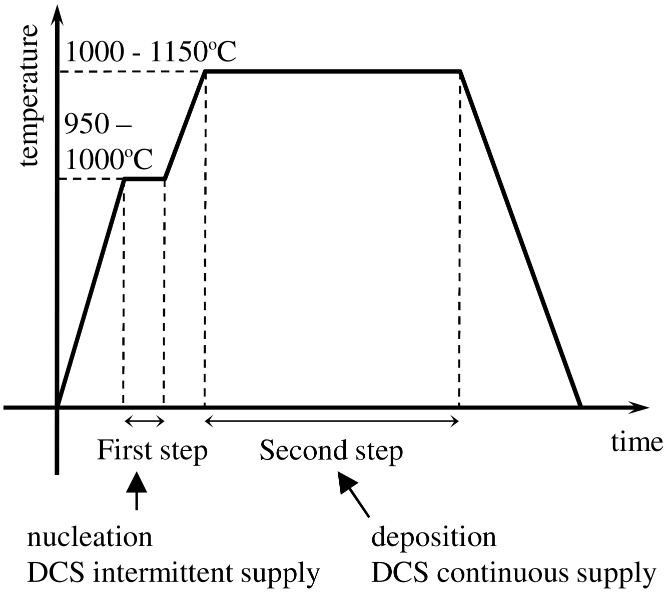

Fig. 2.4: Temperature sequence of 2-step deposition method.

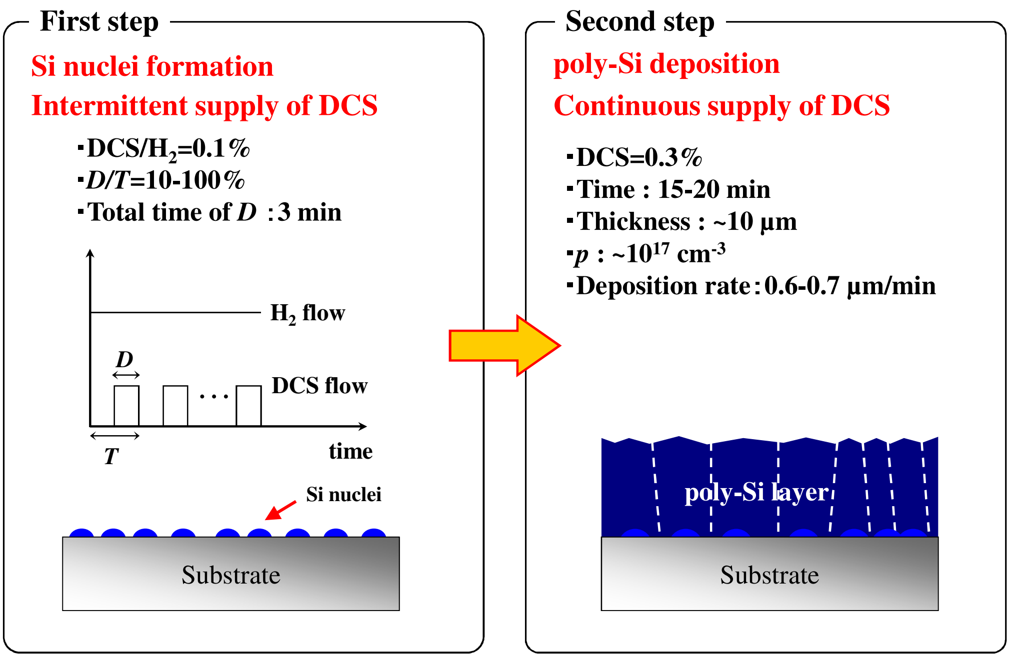

Fig. 2.5: Scheme of an intermittent source gas supply method.

Table 2.1: Conditions of poly-Si thin film deposition using thermal-APCVD.

Parameters	Conditions
Substrate	Alumina or silicon wafer
Intermittent ratio *D/T* (%)	10-100 or 1-step
Temperature (°C)	First step: 950-1000 Second step: 1000-1150
Pressure	Atmospheric
Time (min)	First step: 3 (total of DSC supplying time) Second step: 15-20
DCS flow rate (sccm)	First step: 20 Second step: 60
BCl3/Ar flow rate (sccm)	15 (only in second step)
H_2 flow rate (slm)	20

Table 2.2: Features of alumina substrate.

Parameters	Conditions
Purity (%)	99.9
Density (g/cm^3)	3.97
Vending strength at 25 °C (MPa)	660
Thermal expansion coefficient at 25-800 °C (1/K)	8×10^{-6}
Thermal conductivity at 25 °C (W/m·K)	33
Resistivity (Ω·cm)	10^{15}
Relative permittivity at 25 °C, 10 GHz	10
Roughness (µm)	~0.02

cells on highly reflective alumina substrate have been researched and achieved high short circuit current density [2.13, 2.14]. Impurities in alumina are chemically strongly bound and stayed in a matrix of substrate, so that only a very limited amount of contamination is released during deposition process. Poly-Si thin film solar cells on alumina substrate were already investigated [2.15]. However, crystallographic and electronic properties of poly-Si thin film itself on alumina substrate have not been reported.

Poly-Si thin films on ceramic substrates may have different structure and electronic properties (nucleation density, in-grain crystallinity, grain boundaries and tail states, carrier concentration, Hall mobility and so on) from ones deposited on silicon substrates. These different properties might be influenced by the difference of thermal expansion coefficients between alumina and silicon. Thermal expansion coefficients of alumina substrates and silicon are 8×10^{-6} and 4.2×10^{-6} [K^{-1}], respectively. Poly-Si thin films were deposited both on alumina substrates and reference silicon wafers, comparing with each case. Surface of silicon substrates was very smooth, while RMS roughness of surface of alumina substrates was relatively high (given feature: ~200 nm, measured value: 380 nm). Before the use of silicon substrate, RCA cleaning of silicon wafer was carried out as shown in Table 2.2. On the other hand, alumina substrates were cleaned by ultrasonic wave cleaning in acceton liquid in 2 min at room temperature.

When the ceramics are used as the substrate, some buffer intermediate layers should be employed in order to prevent some metal impurities included in substrates from diffusing into a poly-Si layer during the high temperature deposition period. The intermediate layers such as SiO_x, SiN_x, SiC, and etc. has been proposed [2.13-2.17], and in this Chapter, SiO_x and SiN_x layers deposited by plasma-enhanced CVD (PECVD) were adapted as intermediate layers. In addition, SiO_2 layer obtained by thermal oxidation of silicon wafer was

Table 2.3: RCA cleaning procedure.

No	Process	Chemicals	Conditions
1	SPM	H_2SO_4 (97%) → 1:1 of H_2SO_4 (97%):H_2O_2 (30%)	15 min at 80 ℃ → 10 min at 80 ℃
2	Rinse	Deionised H_2O (18M)	1 min at 20 ℃
3	HF	HF (5%)	1 min at 20 ℃
4	Rinse	Deionised H_2O (18M)	1 min at 20 ℃
5	RCA-1 (SC-1)	1:5:1 of NH_3 (27%): H_2O: H_2O_2 (30%)	5 min at 80 ℃
6	Rinse	Deionised H_2O (18M)	1 min at 20 ℃
7	HF	HF (5%)	1 min at 20 ℃
8	RCA-2 (SC-2)	1:5:1 of HCl (27%):H_2O:H_2O_2 (30%)	5 min at 80 ℃
9	Rinse	Deionised H_2O (18M)	1 min at 20 ℃
10	HF	HF (5%)	1 min at 20 ℃
11	Rinse & dry	Deionised H_2O (18M)	1 min at 20 ℃

Table 2.4: PECVD conditions for plasma-SiO_x and SiN_x formation.

Parameters	SiO_x	SiN_x
RF power (W)	75	40
Gas flow rate (sccm)	TEOS: 7 O_2: 300	SiH_4/N_2: 50 NH_3: 80
Time (min)	7.5	10
Temperature (°C)	300	300
Pressure (Pa)	80	80
Film thickness (nm)	~500	~400

Table 2.5: Oxidation conditions for thermal-SiO_2 formation.

Parameters	Conditions
Temperature (°C)	1000
Oxidation time (min)	90
O_2 flow rate (slm)	0.5
Film thickness (nm)	~500

also employed as the reference. Each intermediate layer is denoted as plasma-SiO_x, plasma-SiN_x, and thermal-SiO_2, respectively, and the conditions of formation are arranged in Table 2.3 and 2.4.

2.3. Grain size controlling

Before the deposition on alumina substrates, poly-Si thin films were deposited on silicon wafers with thermal-SiO_2, as a standard model for the investigation of deposition itself. In this section, the conditions of nucleation and grain size of poly-Si thin films deposited by an intermittent source gas supply method on silicon wafers with thermal-SiO_2 intermediate layers are discussed.

2.3.1. Nucleation density and grain size controlling

Figure 2.6 shows the surface-SEM pictures of silicon nuclei after the first step with different intermittent ratio, *D/T*. The density of the silicon nuclei clearly decreased with reducing *D/T.* The nucleation density could be controlled in the range from 10^6 to 10^{10} cm^{-2}.

Figure 2.7 show the surface- and cross-SEM images of poly-Si thin films after the second step of deposition with different intermittent ratio *D/T* at the prior first step. It can be clearly observed that the grain size was enlarged with reducing *D/T*. Average grain size by the deposition at *D/T* of 100% was 2-3 μm. On the other hand, grain sizes were enlarged from 2-3 to 15-20 μm by an intermittent source gas supply with decrease of *D/T* from 100 to 10%. Relationship between the nucleation density and *D/T*, and grain size and *D/T* are shown in Fig. 2.8 and 2.9, respectively.

(a) *D/T*=10%

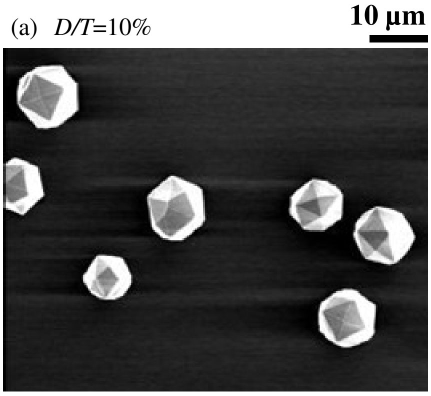

(b) *D/T*=30%

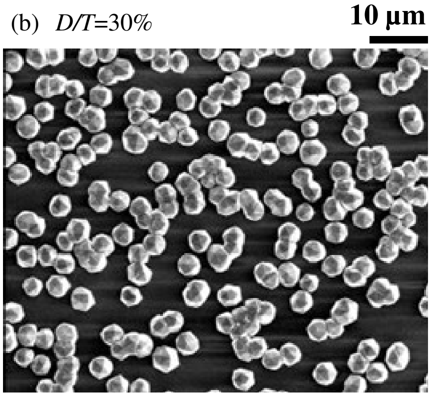

(c) *D/T*=100%

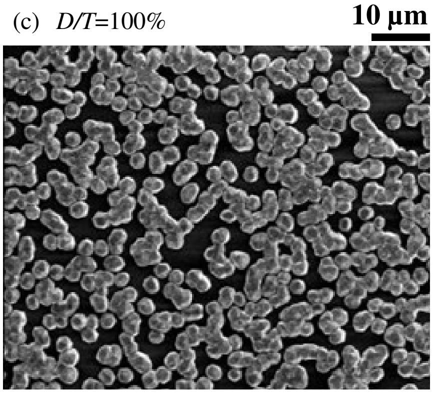

Fig. 2.6: SEM images of the silicon nuclei after the first step with different intermittent ratio *D/T*.

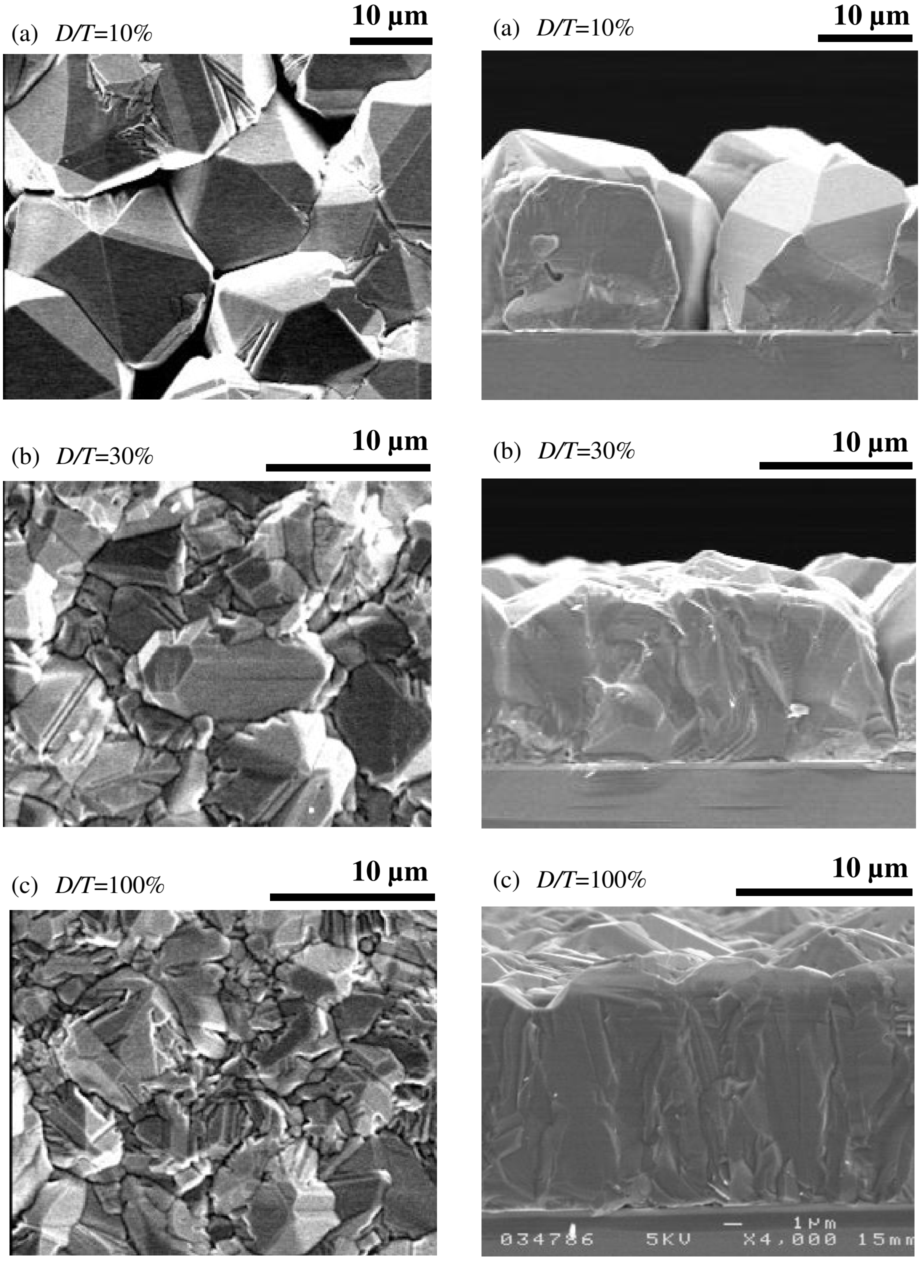
(a) *D/T*=10% (a) *D/T*=10%

(b) *D/T*=30% (b) *D/T*=30%

(c) *D/T*=100% (c) *D/T*=100%

Fig. 2.7: Surface- and cross-SEM images of poly-Si thin films after second step with different intermittent ratio *D/T*.

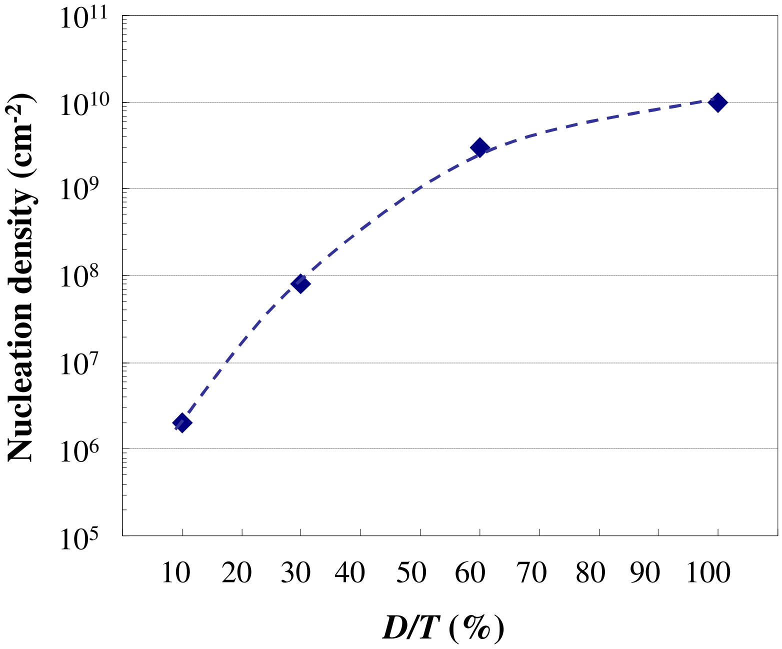

Fig. 2.8: Nucleus density after the first step as a function of *D/T*.

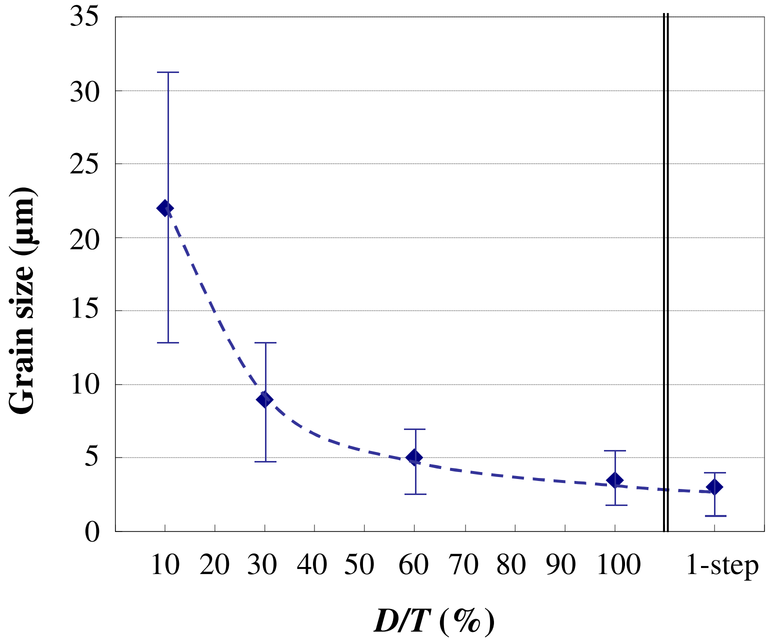

Fig. 2.9: Grain size of poly-Si thin films as a function of *D/T*.

2.3.2. Discussion of grain size controlling mechanism

When heterogeneous nucleation of silicon occurs on the surface of a foreign substrate which does not allow epitaxy, growth takes place in island mode (also called Volmer-Weber mode). Three-dimensional grains are formed, and they retain the shape until they coalesce with each other. The grain size in poly-Si thin films is determined on one hand by the early phase deposition, i.e., the nucleation phase, and on the other hand by competitive grain growth. During the nucleation phase, nuclei are formed and start capturing free silicon atoms on the substrate surface. While these existing grains grow, new ones may be formed in the spaces between them. After coalescence however, grains grow further epitaxially, continuing the underlying crystalline structure throughout the layer. Therefore, they form GBs when they reach each other. The relationship between the nucleation density (N_d) and the grain size (L_g) can be roughly approximated by [2.9, 2.10, and 2.18],

$$N_d = 1/L_g{}^2 (cm^{-2}) \cdot \qquad (2.4)$$

Hence, the smaller nucleation density is desirable to accomplish the grain-size enlargement.

In order to understand the fundamental mechanisms of nucleation, “atomic nucleation theories” seems to be suitable. The most complete treatment of the nucleation processes is probably Venables’s rate equation approach [2.19], which not only covers nucleation itself, but also takes other phenomena into account like coalescence and mobility of nuclei. The theory after simplification leads to the following factors. The first factor is the evolution of density of adatoms in time. Here, adatoms are defined as single atoms that are adhered at the surface of the substrate but diffuse freely along the surface. The evolution of adatom density in time is determined by the rate of arrival of adatoms, the frequency of removal of adatoms, the fraction of surface which is already covered, the density of stable nuclei, and the capture number of these nuclei. In steady state, the atoms appearing on the surface either to get caught by the stable nuclei or are removed after an average residence time. At the given temperature in CVD, the removal rate does not change irrespective of the other parameters, and is likely to be determined by surface reactions. During the deposition of silicon with chlorinated species like this study, the etching reaction,

$$\mathrm{Si\ (site) + 2HCl\ (gas) \rightarrow SiCl_2\ (gas) + H_2\ (gas)}, \qquad (2\text{-}5)$$

plays a crucial role. The second factor is the increase of stable nuclei per unit time, which is equal to the nucleation rate minus the rate at which the number of stable clusters decreases through merging processes. Third factor describes how the coverage increases when the stable nuclei grow.

The intermittent source gas supply method is the deposition technique actively utilizes the function of the etching reaction by HCl. In conventional 1-step deposition with the given temperature and silicon source gas supplying rate, the approaching rate of atoms on surface and the growth rate of stable nuclei are much larger than the atoms' removal rate, thus the nucleation occurs everywhere the surface and the nucleation density becomes high. When silicon grains contacted the neighbor grains already in the initial stage of deposition, the grains grew only in the perpendicular direction to the substrate. On the other hand, by introducing the intermittent supply method, some of the very small and unstable silicon clusters are desorbed and/or etched away during the intermission time because the etching becomes dominant. Once some nuclei start to grow, the nuclei are likely to preferentially adsorb precursors. Therefore, the size of the individual nuclei was enlarged with reducing *D/T*, while the number of the nuclei decreased. In the case of lower *D/T*, it could be seen that the individual grains grew much larger to lateral direction because the isolated grains can continue to grow until colliding with the other grains due to the low nucleation density.

Figure 2.10 shows the X-ray diffraction (XRD) patterns of poly-Si thin films fabricated with different *D/T*. The poly-Si thin film obtained by 1-step deposition showed a strong (220) preferential orientation peak in XRD pattern. This result corresponds to many reports of silicon deposited on foreign substrates, which mentioned that poly-Si thin films have a strong [110] preferential orientation [2.20]. The dominance of this orientation was linked to some properties of <110> grains, which make them highly successful in competitive growth, namely the high growth rate of the {110} planes and a low probability of developing slow growing {111} facets. With reducing the intermittent ratio *D/T*, intensity of (220) preferential orientation decreased and (111) orientation dominated. This explains that (111) plane remains without desorbed during the intermission time because (111) plane is more stable to etching than (220) plane relating to the difference of surface energy [2.21].

2.4. Substrate type dependency

2.4.1. Intermediate layer dependency

One more cushion before depositing on alumina substrates, the influences of intermediate layers, thermal-SiO_2, plasma-SiO_x and plasma-SiN_x layers, were investigated on silicon wafers. As shown in the SEM images of Fig. 2.11, the nucleus density on the plasma-SiN_x layer was extremely larger than that on both thermal-SiO_2 and plasma-SiO_x layers.

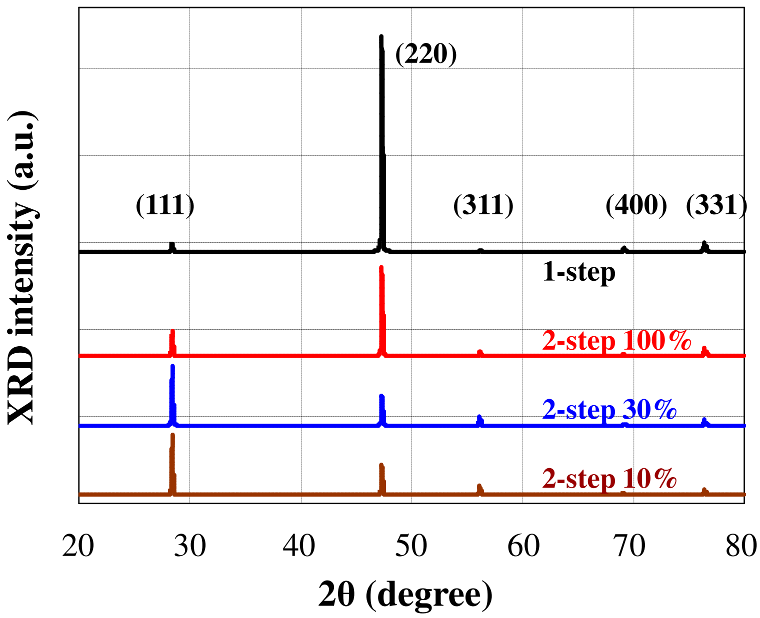

Fig. 2.10: XRD patterns for poly-Si thin films fabricated with different intermittent ratio.

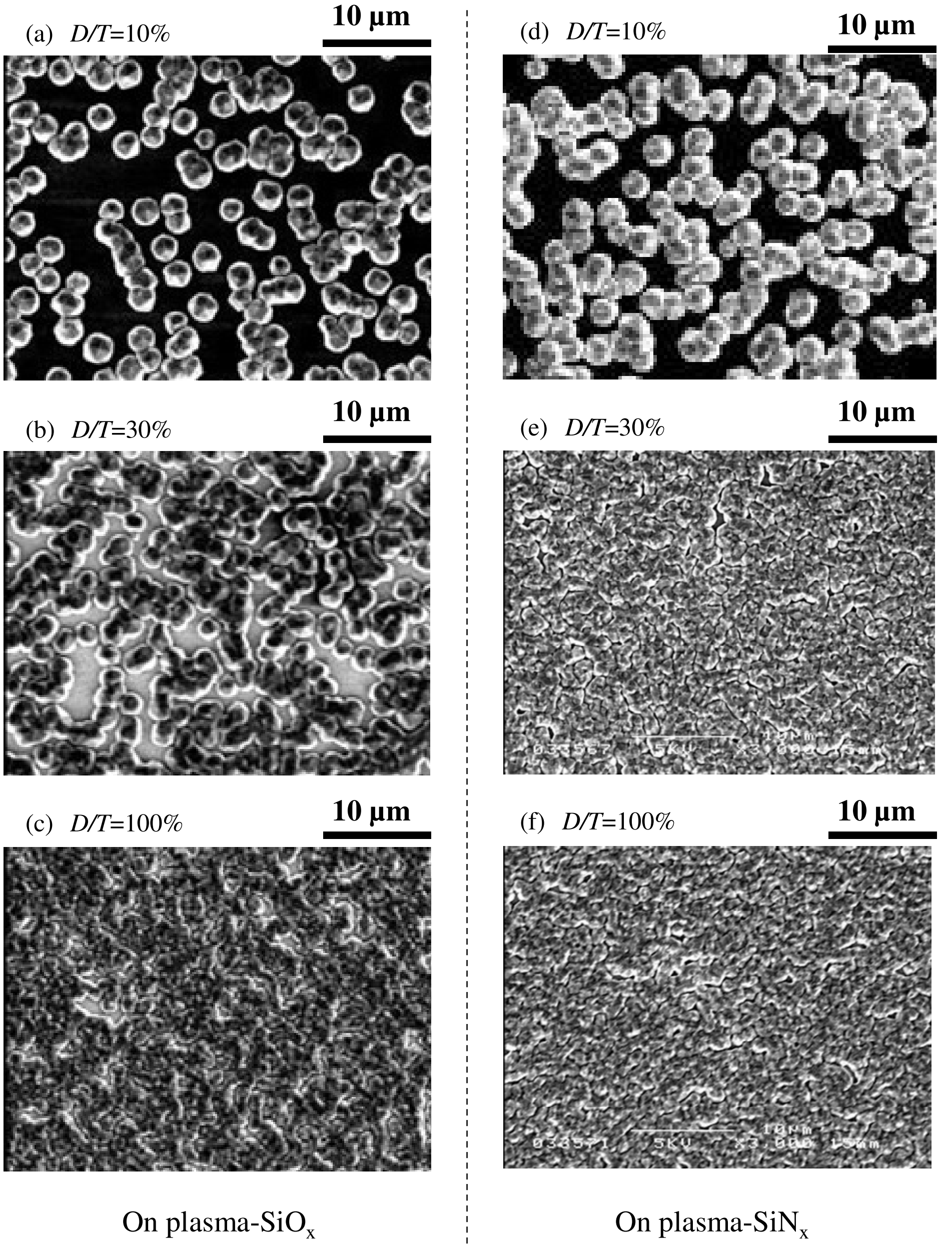

Fig 2.11: SEM images of the silicon nuclei after the first step with different *D/T* on plasma-SiO_x and SiN_x intermediate layers.

On SiO_2 layers, silicon precursors adhered on the surface of the substrate are likely to react with SiO_2 and be evaporated as SiO that has high vapor pressure [2.12], as give by,

$$Si + SiO_2 \rightarrow 2SiO\uparrow . \qquad (2.6)$$

Then, the nucleus density would be relatively small on the SiO_2 layers. Since the reaction expressed by equation above cannot be shown on the SiN_x layer [2.12], the nucleus density on the SiN_x layer became so large. Additionally, the nucleus density on the plasma-SiO_2 layer was markedly larger than that on the thermal-SiO_2. It might be caused by the difference of chemical composition of Si and O between thermal-SiO_2 and plasma-SiO_x. It was reported that the deposited SiO_x are likely to have Si-rich surface rather than stoichiometric composition of thermal grown SiO_2 [2.12], and silicon clusters likely adhere onto substrate to form silicon nuclei in plasma-SiO_x case.

Figure 2.12 shows SEM images of poly-Si thin films after second step of deposition onto different intermediate layers with different intermittent ratio *D/T*. The nucleation density and grain size as a function of *D/T* on each intermediate layer is shown in Fig. 2.13 and 2.14, respectively. From the view point of the range of grain size controlling, thermal-SiO_2 layer is ideal as an intermediate layer, but obviously it can not be applied when the substrate is not silicon. The nucleus density on the SiN_x layer was so large that the layer would be difficult to use as an intermediate layer for the deposition of large grain poly-Si thin films. Hence, plasma-SiO_x is expected as the proper intermediate layer for the deposition of poly-Si thin films with grain size controlling deposited on foreign substrates.

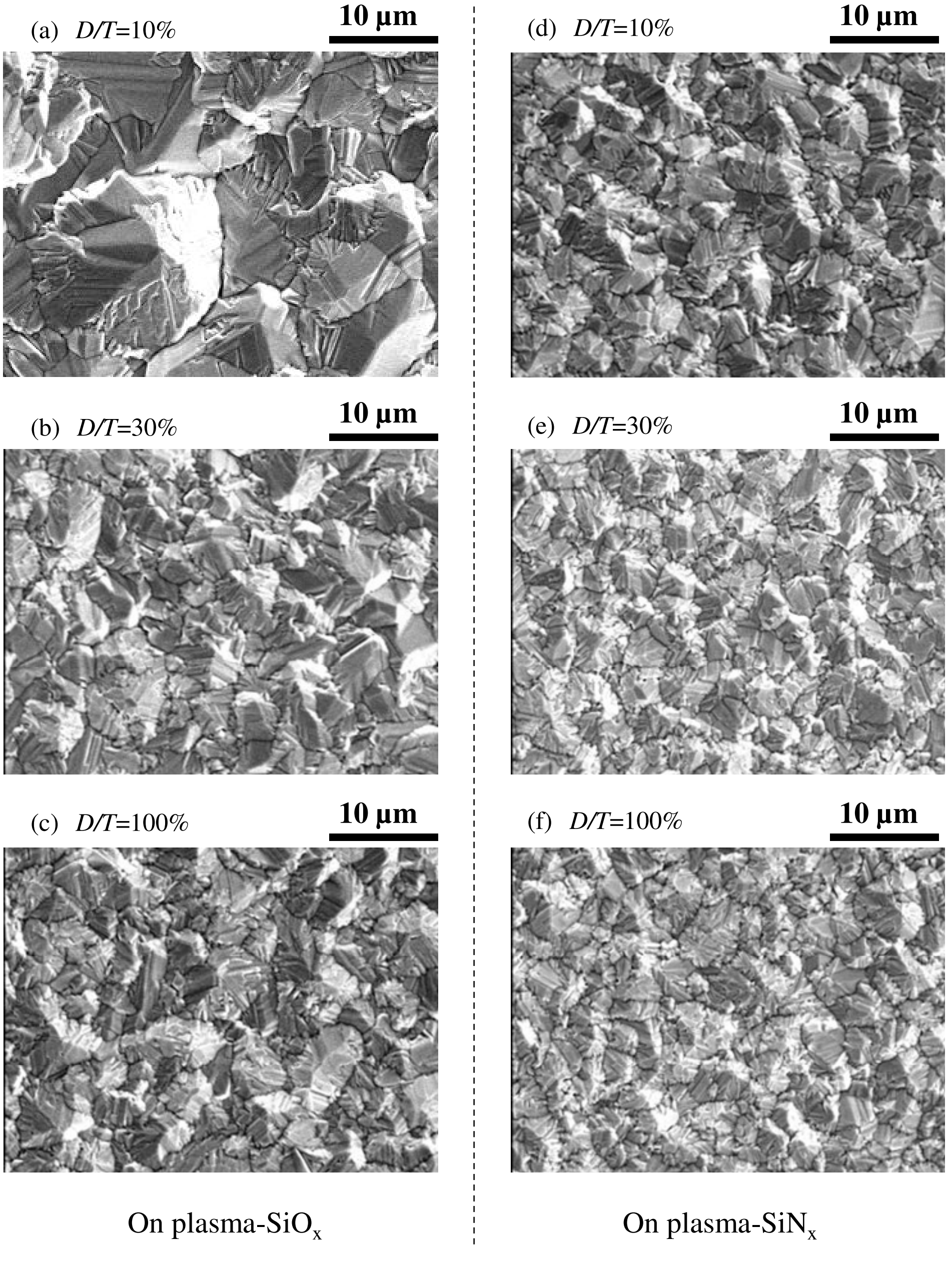

Fig 2.12: SEM images of the poly-Si thin films after the second step with different *D/T* on plasma-SiO_x and SiN_x intermediate layers.

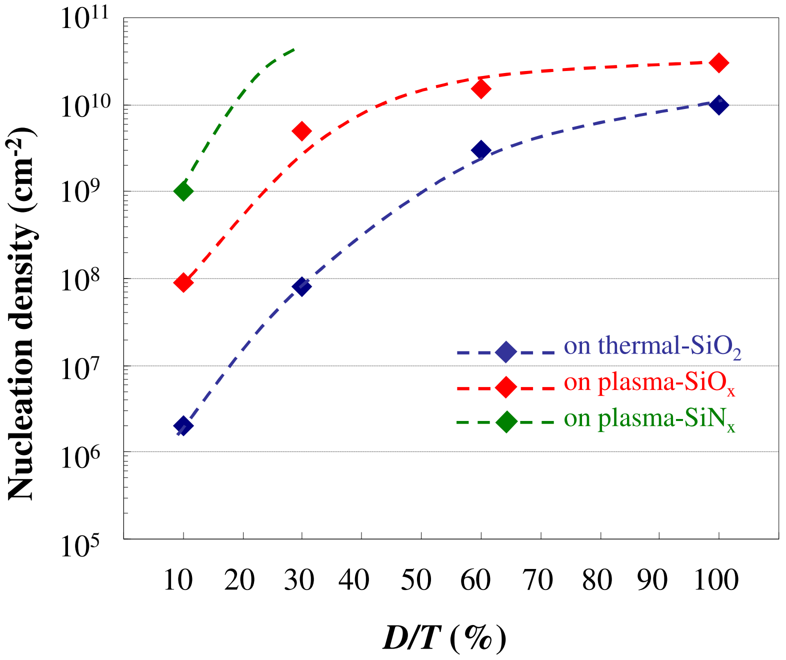

Fig 2.13: Nucleation density on different intermediate layers as a function of *D/T*.

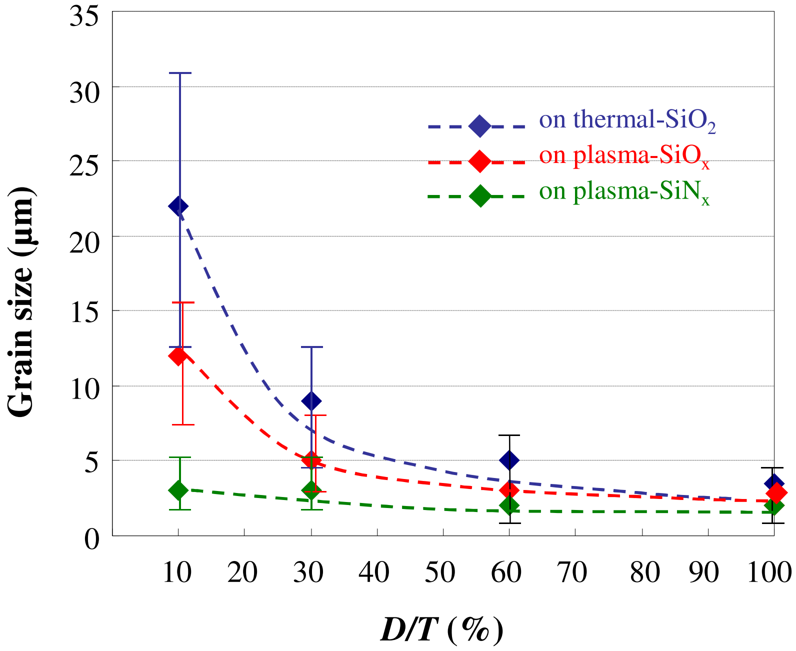

Fig 2.14: Grain size of poly-Si thin films on different intermediate layers as a function of *D/T*.

2.4.2. Deposition on alumina substrate

The poly-Si thin films were deposited by thermal-APCVD on alumina substrates with and without a plasma-SiO_x intermediate layer using the intermittent source gas supply method. The grain size of poly-Si thin film would depend on the intermittent ratio *D/T* and on existence or nonexistence of an intermediate layer. Fig. 2.15 shows SEM images of the surface morphology of poly-Si thin films on alumina substrates with and without a plasma-SiO_x intermediate layer with different intermittent ratio *D/T*. Grain size of poly-Si thin films on alumina with a plasma-SiO_x intermediate layer was successfully controlled by the intermittent gas supply as well as the case of the deposition on silicon substrate as shown in Fig. 2.16, while no significant change of grain size was observed in the case of without a plasma-SiO_x intermediate layer. The tendency of orientation was also almost the same as the case of deposition on silicon substrates if grain size controlling could be applied as shown in Fig. 2.17. These results imply that the nucleation density can be determined by the *D/T* and the existence of SiO_x intermediate layer rather than by the surface roughness of alumina substrate (RMS roughness was around 380 nm). In case of deposition on plasma-SiO_x with *D/T*=10%, the well-grain-enlarged poly-Si thin film, whose grain size was comparable to 10 μm, was obtained. This would lead to the high efficient poly-Si thin film solar cells fabricated on the cheaper foreign substrates.

Finally, Fig. 2.18 shows the result of secondary ion mass spectroscopy (SIMS) which reveals the impurities incorporated into poly-Si thin films. By introducing the plasma-SiO_x intermediate layer, the diffusion of undesirable atoms such as oxygen and iron was suppressed very well by the factor of 1/4. Provably, more improvement can be expected by changing the quality of SiO_x layer such as film density.

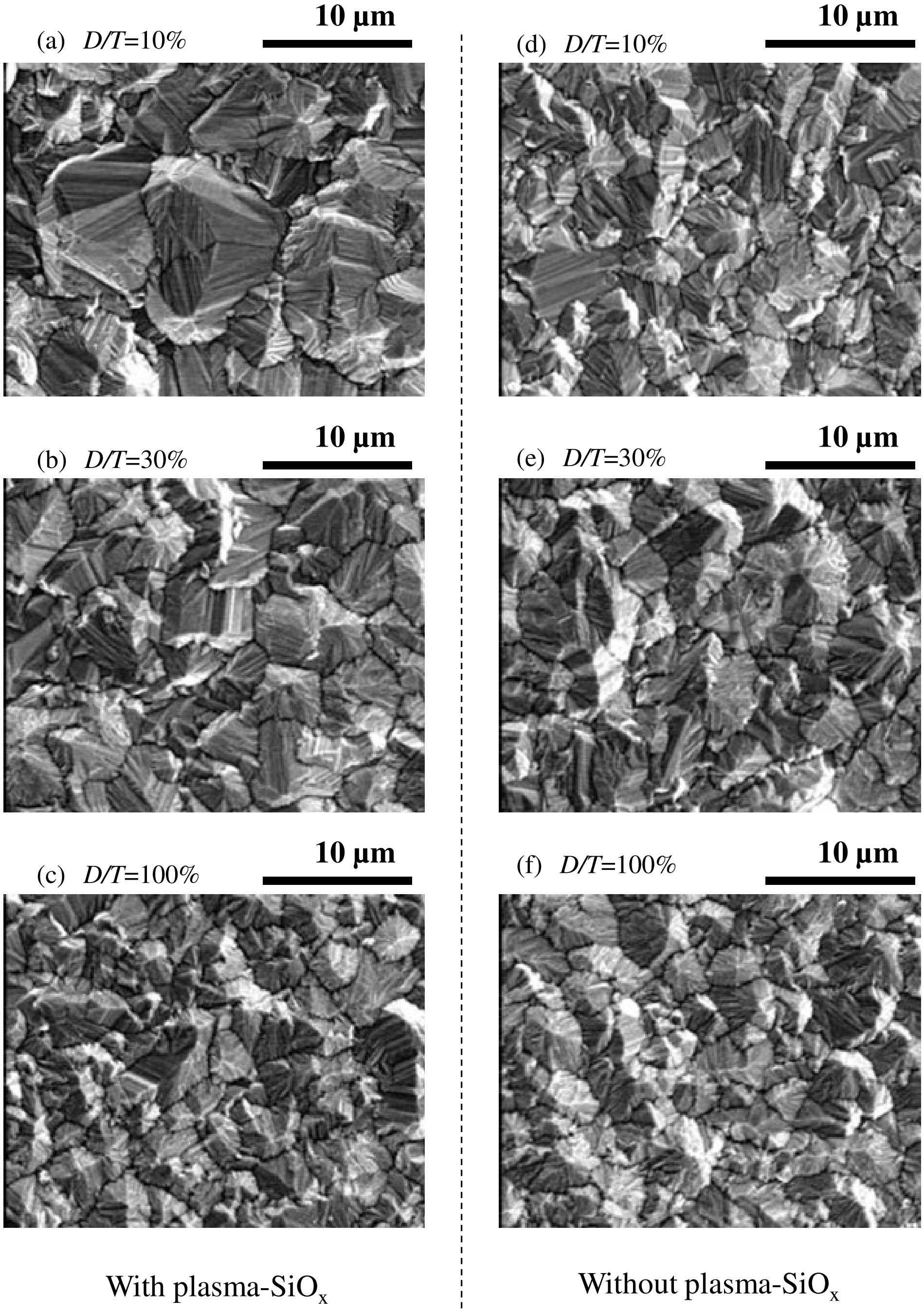

Fig. 2.15: SEM images of poly-Si thin films deposited on alumina substrates with and without a plasma-SiO_x intermediate layer with different *D/T*.

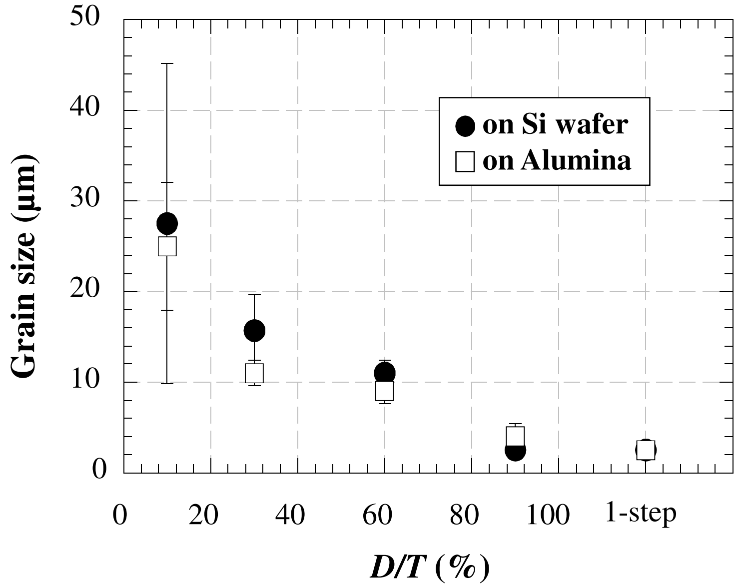

Fig. 2.16: Grain size of poly-Si thin films on alumina substrates with different *D/T*, comparing with the case of deposition on silicon wafer.

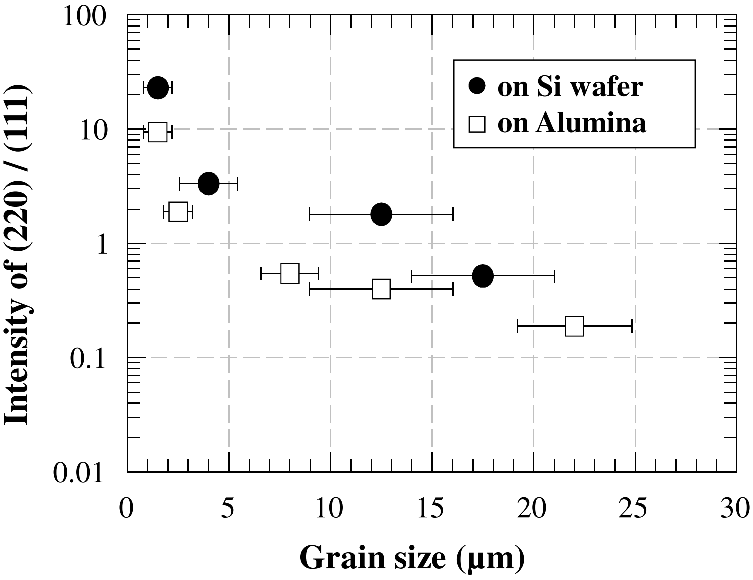

Fig. 2.17: Intensity ratio of (220)/(111) orientations of poly-Si thin films on alumina substrate with different grain size, comparing with the case of deposition on silicon wafer.

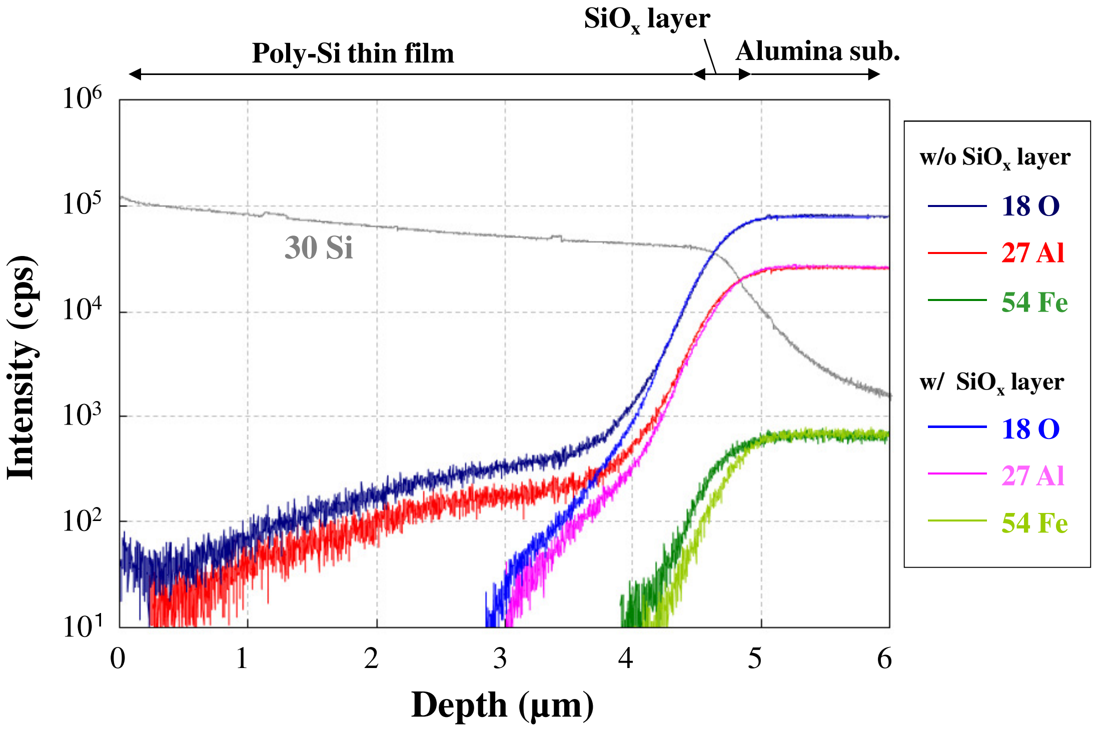

Fig. 2.18: SIMS profiles of diffused atoms (Al, O, Fe) into poly-Si thin films in case of with and without plasma-SiO$_x$ intermediate layer.

2.5. Summary

The grain size of poly-Si thin films could be successfully controlled directly in deposition period by the 2-step deposition method with nucleation controlling using the intermittent source gas supply technique. The nucleus density could be controlled in the range from 10^6 to 10^{10} cm^{-2} on both silicon and alumina substrates with SiO_x intermediate layers. Then, the grain size could be controlled in the range from a few μm to over 10 μm, the suitable value for solar cell designing. It can be concluded that the deposition of large grain poly-Si thin films fabricated by using the intermittent source gas supply method is applicable effectively to the low-cost processing of poly-Si thin film solar cells.

References of Chapter 2

[2.1] A. Takami, S. Arimoto, H. Morikawa, S. Hamamoto, T. Ishihara, H. Kumabe, and T. Murotani: Proc. of 12th European Photovoltaic Solar Energy Conference (1994) p.59.

[2.2] R. Auer, J. Zettner, J. Krinke, G. Polisski, T. Hierl, R. Hezel, M. Schulz, H. P. Strunk, F. Koch, D. Nikl, and H. V. Campe: Proc. of 26th IEEE Photovoltaic Specialists Conference (1997) p.739.

[2.3] C. Hebling, S. W. Glunz, J. O. Schumacher, J. Knobloch: Proc. of 14th European Photovoltaic Solar Energy Conference (1997) p.2318.

[2.4] H. Morikawa, Y. Kuwama, Y. Matsuno, S. Hamamoto, K. Imada, T. Ishihara, K. Kojima, and T. Ogama: Tech. Dig. of 11th Int’l Photovoltaic Solar Energy Conference (1999) p.543.

[2.5] A. G. Aberle: Proc. of 4th World Conference on Photovoltaic Energy Conversion (2006) p.1418.

[2.6] B. Rau, J. Schneider, E. Conrad, S. Gall, and W. Fuhs: Tech. Dig. of 15th Int’l Photovoltaic Science and Engineering Conference (2005) p.778.

[2.7] I. Gordon, L. Carnel, D. Van Gestel, G. Beaucarne, and J. Poortmans: Thin Solid Films, Vol. **516**, Issue 20 (2008) p.6984.

[2.8] A. Slaoui, E. Pihan, and A. Focsa: Solar Energy Materials and Solar Cells, **90** (2006) p.1542.

[2.9] G. Beaucarne, S. Bourdais, A. Slaoui, and J. Poortmans: Thin Solid Films, **403-404** (2002) p.229.

[2.10] T. Yamazaki: Y. Uraoka, and T. Fuyuki, Thin Solid Films, **487** (2005) p.26.

[2.11] Y. Ishikawa: Ph. D. Thesis, Graduate School of Materials Science, Nara Institute of

Science and Technology (2003) p.82.

[2.12] W. A. P. Claassen, and J. Bloem: J. Electrochem. Soc., **127** (1980) p.1836.

[2.13] A. M. Barnett, J. A. Rand, R. B. Hall, J. C. Bisaillon, E. J. Delledonne, B. W. Feyock, D. H. Ford, A. E. Ingram, M. G. Mauk, J. P. Yaskoff, and P. E. Sims: Solar Energy Materials and Solar Cells, **66** (2001) p.45.

[2.14] A. Slaoui, S. Bourdais, G. Beaucarne, J. Poortmans, and S. Reber: Solar Energy Materials and Solar Cells, **71** (2002) p.245.

[2.15] G. Beaucarne, S. Bourdais, A. Slaoui, and J. Poortmans, Solar Energy Materials and Solar Cells, **61**, (2000) p.301.

[2.16] J. Isenberg, S. Reber, J. Aschaber, and W. Warta: Proc. of 19th European photovoltaic Solar Energy Conference (2000) p.1463.

[2.17] S. Bau, S. Janz, T. Kieliba, C. Schetter, S. Reber, and F. Lutz, Proc. of 3rd World Conference on Photovoltaic Energy Conversion (2003) p.1178.

[2.18] Y. Ishikawa, Y. Uraoka, and T. Fuyuki: Jpn. J. Appl. Phys., **42** (2003) p.6759.

[2.19] J. A. Venables: Philos. Meg., **27** (1973) p.697.

[2.20] Y. Ishikawa, Y. Yamamoto, T. Hatayama, Y. Uraoka, and T. Fuyuki: Solar Energy Materials and Solar Cells, **74** (2002) p.255.

[2.21] Fumio Shimura: “Crystal Technology of Silicon Semiconductor”, Maruzen (1993) p.30, in Japanese.

Chapter 3

Crystallographic and electronic properties of grain size-controlled poly-Si thin films

3.1. Introduction

Performance of polycrystalline silicon (poly-Si) thin film devices largely depends on charge carrier transport properties dominated by the grain boundaries (GBs), as discussed in previous Chapters. In order to decrease the influence of GBs, it is necessary to enlarge grains to sizes larger than the film thickness, and particularly in solar cell devices, the grain size of poly-Si has strong effect on solar cell performance. In Chapter 2, to enlarge grain size, an intermittent gas supply was employed for the nucleation controlling in thermal chemical vapor deposition in atmospheric pressure (thermal-APCVD) and the grain size of poly-Si thin films with thickness of around 10 μm deposited both on alumina and silicon substrates with SiO_x intermediate buffer layers was completely controlled in the range from a few μm to over 10 μm by changing the source gas supplying condition.

In this Chapter, enlargement of grain size was evaluated from the point of view of the crystallinity, i.e., the amount of crystalline disorders. In fact, there’s no significant report which investigates about crystallographic properties of poly-Si thin films fabricated on alumina substrates in detail. The possibility to fabricate poly-Si thin films with controlled grain size on different substrates is discussed, comparing with standard substrates of silicon wafers.

3.2. Role of the deposition temperature in APCVD

In Chapter 2, the deposition temperature was fixed at 950 °C in the first step and 1050 °C in the second step to focus on investigating the source gas supply conditions of poly-Si deposition. However, it is considerable that the deposition temperature has influences to the crystalline quality. Thus, the role of deposition temperature to crystalline quality was investigated in this section. Deposition temperature was varied from 1000 °C to 1150°C in 1 step deposition on oxidized silicon. Obtained grain size was around 2-3 μm in all poly-Si thin films and film thickness of each case was almost the same at around 10 μm. The crystallinity of the poly-Si thin films was investigated by Raman scattering spectroscopy with Ar laser at 514 nm excitation, and X-ray diffraction (XRD) measurement with diffractometer Bruker D8 CuKα with energy dispersive SOL-X detector. Raman spectra were numerically fitted by Lorentzian curve to extract the TO-LO (transverse optical mode, longitudinal optical mode) band parameters.

Figure 3.1 shows full width at half maximum (FWHM) of TO-LO phonon band of Raman spectra of poly-Si thin films as a function of deposition temperature. With an increase of the deposition temperature, FWHM of the TO-LO phonon band became narrower, becoming close to that of crystalline silicon (c-Si) due to improvement of crystallinity. At the deposition temperature of 1000 °C, Raman band becomes much wider, which means the resulting silicon lattice contained higher disorder for which higher defect density can be expected. Peak position of TO-LO phonon band was not shifted as a function of deposition temperature.

Lattice constant was also influenced by the deposition temperature. Lattice constant of the poly-Si thin films and the stress measured by XRD as a function of the deposition temperature are shown in Fig. 3.2. At low temperature, lattice constant was smaller than that of the standard c-Si lattice constant (5.4309 Å), and it became closer to the c-Si value with increasing the deposition temperature. Residual stress can be determined from the shift of a diffraction line according to [3.1]:

$$\sigma_1+\sigma_2=\frac{-E}{v}\cdot(d_{\exp}-d_o)/(d_o), \qquad (3.1)$$

Where E is the Young's modulus, v is the Poisson's ratio and d_{exp} is the lattice spacing obtained from the XRD results. The determined stress is the sum of the two main stress tensor components $\sigma_1+\sigma_2$ in the plane of the poly-Si thin films. The stress was calculated using a value of 165.9×10^9 Pa for the Young modulus and the Poisson's ratio of 0.217 [3.1]. Thermal stress due to the difference of the thermal expansion coefficients between the SiO_2 (5.0×10^{-7} K^{-1}) and poly-Si thin films (4.2×10^{-6} K^{-1}) was not considered in this estimation because the no significant effect could be assumed when SiO_2 layer was enough thin. Thus, internal stress of poly-Si thin films was caused by internal factors.

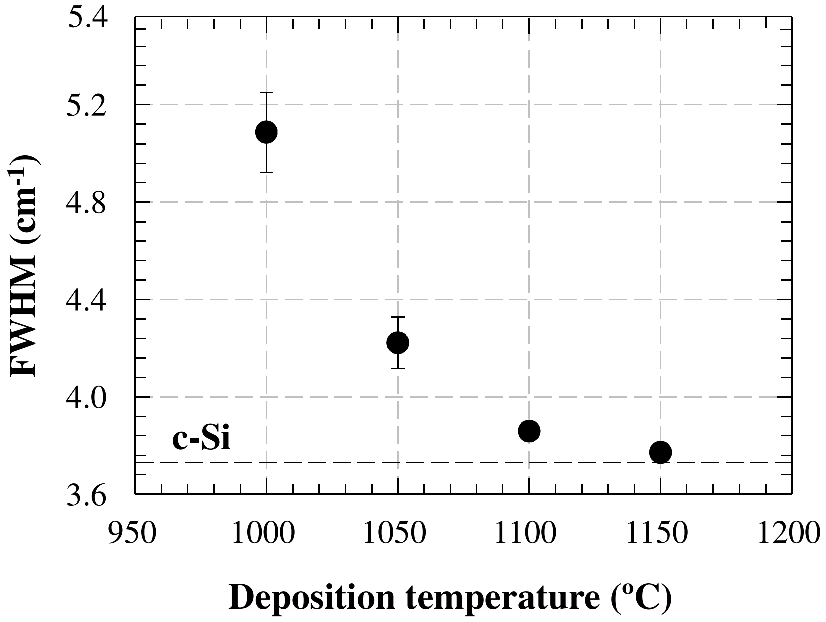

Fig. 3.1: FWHM of TO-LO phonon band of poly-Si thin films as a function of deposition temperature.

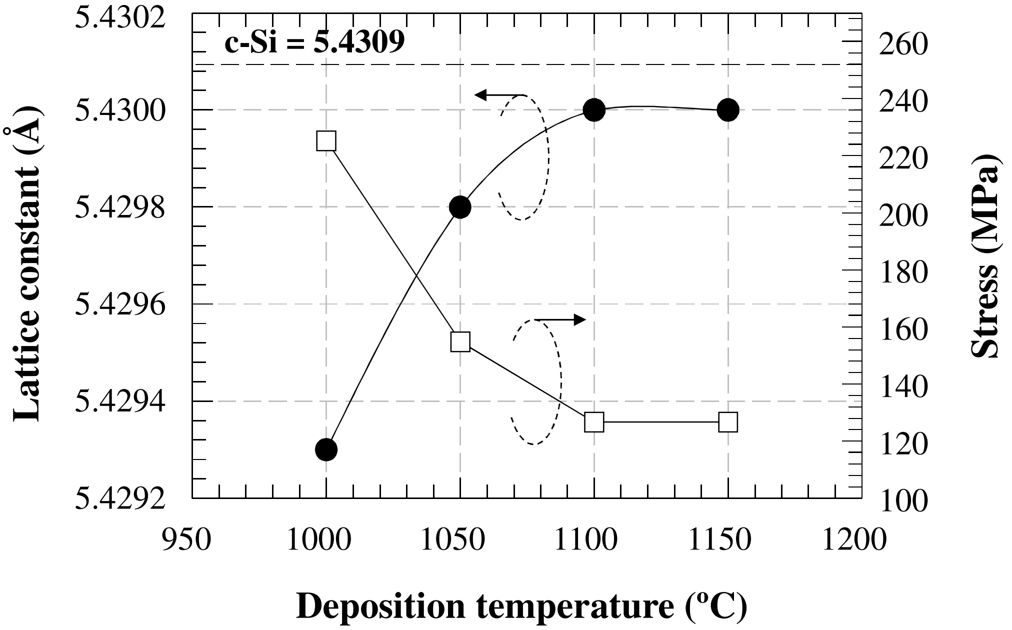

Fig.3.2: Lattice constant of poly-Si thin films and the measured value of lattice stress in poly-Si thin films as a function of deposition temperature.

The internal stress can have several origins such as; 1. incorporation of atoms, residual gases or chemical reaction, 2. differences of the lattice constant of the crystalline substrate and the film during epitaxial growth, 3. variation of grain size, 4. re-crystallization processes, 5. microscopic voids and special arrangement, and 6. phase transformation. Stress in poly-Si thin films would be caused by a combination of several above mentioned factors, e.g., silicon atoms could not find stable sites during crystal growth at 1000 °C, resulting in crystalline disorder, i.e., dangling bonds or dislocation formation. These are origin of broadening of the FWHM of TO-LO phonon Raman band, shrinking of the lattice constant and probably also in weaker (220) preferential orientation

Deposition temperature could strongly influence the character of poly-Si thin films. For later experiments in this thesis, the deposition temperature was fixed at 1100 °C in second-step because the better electronic properties may be expected without stressing the CVD apparatus. And in this case, it was also confirmed that deposition temperature of 1000 °C in the first step would bring the effective grain size controlling as well as mentioned in Chapter 2.

3.3. Crystalline quality of poly-Si thin films with different grain size

A series of measurements by means of Raman scattering measurement, XRD measurement, and photoluminescence (PL) measurement were performed in order to investigate the crystallographic properties of grain size-controlled poly-Si thin films deposited on alumina and silicon substrates with plasma-SiO_x intermediate layers. The PL measurement was done at 7 K with a excitation laser with wavelength of 980 nm and power of 40 mW/cm^2, using Ge detector and lock-in amplifier.

3.3.1. Results of measurements

Figure 3.3 shows lattice constant calculated from XRD data of grain size-controlled poly-Si thin films on alumina and silicon substrates. Lattice constant was influenced by enlargement of grain size of poly-Si thin films on alumina substrates, while it was almost constant regardless of the grain size in the case of deposition on silicon substrates. The lattice constant of poly-Si thin films on alumina substrates showed large shift from c-Si value in the case of small grain size and was dramatically improved with an increase of grain size, becoming closer to that of c-Si.

Figure 3.4 shows the result of Raman scattering measurement; FWHM and peak position of the TO-LO phonon band (at 520.5 cm^{-1} in c-Si) as a function of the grain size. Peak position and FWHM of poly-Si thin film with small grains on alumina substrate were shifted to higher wave number (524.5 cm^{-1}) and became broader (5.5 cm^{-1}). With an increase of grain size, FWHM and peak position of the TO-LO phonon band were drastically shifted to those of c-Si values, just the same tendency as lattice constant from XRD. Even in case of poly-Si thin films on silicon substrates, the slight shift of FWHM and peak position from c-Si and improvement by grain size enlargement were observed.

Figure 3.5 and 3.6 show PL spectra of the poly-Si thin films with different intermittent ratio *D/T* (different grain size) deposited on silicon and alumina substrates, respectively. All PL spectra are normalized by peak intensity of the tail-to-tail part (around 0.95-1.0 eV). The most remarkable feature is the difference of peaks at around 1.08 eV among samples. This peak indicates TO phonon replica of bound excitons (BE) at B atoms [3.2], and

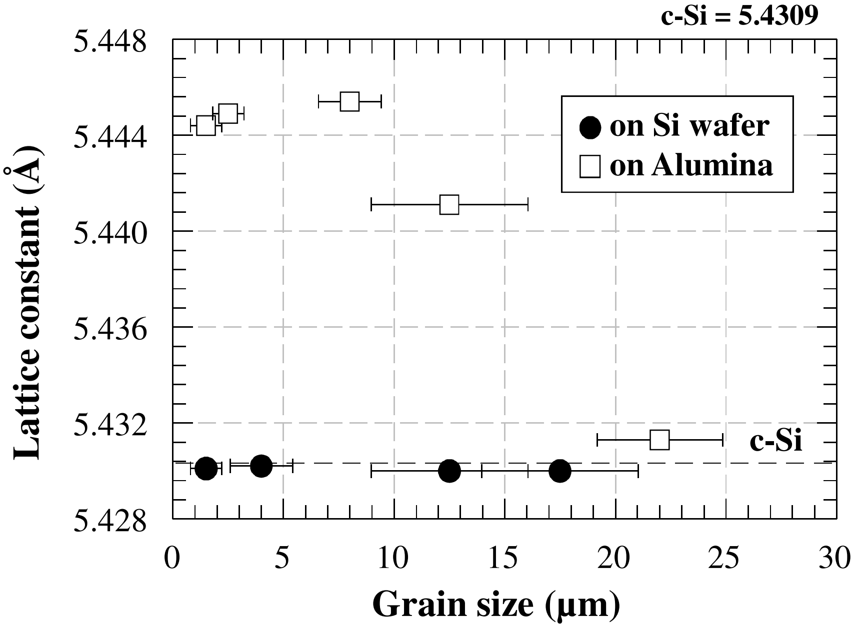

Fig. 3.3: Lattice constant of poly-Si thin films with different grain size on silicon and alumina substrates with SiO_x intermediated layer as a function of grain size.

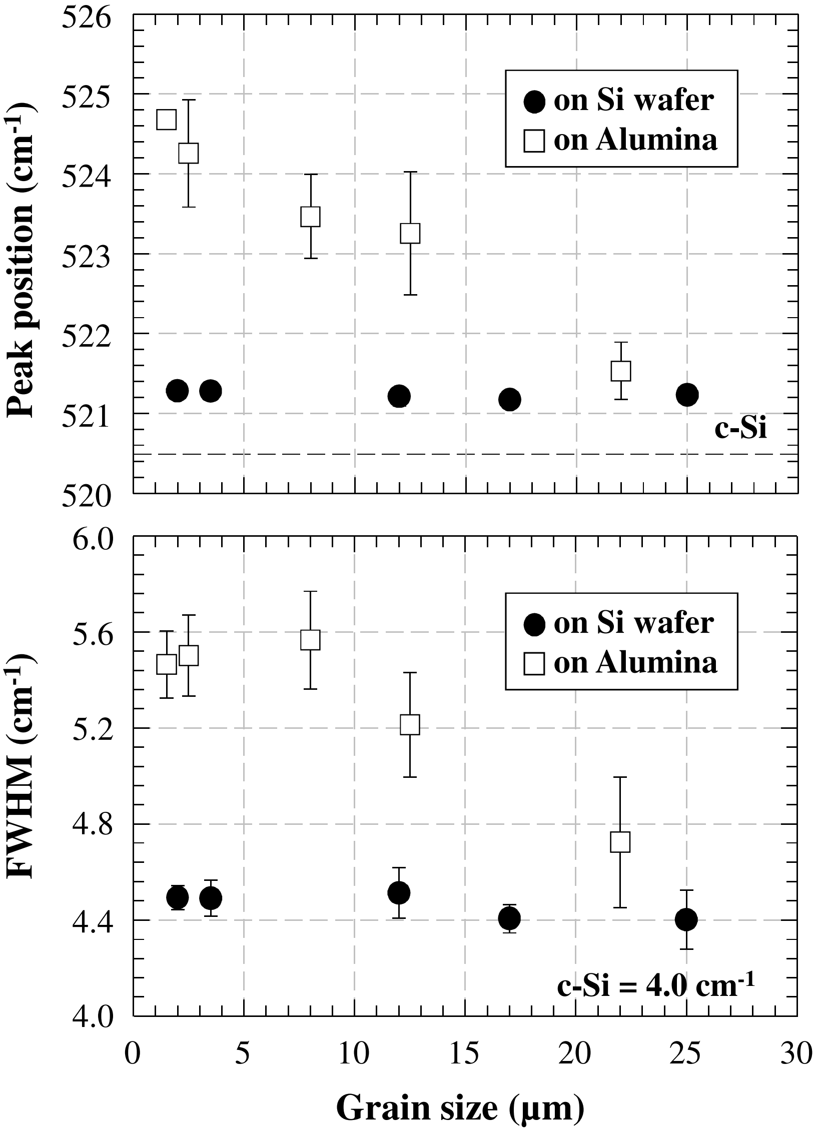

Fig. 3.4: FWHM (upper) and peak position (down) of TO-LO phonon band of poly-Si thin films with different grain size on silicon and alumina substrates with SiO_x intermediated layer as a function of grain size.

in the case of silicon substrates, started to be appear and increased with the grain size enlargement. Moreover, peak position of TO-BE peak became closer to that of c-Si (1.092 eV) with an increase of the grain size. In addition, peak at around 1.12 eV which is related to transverse acoustic (TA) phonon replica of BE [3.2, 3.3] could be observed in poly-Si thin film on silicon with the largest grain size. On the other hand, poly-Si thin films on alumina substrates showed no TA-BE peaks and very small TO-BE peak only in the case of biggest grain size. This tendency of peak appearance and sharpening with grain size enlargement was also seen in so called D1 peak (around 0.80 eV) which is related to dislocations. As one more interesting thing in the case of alumina substrates, large peak shift of tail-to-tail peak to higher energy (0.926 to 0.986 eV) was observed with an increase of grain size.

3.3.2. Discussion

By using the intermittent source gas supply method, grain size of poly-Si thin films was controlled in the range from a few μm to over 10 μm in the case of deposition temperature at 1000 °C in the first step and 1100 °C in the second step. The result of XRD and Raman scattering measurement showed the same tendency; poly-Si thin film with small grains on alumina substrate gave very large shift from c-Si value and became closer to that of c-Si with grain size enlargement. The shifts of these values from c-Si indicate the large internal compressive stress and large amount of disorders in poly-Si thin films with small grains on alumina. The internal stress would be caused by the difference of thermal expansion coefficient. The theoretical thermal stress (σ_{th}) due to the different thermal expansion coefficients is given by,

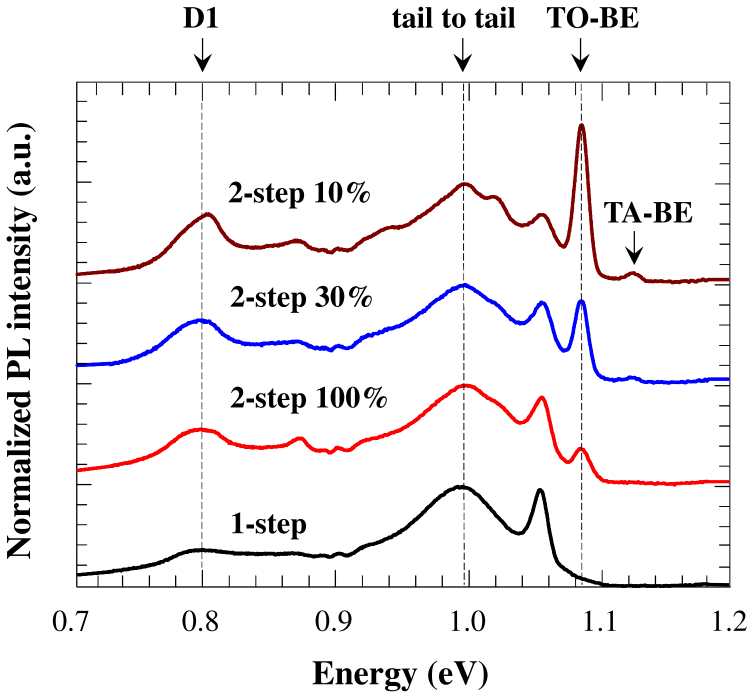

Fig. 3.5: PL spectra of poly-Si thin films on silicon substrates fabricated with different intermittent source gas supply conditions.

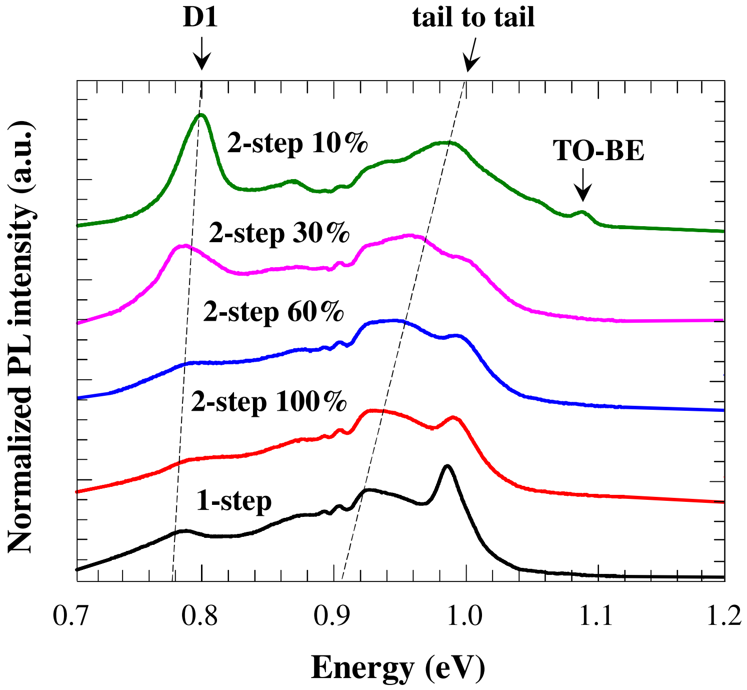

Fig. 3.6: PL spectra of poly-Si thin films on alumina substrates fabricated with different intermittent source gas supply conditions.

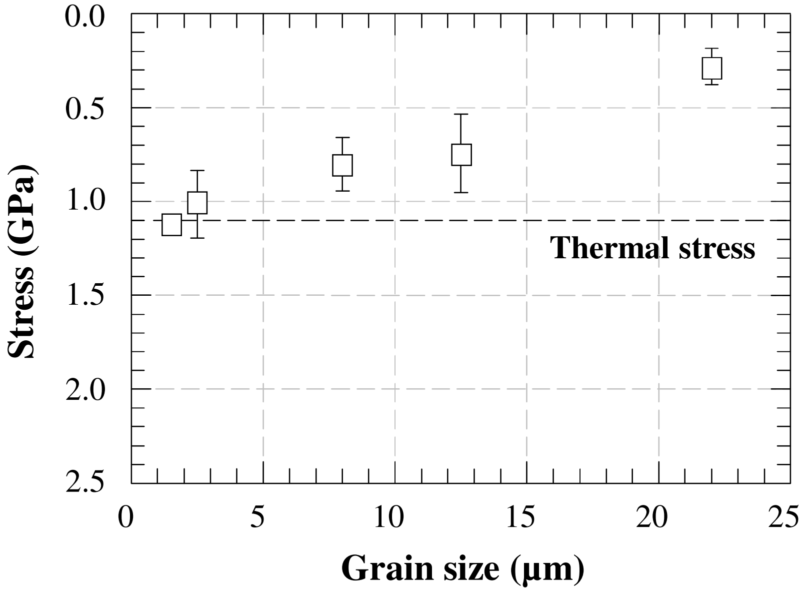

Fig. 3.7: Calculated inner stress from Raman peak shift of poly-Si thin films on alumina substrate with SiO_x intermediate layer as a function of grain size.

$$\sigma_{th} = E \cdot (\alpha_1 - \alpha_2) \cdot (T_{low} - T_{high}) / (1 - \nu), \qquad (3.2)$$

where E is the Young's modulus, α_1 and α_2 are the thermal expansion coefficients of different materials, T_{low} and T_{high} are low and high temperature in process and v is the Poisson's ratio [3.4]. The calculated thermal stress was around 1.1 GPa during temperature cycles from 1100 °C to room temperature. And the internal stress (σ_{in}) of poly-Si thin films could be calculated from the shift (Δ) of Raman TO-LO peak using the equation [3.5, 3.6],

$$\sigma_{in} = -250 \times \Delta, \qquad (3.3)$$

as shown in Fig. 3.7. The internal stress of poly-Si thin films with small grains on alumina substrate was almost the same as the thermal stress. Grain size enlargement can be said to be effective not only to grain boundary reduction but to internal stress relaxation, resulting in crystallinity improvement within the grains. This is probably due to the reduction of interaction between grains such as collision.

PL result reflects the crystallinity related to photo-generated carrier's activity, therefore, it is very important for photovoltaic application. The appearance, sharpening and position shift of TO-BE, TA-BE, D1 and tail-to-tail peaks can be used to judge the crystalline quality of poly-Si thin films, because they will be shifted to lower energy and broadened by residual strain which results from dislocations and point defects [3.2, 3.7-3.11]. In the case of poly-Si thin films on silicon substrates, TO-BE peak clearly increased with grain size enlargement as shown in Fig. 3.5, confirming the crystallinity improvement in agreement with Raman and XRD results. Large shift to lower energy of tail-to-tail peak and difficulty of appearance of other peaks in poly-Si thin films with small grains on alumina substrates explained poor crystallinity due to large stress discussed above, however, grain size enlargement could be the help or must be applied to improve the crystallinity.

3.4. Electronic properties of poly-Si thin films with different grain size

3.4.1. Macroscopic analysis (Hall effect measurement)

Electronic properties as a function of grain size are discussed in this section. Figure 3.8 shows carrier concentration and Hall mobility as a function of grain size on silicon and alumina substrate, measured by using Van der Paw method. Carrier concentration of the samples was 1×10^{17} cm^{-3}. It was reported that the relation between acceptor concentration and the hole carrier concentration is almost 100% [3.12]. But poly-Si thin films with smallest grain size on alumina substrate have lower carrier concentration down to 4×10^{16} cm^{-3} in spite of the coinstantaneous deposition on silicon and alumina substrates. Poly-Si thin films with small grain size on alumina substrate have largest stress and crystalline disorder as discussed above. Stress might influence relation between the acceptor concentration and the hole concentration, making acceptors inactive. The correlation between the stress and carrier doping efficiency is still unknown and it should be further investigated. Hall mobility was improved with an increase of the grain size in poly-Si thin films on both substrates due to the decrease of the number of grain boundaries. Hall mobility of poly-Si thin films on silicon was larger than that of poly-Si thin films on alumina substrate in spite of almost the same grain size, due to the fact that the poly-Si thin films on alumina substrate had deep tail states and deteriorated grain quality.

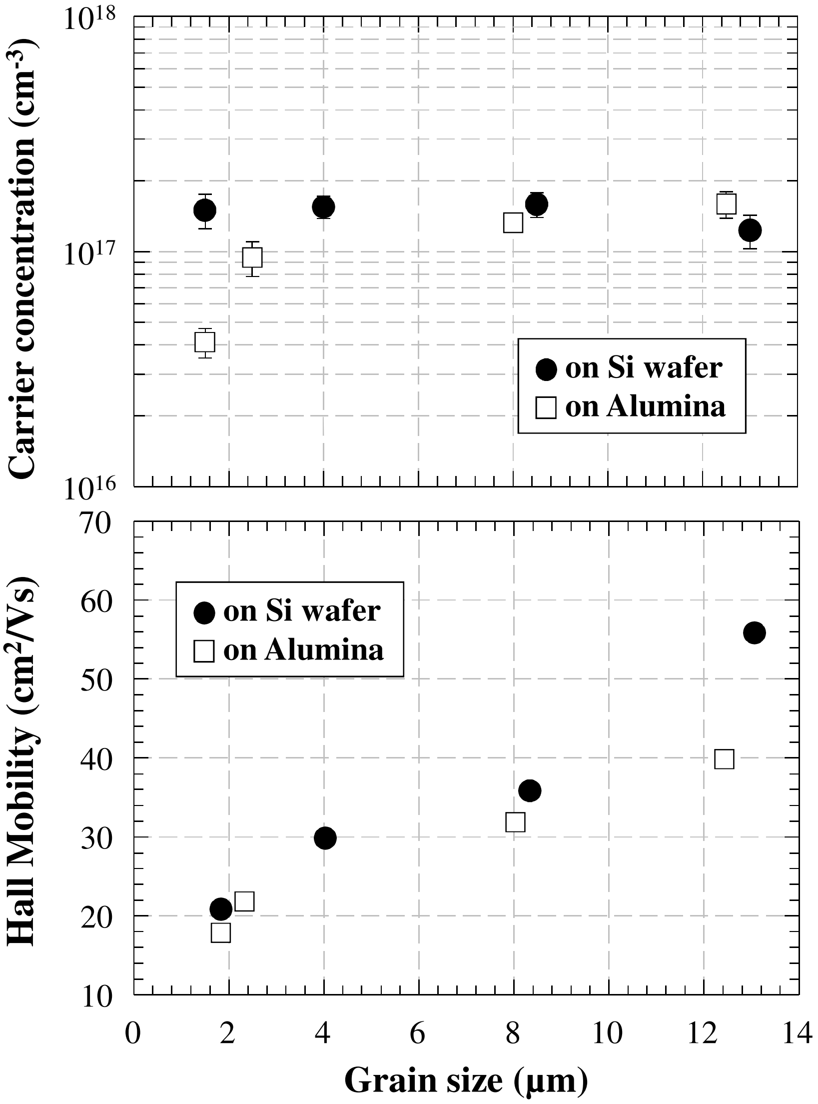

Fig. 3.8: Carrier concentration (upper) and Hall mobility (down) of poly-Si thin films with different grain size on silicon and alumina substrates with SiO_x intermediate layer as a function of grain size.

The mobility of majority carriers in poly-Si thin film would be largely dominated by the carrier scattering at the potential barriers due to defects especially at grain boundaries [3.13]. For the photovoltaic application, the relation ship between crystallographic defects and minority carrier transport property should be investigated in further study.

3.4.2. Microscopic analysis (KFM measurement)

In order to make the microscopic characterization at the local point of GBs, Kelvin Force Microscopy (KFM) was performed. For the KFM measurement, poly-Si thin film samples with a special structure with base contact were fabricated as follows and as shown in Fig. 3. 9. In this structure, the plasma-SiO_x intermediate buffer layer formed on a low resistivity (0.004 Ω·cm) silicon wafer was used as a substrate. Before the deposition of a poly-Si thin film, 80-μm-diameter holes were opened at an interval of 450 μm in the SiO_x film by a photolithography process. The holes act as the base contact. The p-type poly-Si thin films were deposited by 1-step method at 1100 °C. In this structure, grain size enlarging by an intermittent source gas supply method could not work effectively because the epitaxial growth of silicon at contact holes dominated rather than silicon nuclei formation in first-step. Finally, an Al electrode was formed to the rear side of silicon substrate.

These fabricated poly-Si thin films were evaluated by KFM measurement at room temperature and ambient conditions using Veeco Dimension 3100. Pt/Ir coated cantilever with resonance frequency of 75 kHz was used. Figure 3.10 shows the two images from KFM measurement; local topography and KFM potential image. Potential image showed the contrast at GBs as relative higher surface potential. Figure 3.11 shows line profiles of height and surface potential at a distinctive GB as indicated points between A and B in Fig. 3.9. At GB, the potential clearly increased by 40-60 mV higher than inner grain.

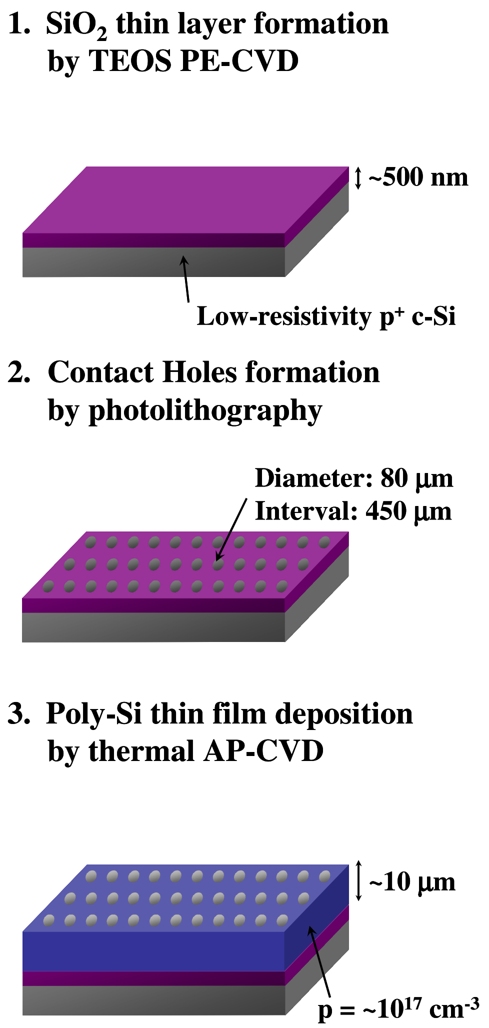

Fig. 3.9: Schematic illustration of process sequence of poly-Si thin film sample fabrication for KFM measurement.

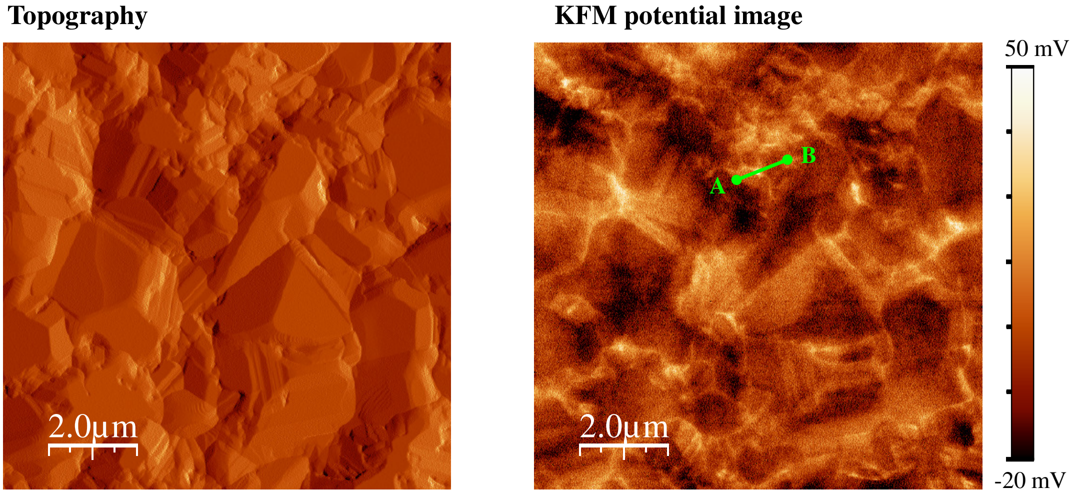

Topography

KFM potential image

Fig. 3.10: Topography (left) and KFM potential image (right) of poly-Si thin film.

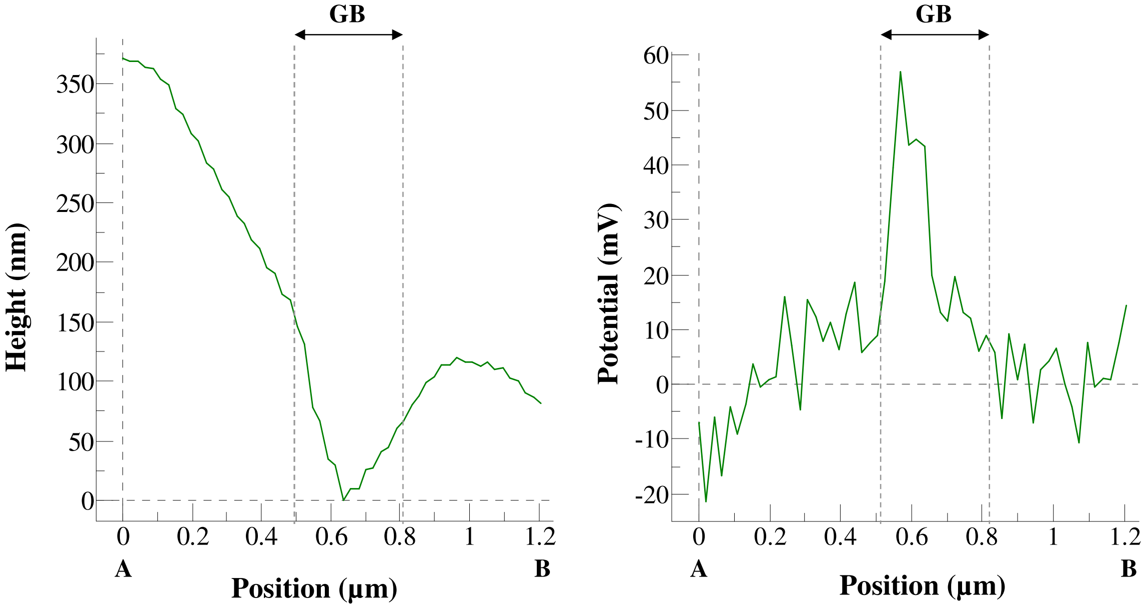

Fig. 3.11: Line profiles of height (left) and surface potential (right) at a distinctive GB as indicated points between A and B in Fig. 3.10 in poly-Si thin film.

In the measurement in this study, the absolute value is not calibrated, however, it is possible to compare potential values at several GBs in one KFM image. Figure 3.12 shows the band diagram of p-type poly-Si within the grain and at a GB in the case of KFM measurement using Pt coated cantilever. Work function of Pt is approximately 5.4 eV, while for p-type silicon it is around 4.3 eV. The larger surface potential obtained from KFM measurement corresponds to larger contact potential difference, i.e., the band bending to valence band.

This potential bending to valence band would be caused by the interface states at GBs. The interface state at GBs is fully occupied by majority carriers when the Fermi level at GBs lies closer to a band edge than the interface state level [3.13]. Then, in p-type poly-Si thin films, the GBs are generally positive charged. The positively charged GBs will induce the band bending as shown in Fig. 3. 12. The barrier height of potential bending (ϕ_b) is described as [3.14],

$$\phi_b = qN_T^{\ 2} / 8\varepsilon N_a \,, \qquad (3.4)$$

where q is elementary electric charge, ε the dielectric permittivity, N_a the acceptor concentration and N_t the interface state density at GBs. The interface states at GBs act also as recombination center for minority carriers as well as induce the potential barrier for majority carriers. Then, the inter face recombination velocity at GBs (S_{GB}) can be estimated from N_T, as follows,

$$S_{GB} = \sigma_n v_{th} N_T \,, \qquad (3.5)$$

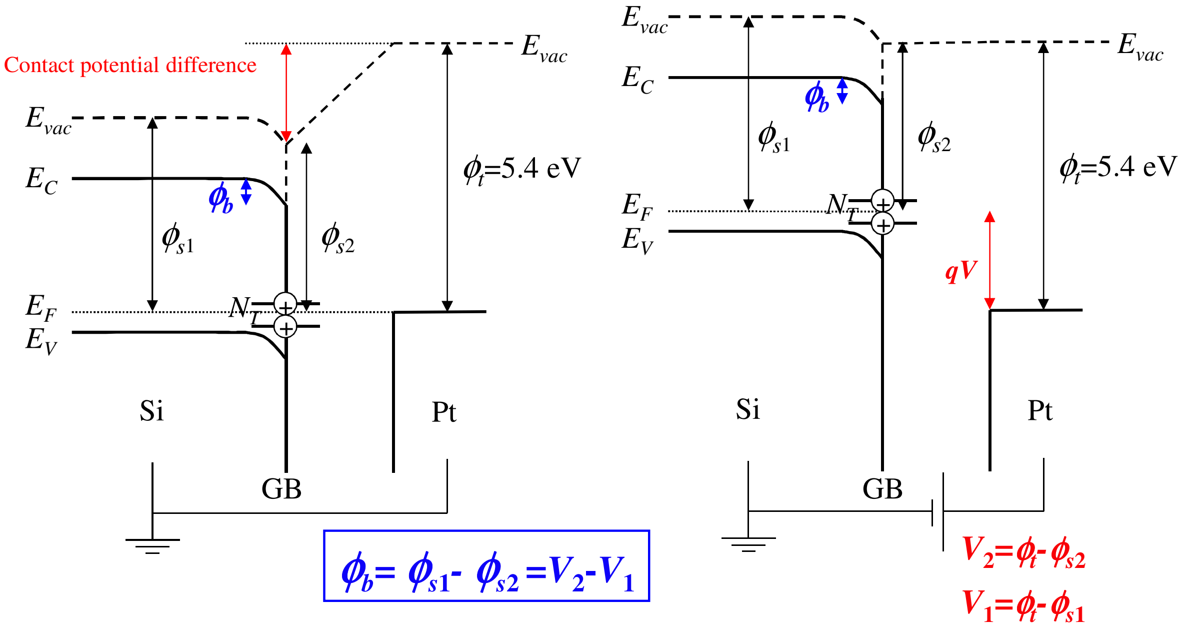

Fig. 3.12: Band diagram of p-type poly-Si within the grain and at a GB in the case of KFM measurement using Pt cantilever.

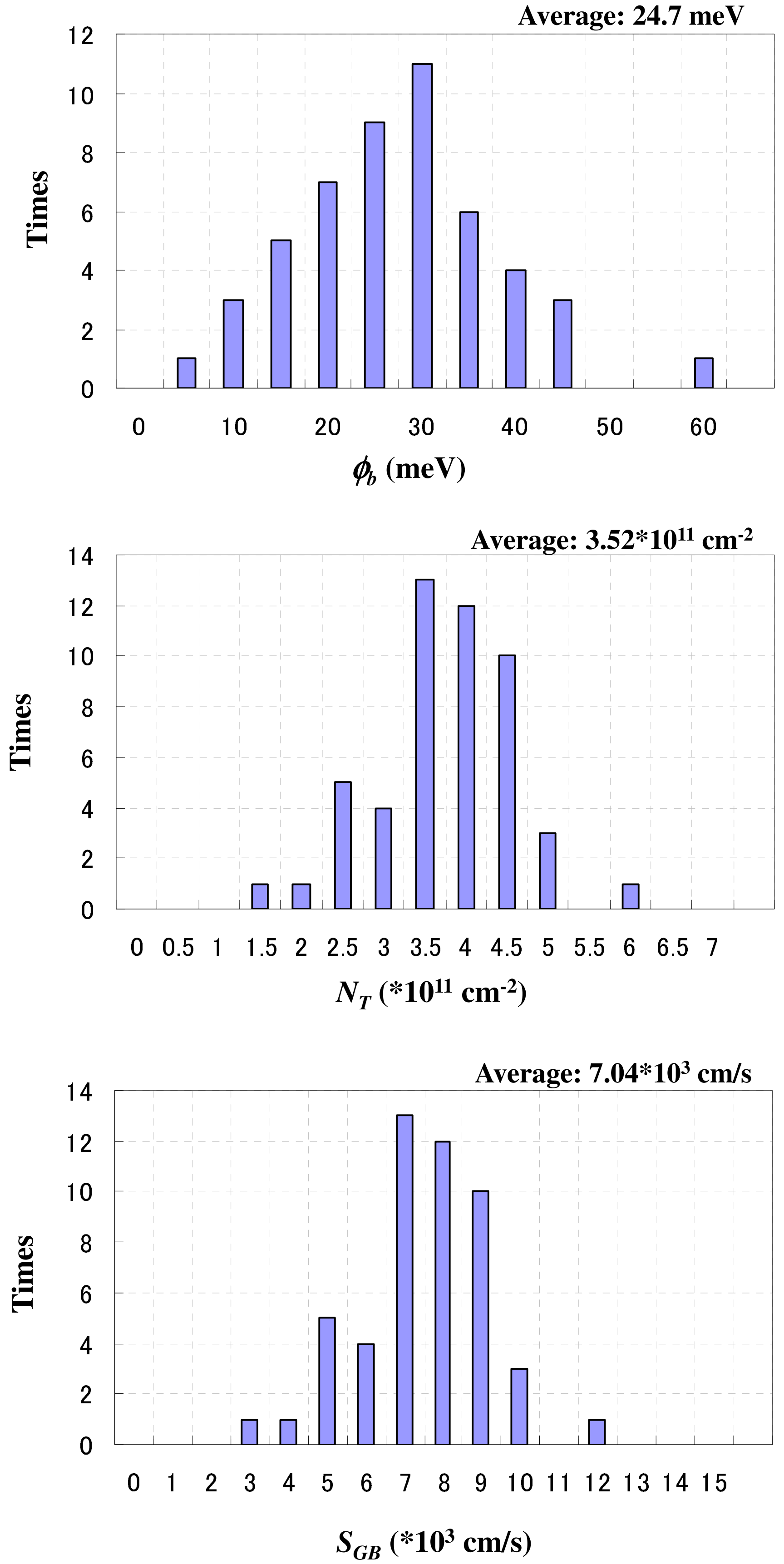

Fig. 3.13: Histograms of ϕ_b, N_T, and S_{GB} of arbitrary 50 GBs in poy-Si thin film.

where σ_n is the capture cross section and v_{th} is the thermal velocity.

Using equation (3.4) and (3.5), N_T and S_{GB} are calculated with the assuming that N_a, σ_n, and v_{th} are 1.0×10^{17} cm^{-3}, 1.0×10^{15} cm^2, and 2.0×10^7 cm/s, respectively [3.15, 3.16]. The results of arbitrary 50 GBs are arranged in histograms in Fig. 3.13. The average N_T and S_{GB} are 3.52×10^{11} cm^{-2}, and 7.04×10^3 cm/s, respectively, in this case of poly-Si thin film with small grains on silicon substrate and the value $L_g/2S_{GB}$ equals to 1.42×10^{-9} s, much less than the target of 5.0×10^{-8} s. Unfortunately the measurement of large grain poly-Si thin film has not been performed yet, but the simple assumption of just the difference of grain size (of course it is not true) brings one order higher value of $L_g/2S_{GB}$ in case of poly-Si thin film with enlarged grain. Additionally, the quality of intra grain would be improved as already shown in this Chapter. However it is expected that poly-Si thin films on alumina substrate has much less quality, so more and more improvement is necessary.

3.5. Summary

Grain size of poly-Si thin films was successfully enlarged by intermittent gas supply method up to 20 μm. With an increase of the grain size, crystalline quality of poly-Si thin films was improved, as shown by Raman and PL results. Hall mobility was improved up to 60 cm^2/Vs in the case of the biggest grain size due to the decrease of the number of the grain boundaries. Grain size of poly-Si thin films on alumina substrates with SiO_x buffer layer could be controlled by the same intermittent gas supply method. Poly-Si thin films on alumina substrate have larger compressive stress caused by difference of the thermal expansion coefficients between alumina substrate and silicon thin films. With an increase of grain size on alumina substrate, crystalline disorder and stress were improved. The improvement was dramatically larger than in the case of poly-Si thin films on silicon substrates.

Stress and crystalline disorder of poly-Si thin films on alumina substrates are larger than those on silicon in spite of almost the same grain size. According to Raman and XRD results, stress and crystalline disorder could be mainly caused at GBs. As a result, Hall mobility of poly-Si thin films on alumina substrate is deteriorated. GBs condition influenced by stress and crystalline disorder suppressed improvement of electronic properties. It can be concluded that enlargement of grain size is essential in order to achieve good electronic properties.

KFM measurement for microscopic characterization revealed that the value $L_g/2S_{GB}$ equals to 1.42×10^{-10} s, much less than the target of 5.0×10^{-8} s, in this case of poly-Si thin film with small grains on silicon substrates. The simple assumption of just the difference of grain size brings one order higher value of $L_g/2S_{GB}$ in case of the poly-Si thin film with enlarged grain. Additionally, the quality of intra grain would be improved. However, poly-Si thin films on alumina substrate were expected to be much less quality, therefore, more improvement of crystallinity is necessary.

References of Chapter 3

[3.1] A. J. M. M. van Zutphen, P. Šutta, F. D. Tichelaar, A. von Keitz, M. Zeman, and J. W. Metselaar: Journal of Crystal Growth, **223** (2001), p.332.

[3.2] A. V. Mudryi, A. L. Patuk, I. A. Shakin, A. G. Ulyashin, R. Job, W. R. Farhrner, A. Fedotov, A. Mazanik, and N. Drozodov: Solar Energy Materials and Solar Cells, **72** (2002) p.503.

[3.3] H. Nakayama, Y. Nishino, and Y. Hamakawa: Appl. Phys. Lett., **38** (1981) p.63.

[3.4] S. A. Campbell: "The science of Microelectronic Fabrication", Oxford University Press (1996).

[3.5] N. H. Nickel, P. Lengsfeld, and I. Sieber: Pys. Rev., **B61** (2000) p.15558.

[3.6] E. Annastassakis: Proc. of the 4th Int'l School ISPPM, edited by K. Kassavod (1985) p.128.

[3.7] R. Sauer, J. Weber, J. Stolz, E. R. Weber, K. H. Kusters, and H. Alexander: Appl. Phys. A, **36** (1985) p.1.

[3.8] V. D. Kulakowskii: Sov. Phys. Solid State, **20** (1978) p. 802.

[3.9] M. Suezawa, K. Sumino, and Y. Nishina: Jpn. J. Appl. Phys., **21** (1982) L518.

[3.10] N. A. Drozdov, A. A. Patrin, and V. D. Tkachev: JETP lett., **23** (1976) 597.

[3.11] N. A. Drozdov, A. A. Patrin, and V. D. Tkachev: Phys. Status solidi (b), **83** (1977) p.137.

[3.12] T. Yamazaki: Ph. D. Thesis, Graduate School of Materials Science, Nara Institute of Science and Technology (2005) p.55.

[3.13] S. M. Sze: "Physics of semiconductor device, 2nd edition", Wiley (1981) p.254.

[3.14] J. Y. W. Seto: J. Appl. Phys., **46** (1975) p.5247.

[3.15] G. Beaucarne, J. Poortmans, M. Caymax, J. Nijs, and R. Mertens: Solid State Phenomena, **67-68** (1999) p.577.

[3.16] S. A. Edmiston, G. Heiser, A. B. Sproul, and M. A. Green: J. Appl. Phys., **80** (1996) p.6783.

Chapter 4

Defect passivation by high-pressure water vapor heat treatment

4.1. Introduction

Passivation of defects at grain boundaries (GBs) and/or in grains is essential for obtaining high polycrystalline silicon (poly-Si) thin films solar cell performance. Plasma hydrogenation or hydrogen diffusion from SiN:H layer are widely employed in PV industry [4.1-4.8]. Although these passivation methods are well-established, they have disadvantages. Both methods need expensive high vacuum systems, and then they present a barrier for reducing PV cost. Moreover, prolonged hydrogenation also creates new defects on the surface. Development of new simple passivation methods is strongly required. In this Chapter, the high-pressure water vapor heat treatment (HWT) as a new and simple method for passivation of poly-Si-thin films as well as bulk-silicon solar cells was proposed and developed. This method has been developed originally for the improvement of electrical performances of polycrystalline silicon thin film transistors [4.9-4.13], but its advantages, such as ease of performance and the lack of a need for large-scale apparatus or dangerous chemical gases, are suitable for low-cost solar cell production.

In this Chapter, the effect of HWT at approximately 300 °C is investigated on poly-Si thin films deposited on alumina or silicon substrates with SiO_x intermediate layers by using thermal chemical vapor deposition in atmospheric pressure (thermal-APCVD) with an intermittent source gas supplying method, as well as the mono- and multicrystalline silicon solar cells with SiO_x or SiN_x passivation layers formed by PECVD at 300 °C. Firstly, the enhancement of passivation layers of bulk silicon solar cells by HWT is confirmed and discussed. Secondly it is applied to poly-Si thin films, discussing its effect to crystallinity and electronic properties in main.

4.2. HWT experimental method

The detail explanation and conditions of HWT are mentioned as followings [4.9-4.13]. Figure 4.1 shows the image of the chamber for HWT and its schematic experimental setup. Samples were placed in a pressure-proof stainless-steel chamber with 1 cc of pure-water ice. In this study, no vacuuming or gas replacement of the chamber was carried out. By heating the chamber, the water evaporated and the pressure inside the chamber increased. The treatment temperature was varied in the range from 150 to 350 °C, and the pressure inside the chamber changed from 0.62 to 1.65 MPa, depending on the treatment temperature. The treatment time was fixed at 60 min.

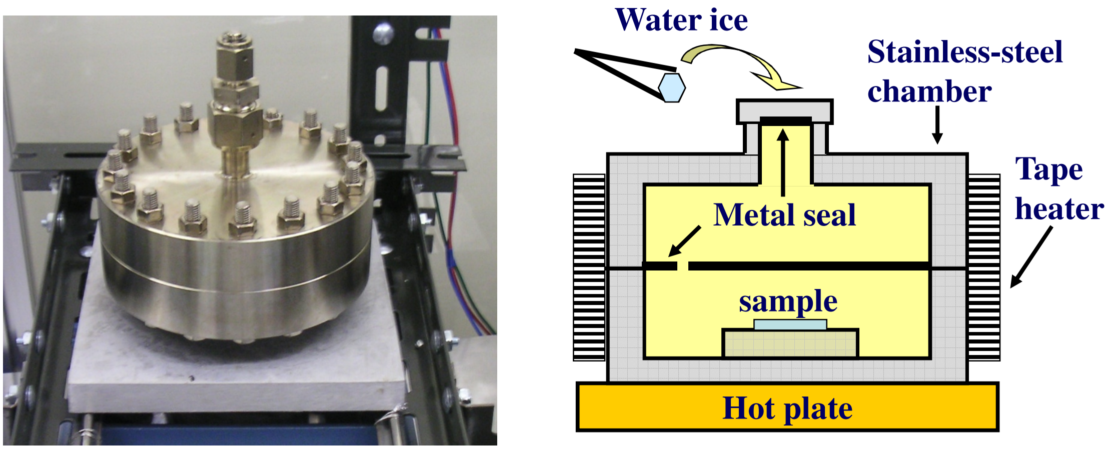

Fig. 4.1: Photograph (left) and schematic image (left) of HWT instrument.

4.3. Applying to bulk crystalline silicon solar cells

Surface and defect passivation technologies are very important for silicon solar cells. For the passivation of p-type silicon wafers, excellent passivation with a very low surface recombination velocity (SRV) has been realized by the combination of a SiO_2 layer grown at high temperature (over 900 °C) with an evaporated and annealed aluminum film (so-called "alneal") [4.14]. However, this passivation method is difficult to integrate into industrial cell fabrication because thermal processes above 900 °C typically lead to a significant degradation of the bulk lifetime [4.15]. Therefore, low-temperature passivation methods are highly desirable. Recently, plasma-enhanced chemical vapor deposition (PECVD) at approximately 400 °C has become the dominant method for low-temperature passivation, and SRVs lower than 100 cm/s have been reported with silicon oxide (SiO_x), hydrogenated silicon nitride (SiN_x:H), and hydrogenated amorphous silicon (a-Si:H) passivation films formed by PECVD. Moreover, several additional treatments have been proposed to improve these films' passivation effect. For example, Rinio *et al.* reported that rapid firing at 800 °C or hydrogenation improves the effective lifetime of minority carriers of SiN_x-passivated silicon substrates, especially at grain boundaries [4.16]. However, to achieve low-cost silicon solar cell fabrication, simpler passivation methods at lower temperatures are preferable.

4.3.1. Experimental

As silicon substrates, p-type Float-Zone (FZ)-grown monocrystalline substrates with a resistivity of 1-5 Ω·cm and a thickness of 300 μm, and p-type Cast-grown multicrystalline substrates with a resistivity of 1-4 Ω·cm and a thickness of 300 μm, were used. Each sample's size was 1×1 cm^2. For samples used for lifetime measurement, $\mathrm{SiO_x}$ thin layers (thickness: approximately 150 nm) were deposited on both surfaces of silicon substrates by PECVD at 300 °C. For solar cell fabrication, an n^+-type emitter layer was formed by $\mathrm{POCl_3}$ gas-phase diffusion followed by the evaporation of grid-type electrodes on both sides. Then, $\mathrm{SiO_x}$ or $\mathrm{SiN_x}$ passivation films (thickness: approximately 150 nm) were formed by PECVD at 300 °C with masks on the electrodes. Note that no other improvement techniques such as texturization or back surface field (BSF) were employed in this study, allowing us to focus on the passivation effect.

4.3.2. Lifetime properties

The effective minority carrier lifetime (τ_{eff}) before and after HWT was evaluated by the microwave photoconductance decay (μ-PCD) method with excitation by a laser diode (wavelength: 904 nm) and a microwave frequency of 10 GHz. In the case of monocrystalline substrates, the effective SRV (S_{eff}) was calculated from τ_{eff} using a simple equation:

$$1/\tau_{eff} = 1/\tau_{bulk} + 2S_{eff}/W, \qquad (4.1)$$

where τ_{eff} is effective lifetime, τ_{bulk} is bulk lifetime, S_{eff} is effective SRV and W is substrate thickness. τ_{bulk}=249.0 μs was obtained using chemical passivation with an ethyl alcohol solution containing 3 wt.% iodine.

Figure 4.2 shows the average τ_{eff} of mono- and multicrystalline silicon substrates with $\mathrm{SiO_x}$ layers and the calculated S_{eff} of monocrystalline samples, as a function of HWT temperature. The dashed lines indicate the average values of 16 mono- and 16 multicrystalline

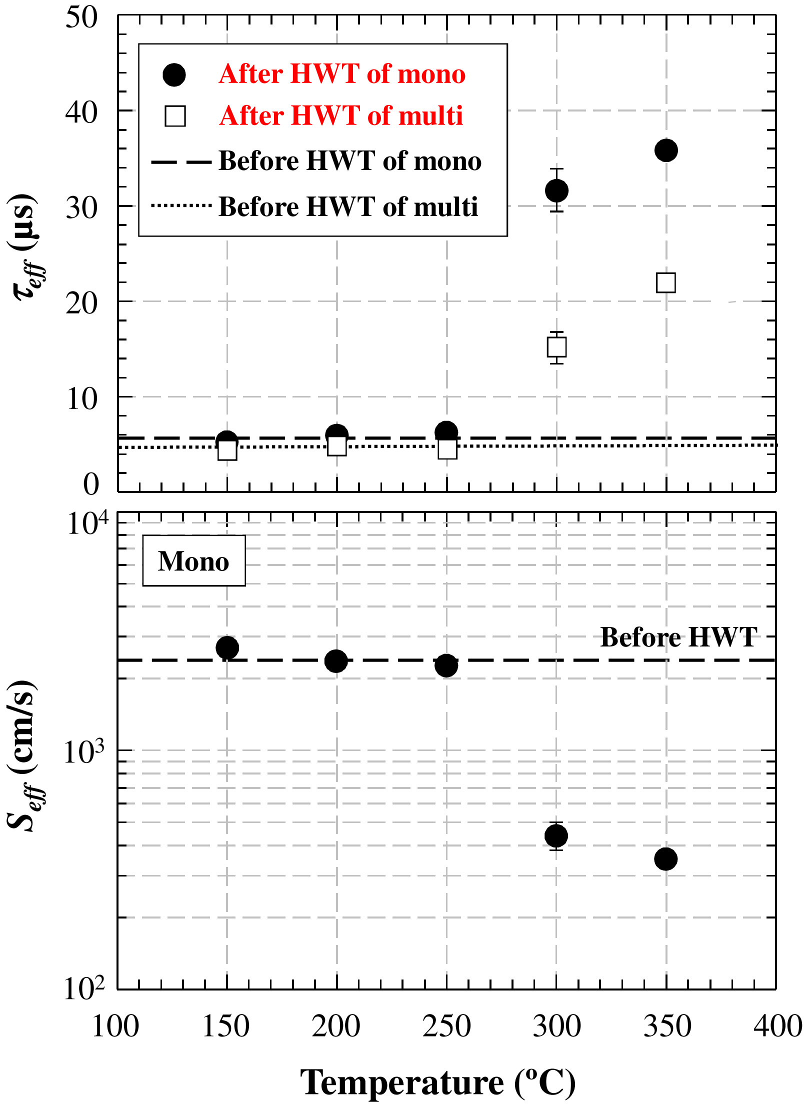

Fig. 4.2: Effective lifetime of SiO_x passivated mono- and multicrystalline silicon substrates and effective SRV of monocrystalline samples, as a function of HWT temperature.

samples before HWT. HWT at each temperature was performed on 2 monocrystalline and 2 multicrystalline samples, except in the case of an HWT temperature of 300 °C, where 8 monocrystalline and 8 multicrystalline samples were used. There was little difference among the samples in the same condition. At temperatures below 250 °C, no significant change in τ_{eff} by HWT was observed, while τ_{eff} was markedly increased by 3- to 5-fold by HWT at over 300 °C (over 1.52 MPa) regardless of substrate type. In monocrystalline samples, S_{eff} was also improved to less than 500 cm/s by HWT at over 300 °C (over 1.52 MPa). Thus, a temperature of 300 °C and a pressure of 1.52 MPa were the lowest treatment temperature and pressure that caused passivation enhancement in this experiment.

4.3.3. Solar cell properties

Table 4.1 shows the photovoltaic properties of mono- and multicrystalline silicon solar cells with SiO_x or SiN_x passivation layers before and after HWT at 1.52 MPa and 300 °C, and Fig. 4.3 shows the illuminated current-voltage characteristics of a typical sample (monocrystalline silicon solar cell with SiO_x). Although the photovoltaic performances of these cells were not satisfactory because of the absence of other improvement structures like texturing or BSF, all photovoltaic parameters, open circuit voltage (V_{oc}), short circuit current density (J_{sc}), and fill factor (*F.F.*) were improved by HWT both for mono- and multicrystalline silicon cells with SiO_x or SiN_x passivation layers. The improvement of V_{oc} means the reduction of saturation current J_0, which suggests the reduction of carrier recombination. Combined with the improvement of J_{sc}, it can be considered that the recombination centers on the silicon surface were reduced by HWT. The improvement in V_{oc}, which could be observed in samples with SiO_x passivation layers, was greater than that observed in samples with SiN_x. Hence, HWT can be assumed to have a stronger relation to the mechanism of SiO_x

passivation than that of SiN_x passivation. On the other hand, with regard to the substrate type, multicrystalline silicon cells exhibited a larger increase in V_{oc} than monocrystalline silicon cells with the same passivation layers. This suggests the possibility of defect passivation including grain boundaries in addition to surface passivation.

To determine whether the effect was caused by ‘high-pressure water vapor’ or by ‘heat’, annealing in atmospheric N_2 at 300 °C was also performed. As a result, only *F.F.* increased owing to contact enhancement between substrate and electrodes upon heating, but no improvements in V_{oc} and J_{sc} were obtained. Thus, it can be considered that ‘high-pressure water vapor’ is essential and effective for improving photovoltaic properties.

The HWT effect was also investigated two-dimensionally using the electroluminescence (EL) imaging method [4.17, 4.18]. The EL emission intensity relates to the effective diffusion length of minority carriers. Therefore, by EL intensity mapping, we can investigate the minority carrier diffusion length distribution and, thus, can detect cracks, electrode breakages, and electronically active crystallographic defects such as grain boundaries, dislocation clusters, and precipitates as dark areas in EL images. Figure 4.4 shows EL images of the fabricated multicrystalline silicon solar cell with a SiO_x passivation layer before and after HWT at 1.52 MPa and 300 °C. The images were obtained using a cooled Si charge-coupled device infrared camera with a 1 sec exposure, applying a 100 mA/cm^2 forward current. After HWT, the EL intensity of the entire cell area markedly increased from 5.4×10^3 to 8.6×10^3 counts. The crystallographic defects clearly detected in the image before HWT became less contrast after HWT (for example, the circled area in Fig. 4.4). Combined with the increase in the point intensity from 4.4×10^3 to 7.0×10^3 counts at the defect indicated by an arrow in the Fig. 4.4, the crystallographic defects as well as the surface could be passivated effectively by HWT.

Table 4.1: Photovoltaic properties of mono- and multicrystalline silicon solar cells with SiO_x or SiN_x passivation layer before and after HWT at 1.52 MPa and 300 °C.

Substrate (passivation)	HWT	V_{oc} (mV)	J_{sc} (mA/cm^2)	*F.F.* (%)	*Eff.* (%)
Mono	Before	574	26.9	70.6	10.9
(SiO_x)	After	580	27.8	72.5	11.7
Multi	Before	572	24.9	73.3	10.4
(SiO_x)	After	580	26.2	69.5	10.6
Mono	Before	579	25.3	68.2	11.6
(SiN_x)	After	582	29.3	72.8	12.1
Multi	Before	577	28.3	69.5	11.6
(SiN_x)	After	582	28.5	72.8	12.4

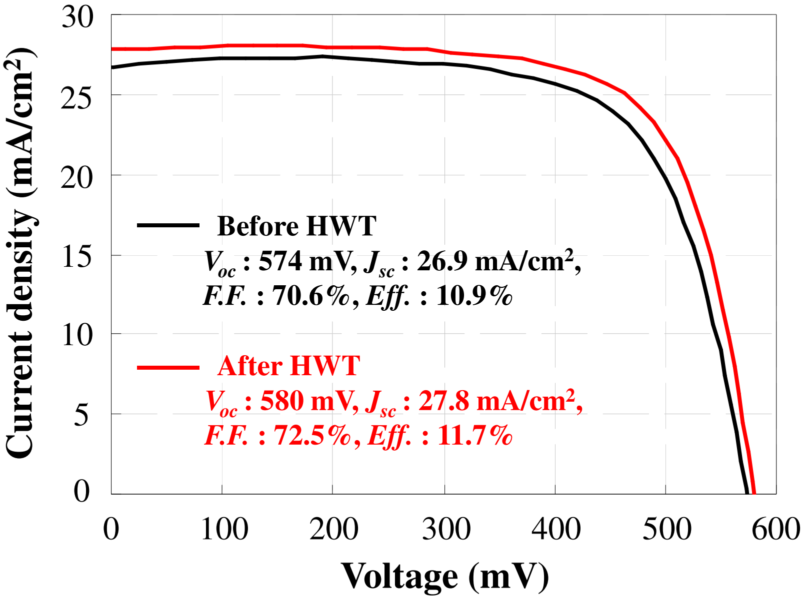

Fig. 4.3: Illuminated current-voltage characteristics of a monocrystalline silicon solar cell with SiO_x before and after HWT at 1.52 MPa and 300 °C.

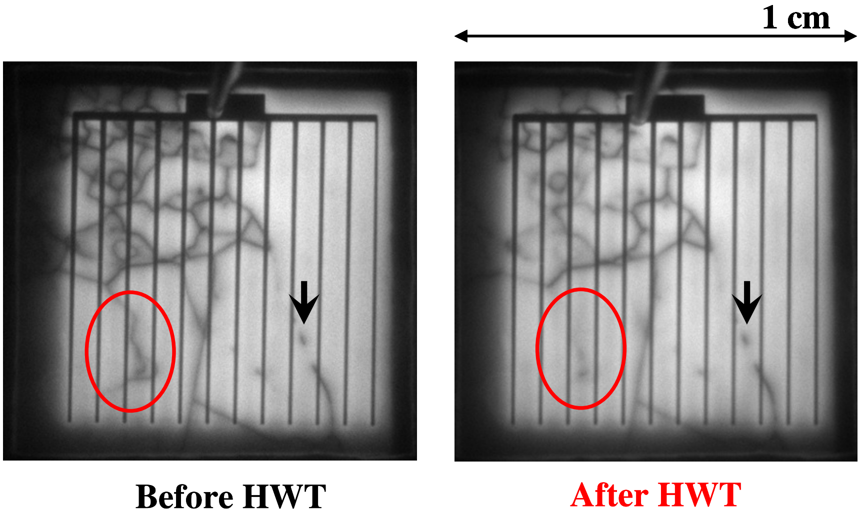

Fig. 4.4: EL images of multicrystalline silicon solar cell with SiO_x passivation layer before (left) and after HWT at 1.52 MPa 300 °C (right).

4.3.4. Discussion of HWT mechanism

To investigate the effect of HWT on the bonding status of passivation films, optical absorption spectra of SiO_x films were obtained using Fourier transform infrared spectrometry (FT-IR). For the measurement, SiO_x films were deposited by PECVD (denoted as PECVD-SiO_x) on both sides of monocrystalline silicon substrates with high resistivity, and then the change in absorption spectra induced by HWT was investigated. As a reference, a SiO_2 layer with almost the same thickness was grown by thermal oxidation of the substrate at 1100 °C (denoted as thermal-SiO_2).

Figure 4.5 shows the FT-IR spectra of three samples, thermal-SiO_2, PECVD-SiO_x before HWT, and PECVD-SiO_x after HWT at 1.52 MPa and 300 °C. The main peak, observed at approximately 1000 cm^{-1}, is the optical absorption band caused by the Si-O-Si antisymmetric stretching vibration mode. In comparison with that of thermal-SiO_2, PECVD-SiO_x showed a smaller and broader absorption band at a lower wavenumber. This indicates that the PECVD-SiO_x film initially had Si-O-Si bonding with low and widely distributed angles with an open and susceptible network. After HWT, the peak wavenumber, peak absorption, and full width at half maximum (FWHM) of the absorption band approached those of thermal-SiO_2. In HWT with a suitable temperature and pressure, a reaction between water vapor and SiO_x is considered to occur as follows. Water was incorporated into the film and caused breakage of the weak Si-O-Si bonds with low bonding angles, resulting in Si-O-H bond formation [4.19]. Then, two Si-O-H groups combined to form more stable Si-O-Si bonds with a larger bonding angle. During formation of this stable Si-O-Si bonding network, the silicon dangling bonds are terminated, and then photovoltaic properties and carrier lifetime are improved because of less surface recombination. In addition, the EL results for multicrystalline silicon revealed that the crystallographic defects were also passivated. This is

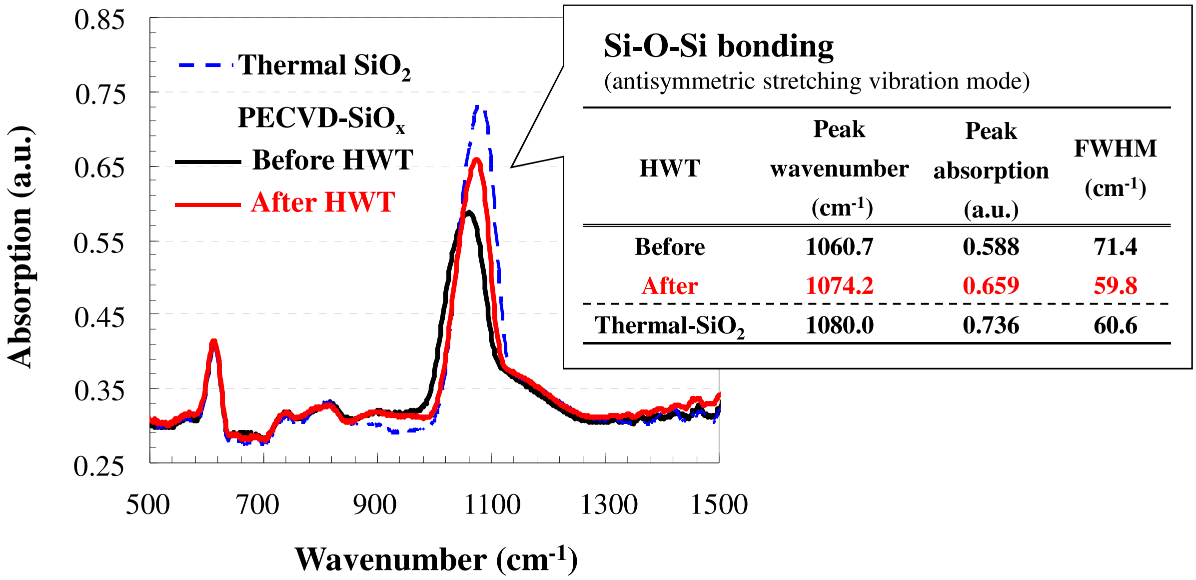

Si-O-Si bonding
(antisymmetric stretching vibration mode)

HWT	Peak wavenumber (cm^{-1})	Peak absorption (a.u.)	FWHM (cm^{-1})
Before	1060.7	0.588	71.4
After	1074.2	0.659	59.8
Thermal-SiO_2	1080.0	0.736	60.6

Fig. 4.5: Optical absorption for PECVD-SiO_x samples before and after HWT. The dashed curve is a reference spectrum of thermal-SiO_2.

probably due to the diffusion of activated oxygen or hydrogen atoms along the line or plane defects and the termination of silicon dangling bonds. The mechanism of SiN_x passivation layer enhancement may be complicated, but termination by oxygen or hydrogen atoms at the interface and at the defects can also be assumed.

4.4. Applying to poly-Si thin films

The utility of HWT to bulk crystalline silicon substrate as well as solar cell device was confirmed in previous section. Especially, it is very important HWT is effective for GB passivation as shown in Fig. 4.4. The defect passivation is more important in poly-Si thin films than in bulk multycrystalline silicon substrates, because the amount of defects including GBs contained in materials is much larger. The dominant technique for the passivation of poly-Si thin films is the plasma-induced hydrogenation [4.1-4.8], however, this method requires a large-scaled, complicated and dangerous apparatus with the need of vacuuming. If HWT could replace the hydrogenation, it would have very impressive impact to poly-Si thin film solar cell fabrication.

HWT (60 min, 300 °C, 1.52 MPa) was performed on poly-Si thin films deposited on alumina and silicon substrates with SiO_x intermediate layers. In this study, the treatment was demonstrated on 10-µm-thick poly-Si thin films with different grain sizes fabricated by two-step thermal-APCVD with an intermittent source gas supply method as described in previous Chapters. Note that these poly-Si thin films had no surface passivation layers, allowing us to concentrate on the defect passivation.

4.4.1. Crystallographic properties

Figure 4.6 shows the results of a Raman scattering measurement using excitation laser of a Cd-He laser of wavelength of 442 nm. The full-width at half maximum (FWHM) and peal position of the TO-LO (transverse optical mode, longitudinal optical mode) phonon band with and without HWT at 1.52 MPa and 300 °C as a function of grain size are shown. Both FWHM and peak position of poly-Si on alumina substrate with each grain size became closer to crystalline silicon (c-Si) value by HWT, indicating the passivation effect which reduces the crystalline defects [4.20-4.22]. However, no significant change could be seen in the case of excitation laser of 785-nm wavelength as shown in Fig. 4.7. The difference of wavelength of excitation laser reflects the information about depth factor by the difference of penetration depth into silicon (442 nm: less than 1 μm, 785 nm: about 10 μm). This indicates HWT is much effective at near surface than deep inside the silicon.

Figure 4.8 shows the photoluminescence (PL) spectra of poly-Si thin films on alumina substrates with small (2-3 μm) and large (10- μm) with and without HWT. The whole intensity of each PL signal was increased by HWT, showing the sharpening of D1 peak at around 0.8 eV, which indicates higher crystallinity as mentioned in Chapter 3 [4.23-4.28]. And the position of tail-to-tail peak shifted a little toward higher energy. These facts would be the evidence of defect passivation by HWT in poly-Si thin films.

4.4.2. Electronic properties

Figure 4.9 shows the relationship between grain size and Hall mobility. The Hall mobility was increased with increasing grain size and improved by HWT at 1.52 MPa and 300 °C for all samples, showing more than 20-cm^2/Vs improvements. The Hall mobility of poly-Si thin film is determined by scattering at GBs, the potential barrier height (ϕ_b) [4.29].

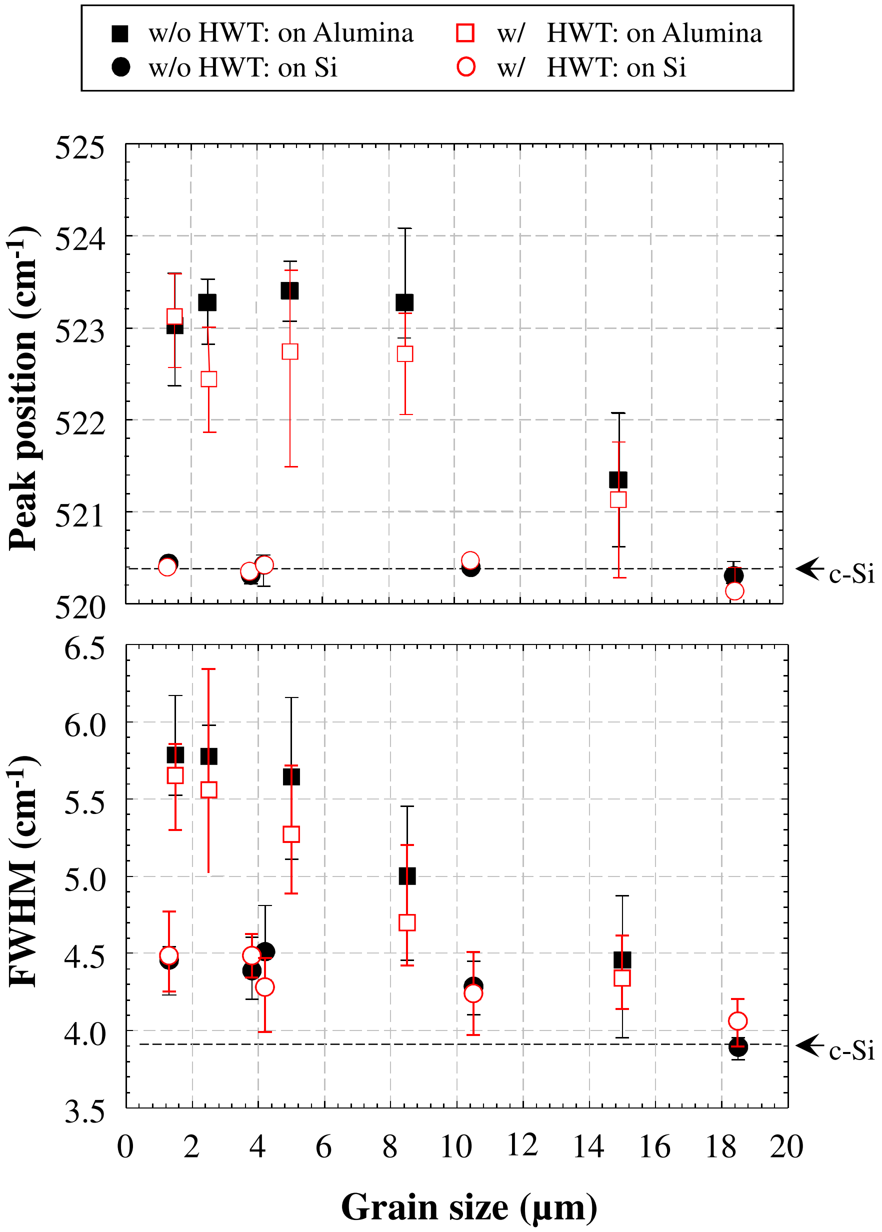

Excitation: 442 nm He-Cd laser

Fig. 4.6: Peak position (upper) and FWHM (down) of TO-LO phonon band of poly-Si thin films with different grain size on silicon and alumina substrates with and without HWT at 1.52 MPa and 300 °C, as a function of grain size, measured with 442 nm He-Cd laser.

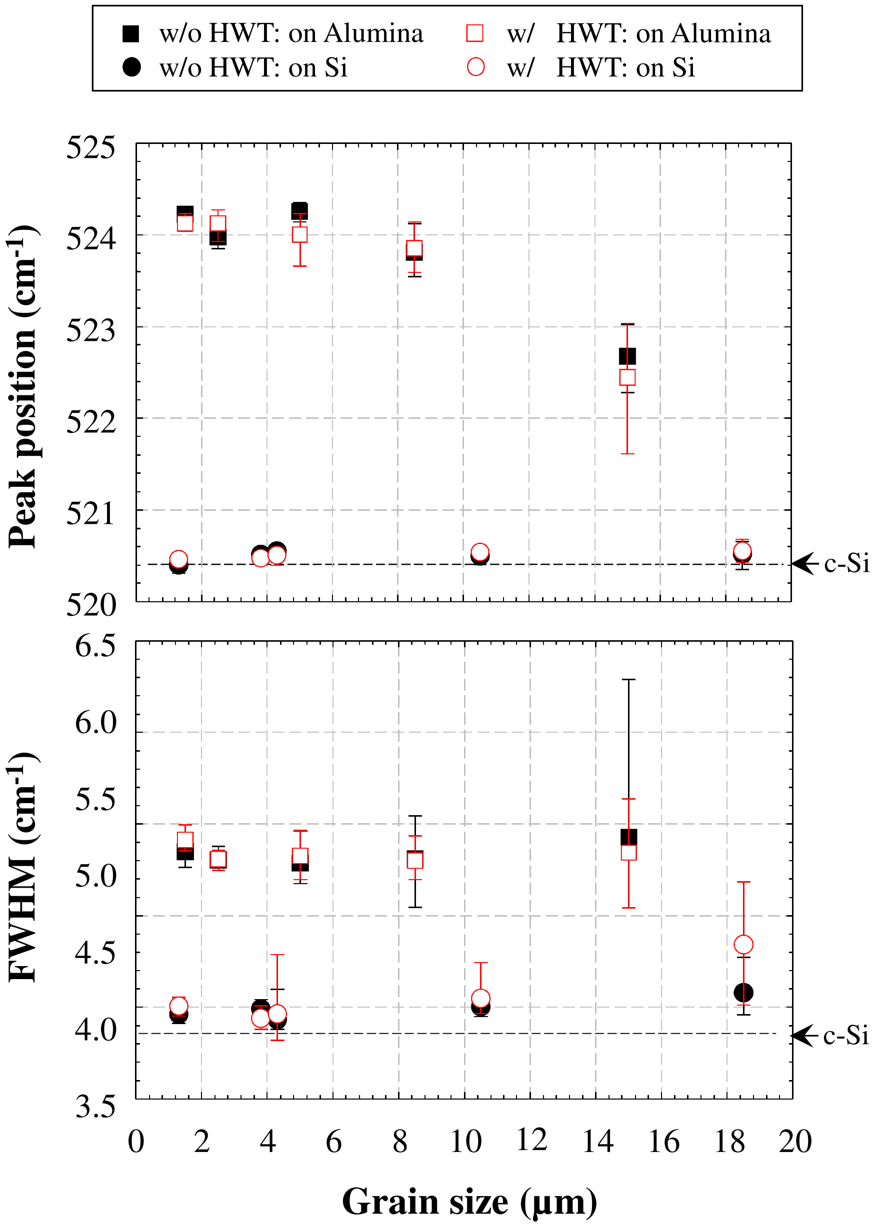

Excitation: 785 nm semiconductor laser

Fig. 4.7: Peak position (upper) and FWHM (down) of TO-LO phonon band of poly-Si thin films with different grain size on silicon and alumina substrates with and without HWT at 1.52 MPa and 300 °C, as a function of grain size, measured with 785 nm laser.

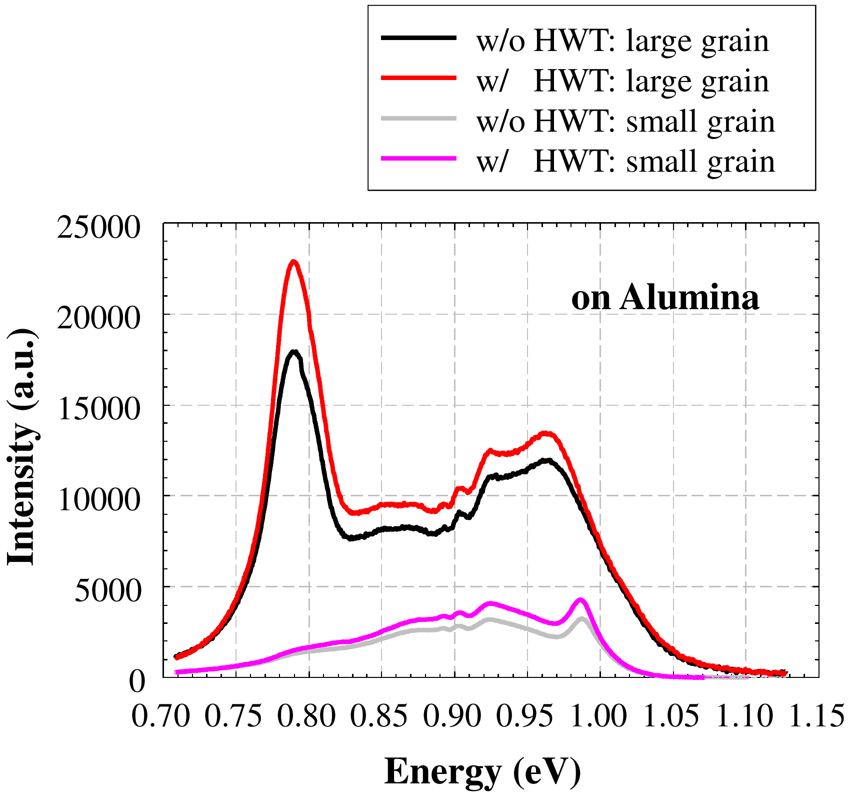

Excitation: 640 nm laser, at 7 K

Fig. 4.8: PL spectra of poly-Si thin films with different grain size on alumina substrates with and without HWT at 1.52 MPa and 300 °C.

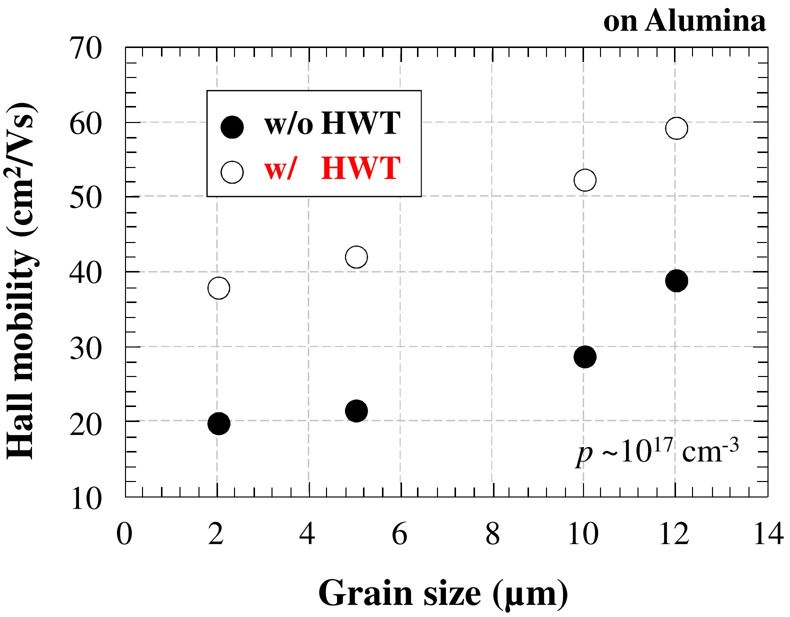

Fig. 4.9: Hall mobility of poly-Si thin films with different grain size on silicon and alumina with and without HWT at 1.52 MPa and 300 °C, as a function of grain size.

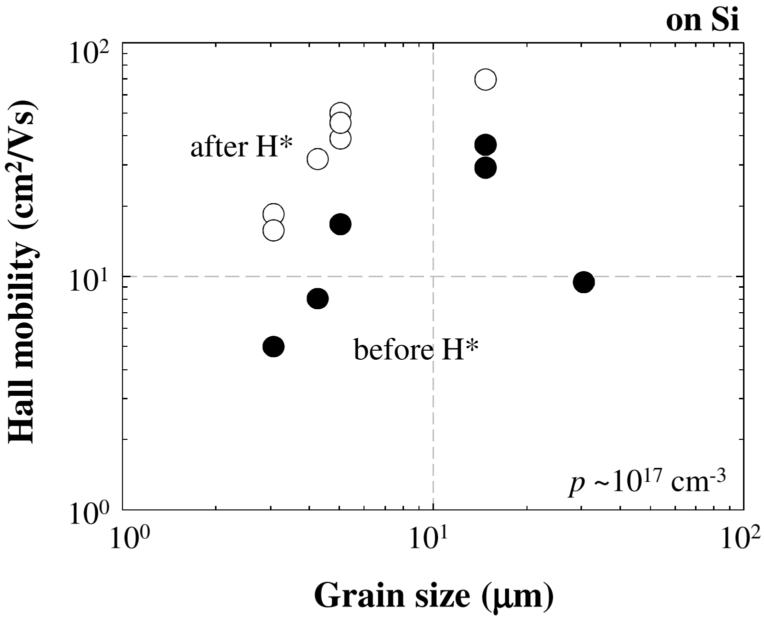

Fig. 4.10: Hall mobility of poly-Si thin films with different grain size on silicon before and after plasma-hydrogenation, as a function of grain size [4.30].

This improvement of the Hall mobility would result from the reduction of ϕ_b at GBs caused by the defect passivation. As the reference, the result of Hall mobility improvement of poly-Si thin films by conventional plasma-induced hydrogenation [4.30] is also shown in Fig. 4.10. The degree of improvements is almost the same between the case of HWT and the case of hydrogenation. Thus, HWT can be said to be very effective and promising method and have a potential to replace the conventional hydrogenation method.

The KFM microscopic characterization at the local point of GBs was also performed, in the same manner as Chapter 3. Figure 4.11 shows the two images of poly-Si thin film after HWT at 1.52 MPa and 300 °C; local topography and KFM potential image. And Fig. 4.12 shows line profiles of height and surface potential at a distinctive GB as indicated points between A and B in Fig. 4.11. At GB, the potential clearly increased by 10-30 mV higher than that of inner grain, but ϕ_b showed relatively decreased values after HWT. The ϕ_b, and calculated N_T and S_{GB} of arbitrary 50 GBs are arranged in histograms in Fig. 4.13, with the comparison to before HWT. The distributions of ϕ_b, N_T and S_{GB} were clearly shifted to lower values after HWT. The average ϕ_b, N_T and S_{GB} after HWT are 17.8 meV, 2.88×10^{11} cm^{-2}, and 5.77×10^{3} cm/s, respectively [4.31-4.33]. In the case of poly-Si thin film with small grains on silicon substrate and the value $L_g/2S_{GB}$ increased to 1.74×10^{-9} s by HWT at 1.52 MPa and 300 °C, assuming that L_g=2 μm. When assuming L_g=14 μm, the value $L_g/2S_{GB}$ can be expected to improve to 1.25×10^{-8} s. This value leads to the estimation of poly-Si thin film solar cells with efficiency of approximately 8% from the simulation of Fig. 1.3.

4.4.3. Discussion of HWT mechanism in poly-Si thin film passivation

The basic idea of the passivation mechanism of HWT for poly-Si thin film can be considered to be the same as the case of bulk crystalline silicon discussed in previous section.

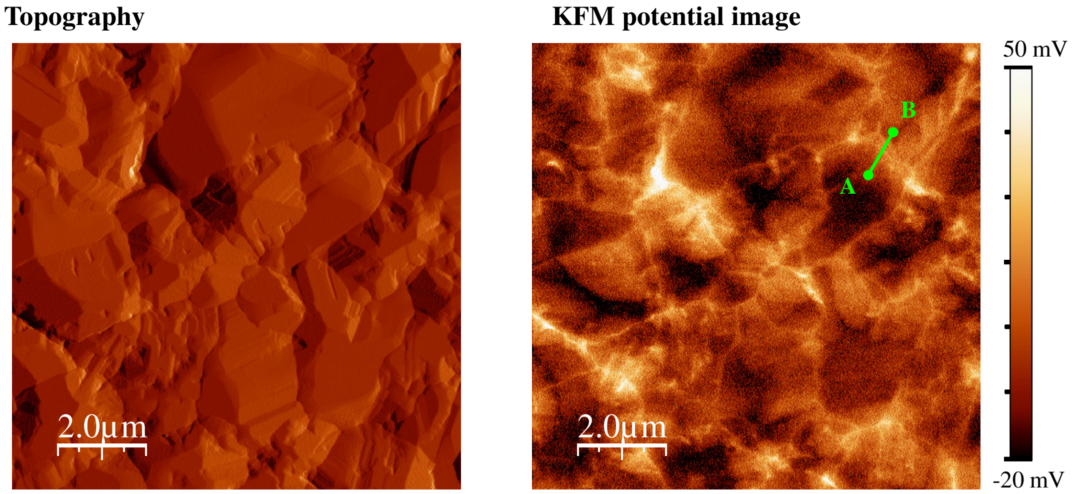

Fig. 4.11: Topography (left) and KFM potential image (right) of poly-Si thin film after HWT at 1.52 MPa and 300 °C.

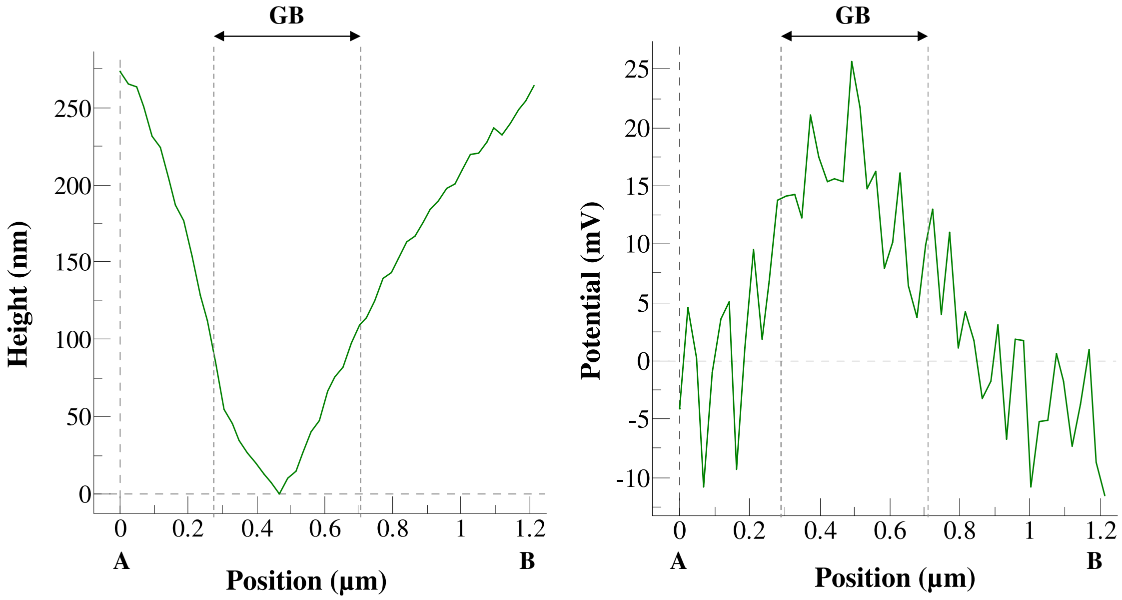

Fig. 4.12: Line profiles of height (left) and surface potential (right) at a distinctive GB as indicated points between A and B in Fig. 4.12 in poly-Si thin film after HWT.

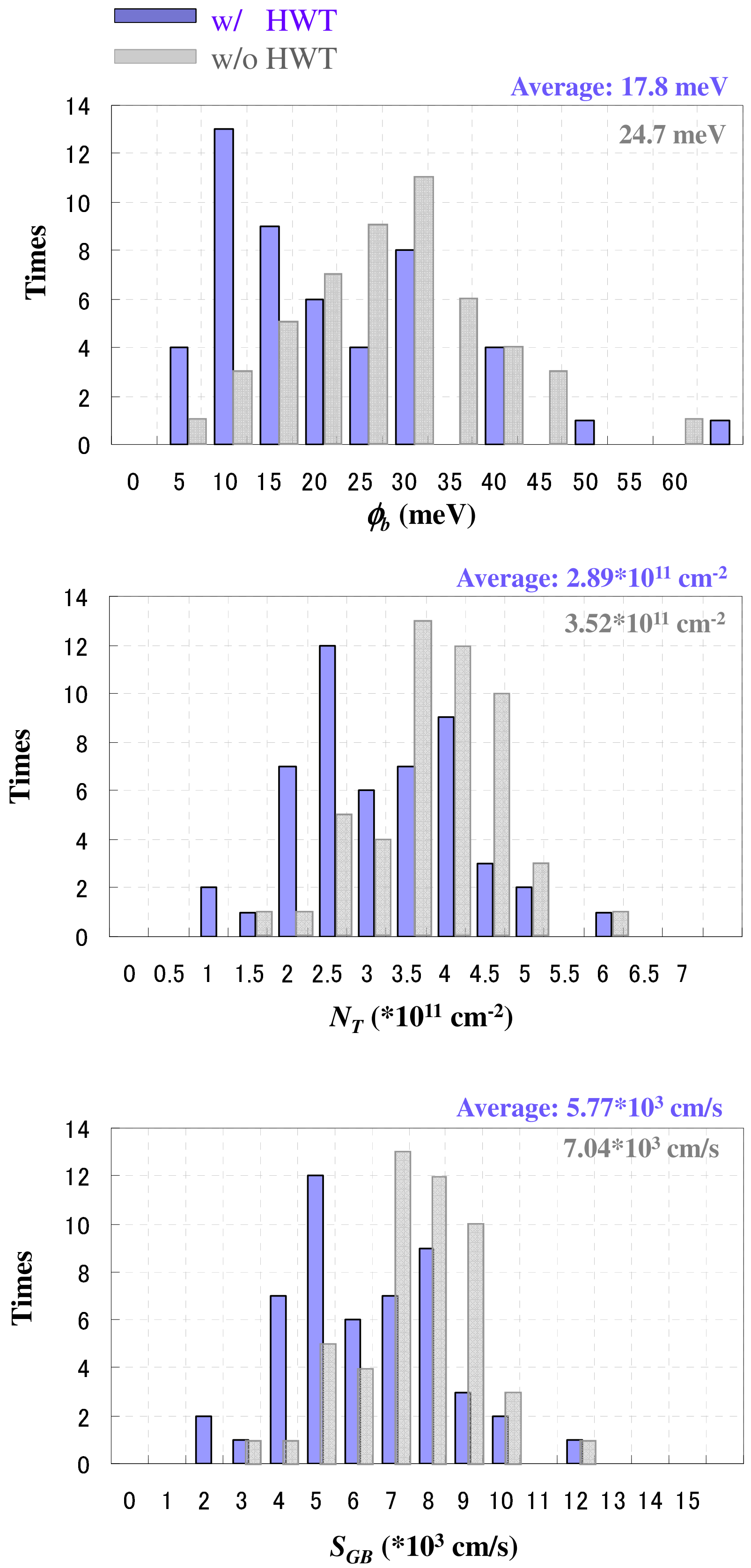

Fig. 4.13: Histograms of ϕ_b, N_T, and S_{GB} of arbitrary 50 GBs in poly-Si thin film before and after HWT.

The dangling bonds were terminated by the stable Si-O-Si bonding network formation at defects. However, in poly-Si thin film, the effect of the diffusion of activated oxygen or hydrogen atoms along GBs is expected to have much larger influence. The diffusion coefficient is much larger at GBs than within the grain [4.34].

Figure 4.14 shows the depth profiles of contained oxygen atoms in poly-Si thin film with or without HWT at 1.52 MPa and 300 °C, measured by secondary ion mass spectroscopy (SIMS). From SIMS result, it was revealed that the poly-Si thin film after HWT contained more oxygen atoms at around surface. These oxygen atoms would passivate the crystalline defects, resulting in the improvements of measurements discussed above. The increase of oxygen was seen within only near surface (-200 nm), which corresponds to the results of Raman with 2 different-wavelength lasers. Of course, it is desirable that whole body of poly-Si thin film is passivated effectively, but conditions near surface is especially important if p-n junction will be formed in this region.

4.5. Summary

As a new technique of passivation with advantages of simple, safe, and at low temperature, HWT was proposed and demonstrated on both bulk crystalline silicon solar cells with SiO_x and SiN_x passivation layers, and poly-Si thin films. By the treatment at 1.52 MPa and 300 °C and, a Si-O-Si bonding network formation which would terminate the silicon dangling bonds was confirmed from FT-IR and SIMS measurement. For bulk crystalline silicon solar cells with SiO_x and SiN_x passivation layers, the reduction of the recombination centers improved the photovoltaic performances, increasing the efficiency by about 1%. From

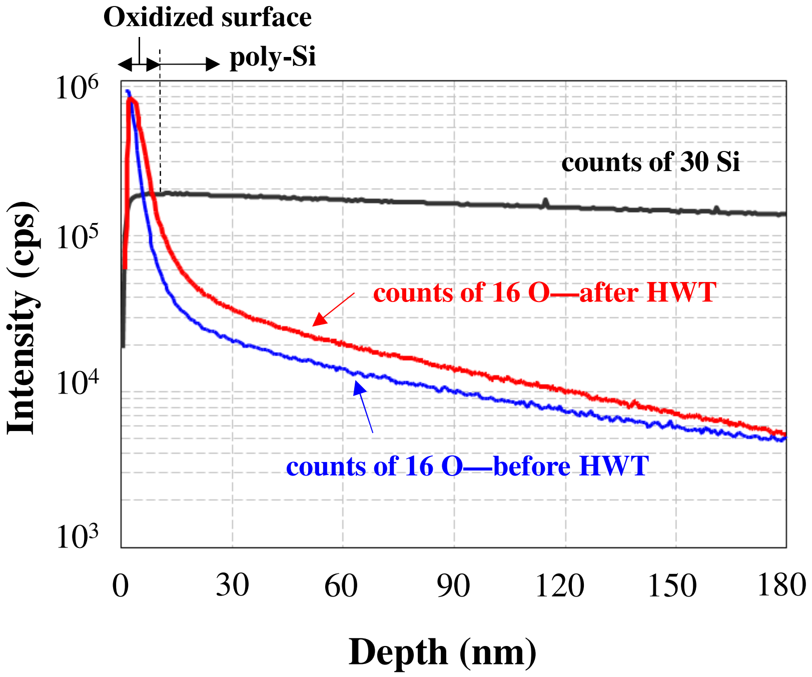

Fig. 4.14: SIMS profiles showing the contents of oxygen in poly-Si thin films before and after HWT at 1.52 MPa and 300 °C.

the investigation of EL emission intensity, the effect of passivation of bulk defect such as grain boundaries was confirmed as well as the surface passivation. The effects of HWT to poly-Si thin films were also observed in improvements of crystallinity, and Hall mobility, and reduction of potential barrier height at GBs. The distributions of ϕ_b, N_T and S_{GB} were clearly shifted to lower values by HWT. More investigations and optimizations will prove that HWT is one of the promising methods for the passivation method of not only bulk crystalline silicon solar cells but also thin film poly-Si solar cells.

References of Chapter 4

[4.1] S. Darwiche, M. Nikravech, D. Morvan, J. Amouroux, and D. Ballutaud: Solar Energy Materials and Solar Cells, **91** (2007) p.195.

[4.2] B. Ren, M. Wang, X. Liu, and Y. Xu: Rare Metals, **25** (2006) p.133.

[4.3] S. Martinuzzi, I. Périchaud, and F. Warchol: Solar Energy Materials and Solar Cells, **80** (2003) p.343.

[4.4] G. Hahn, P. Geiger, D. Sontag, P. Fath, and E.t Bucher: Solar Energy Materials and Solar Cells, **74** (2002) p.57.

[4.5] D. Ballutaud, A. Rivière, M. Rusu, S. Bourdais, and A. Slaoui: Thin Solid Films, **403-404** (2002) p.549.

[4.6] H. F. W. Dekkers, S. De Wolf, G. Agostinelli, F. Duerinckx, and G. Beaucarne: Solar Energy Materials and Solar Cells, **90** (2006) p.3244.

[4.7] C. H. M. van der Werf, H. D. Goldbach, J. Löffler, A. Scarfó, A. M. C. Kylner, B. Stannowski, W. M. ArnoldBik, A. Weeber, H. Rieffe, W. J. Soppe, J. K. Rath, and R. E. I. Schropp: Thin Solid Films, **501** (2006) p.51.

[4.8] C. Boehme, and G. Lucovsky: J. Non-Crystal. Solids, **299-302** (2002) p.1157.

[4.9] T. Sameshima, K. Sakamoto, Y. Tsunoda, and T. Saitoh: Jpn. J. Appl. Phys., **37** (1998) p.1452.

[4.10] T. Sameshima, K. Sakamoto, and K. Asada: Appl. Phys. A, **69** (1999) p.221.

[4.11] K. Sakamoto, and T. Sameshima: Jpn. J. Appl. Phys., **39** (2000) p.2492.

[4.12] P. Punchaipetch, M. Miyashita, Y. Uraoka, and T. Fuyuki: Jpn. J. Appl. Phys., **45**, No. 4 (2006) L120.

[4.13] Y. Uraoka, M. Miyashita, Y. Sugawara, H. Yano, T. Hatayama, T. Fuyuki, and T.

Sameshima: Jpn. J. Appl. Phys., **45**, No. 7 (2006) p.5657.

[4.14] J. Zhao, A. Wang, P. P. Altermatt, S. R. Wenham, and M. A. Green: Proc. of 1st World Conference on Photovoltaic Energy Conversion (1994) p.87.

[4.15] R. R. King, and R. M. Swanson: IEEE Trans. Electron Devices, **38** (1991) p.1399.

[4.16] M. Rinio, M. Kaes, G. Hahn, and D. Borchert: Proc. of 21st European Photovoltaic Solar Energy Conference (2006) p.684.

[4.17] T. Fuyuki, H. Kondo, T. Yamazaki, and Y. Takahashi: Appl. Phys. Lett., **86** (2005) 262108.

[4.18] T. Fuyuki, H. Kondo, Y. Kaji, T. Yamazaki, Y. Takanashi, and Y. Uraoka: Proc. of 31st IEEE Photovoltaic Specialist Conference (2005) p.1343.

[4.19] S. Maekawa, K. Okude, and T. Ohishi: J. Sol-Gel Sci. & Technol., **2** (1994) p.497.

[4.20] S. A. Campbell: “The science of Microelectronic Fabrication”, Oxford University Press (1996).

[4.21] N. H. Nickel, P. Lengsfeld, and I. Sieber: Pys. Rev., **B61** (2000) p.1558.

[4.22] E. Annastassakis: Proc. of the 4th Int’l School ISPPM, edited by K. Kassavod (1985) p.128.

[4.23] A. V. Mudryi, A. L. Patuk, I. A. Shakin, A. G. Ulyashin, R. Job, W. R. Farhrner, A. Fedotov, A. Mazanik, N. Drozodov: Solar Energy Materials and Solar Cells, **72** (2002) p.503.

[4.24] R. Sauer, J. Weber, J. Stolz, E. R. Weber, K. H. Kusters, and H. Alexander: Appl. Phys. A, **36** (1985) p.1.

[4.25] V. D. Kulakowskii: Sov. Phys. Solid State, **20** (1978) p.802.

[4.26] M. Suezawa, K. Sumino and Y. Nishina: Jpn. J. Appl. Phys., **21** (1982) L518.

[4.27] N. A. Drozdov, A. A. Patrin and V. D. Tkachev: JETP lett., **23** (1976) p.597.

[4.28] N. A. Drozdov, A. A. Patrin and V. D. Tkachev: Phys. Status Solidi (b), **83** (1977) p.137.

[4.29] S. M. Sze: "Physics of semiconductor device, 2nd edition", Wiley (1981) p.254.

[4.30] T. Yamazaki: Ph. D. Thesis, Graduate School of Materials Science, Nara Institute of Science and Technology (2005) p.66.

[4.31] J. Y. W. Seto: J. Appl. Phys., **46** (1975) p.5247.

[4.32] G. Beaucarne, J. Poortmans, M. Caymax, J. Nijs, and R. Mertens: Solid State Phenomena, **67-68** (1999) p.577.

[4.33] S. A. Edmiston, G. Heiser, A. B. Sproul, and M. A. Green: J. Appl. Phys., **80** (1996) p.6783.

[4.34] Van Wieringen, and N. Warmholtz: Physica, **22** (1956) p.849.

Chapter 5

Development of poly-Si thin film solar cells on alumina substrates

5.1. Introduction

Much attention has been gathered for poly-Si thin film heading for the photovoltaic applications in view of crystalline quality when fabricated on foreign cheap substrates; alumina. The conversion efficiency over 10% is estimated according to the simulation results for 10-μm-thick poly-Si thin film solar cells when the value $L_g/2S_{GB}$ is over 5.0×10^{-8} s, as mentioned in Chapter 1. In this Chapter, poly-Si thin films investigated in previous Chapters are applied to the solar cell structure. Especially, the profile of p-n junction which strongly affects the photovoltaic performance should be investigated carefully. Particularly in polycrystalline materials, the preferential diffusion of dopant atoms along grain boundaries (GBs) is often observed in conventional technique of emitter formation at a high temperature, which forms p-n junctions along GBs perpendicular to the substrate plane [5.1-5.4]. However, it was reported this kind of perpendicular p-n junction would cause the deterioration of the diode properties [5.5]. Hence, a new process for p-n junction formation without high temperature processing is indispensable for obtaining high efficiency poly-Si thin film solar cells.

In this Chapter, a laser doping (LD) technique for p-n junction formation is proposed as a low temperature processing. First of all, fabrication of bulk crystalline silicon (c-Si) solar cell with LD is investigated and discussed. Next, the interdigitated-electrode structure solar cells using poly-Si thin films on alumina substrates are described and discussed as the trial fabrication.

5.2. Development of laser doping technique in c-Si solar cells

5.2.1. Introduction of this section

Now, laser processing in silicon solar cell fabrication is gathering much attention not only in the field of thin film materials but also bulk c-Si. From the standpoint of cost reduction of silicon solar cells, it is requested to use thinner silicon substrates (under 100 μm). However, in conventional processes of metallization, lithography with wet chemical etching or high temperature annealing in furnaces, the thinner substrates cannot stand the mechanical or thermal stress, resulting in deterioration of fabrication yield. Then, the establishment of new processes suitable for thinner silicon solar cell is necessary. Laser processing is one answer with a lot of advantages; it can be performed at room temperature and in the atmosphere and can form the selective structure directly and easily. Several techniques using lasers such as Laser Fired Contact [5.6], Laser Texturing [5.7], Laser Grooved Buried Contact [5.8] and dielectric layer removal [5.9] have been proposed and developed.

LD technique is also the promising laser process in crystalline silicon solar cell fabrication. Laser doping itself was introduced more than 2 decades ago in the transistor fabrication process for ultra shallow doping using an excimer laser [5.10, 5.11]. However, now it is gathering many attentions as an attractive alternative method to form doping area in silicon solar cell instead of the conventional thermal diffusion (at over 800 °C) method. With the advantages of laser processing, LD can be performed at room temperature and in the atmosphere and can form the selective doping area easily without any lithography processes. The possibility of LD has been studied widely [5.12-5.18] from full surface doping for emitters to selective area doping for highly doped regions underneath electrodes or complex n^+ and p^+ regions at a rear surface for the back contact type structure. Silicon solar cells with laser-doped emitter so far resulted in efficiencies up to 15.4% [5.14].

In order to extend the LD utility for further applications such as shallow emitter or back surface field (BSF) formation which are favorable for high efficiency silicon solar cells, several doping areas with different conditions should be formed. Therefore, in this study, we applied a pulsed laser with 355-nm wavelength for the doping of both phosphorous and boron atoms into p-type monocrystalline silicon and tried to control the doping conditions by changing the laser output power. By using the short wavelength laser instead of a commonly-used green laser (wavelength of 532 nm), controlling of doping profiles at shallower region would be expected, depending on the penetration depth of light into silicon substrate. Also we tried to develop the silicon solar cell fabrication process at very low temperature (below 100 °C) using this LD technique and solar cell properties were investigated relating to the doping conditions.

5.2.2. Experimental

As monocrystalline silicon substrates, p-type Czochralski-grown substrates with a thickness of 150 μm and a resistivity of 1-4 Ω·cm were used. After cutting into 1×1 cm^2 size and RCA cleaning, the dopant contained liquids were spin-coated onto the polished surface. The phosphorus contained liquid and boron contained liquid were used for n^+ emitter and p^+ BSF formation, respectively. Then, they were subsequently dried on a hotplate at 100 °C to obtain the solid phase doping precursors, phosphorus silicate glass (PSG) or boron silicate glass (BSG). Then, PSG- or BSG-coated samples were irradiated by the laser at room temperature in the atmosphere as shown in Fig. 5.1. In this study, a Nd^{3+}:YAG pulsed laser with wavelength of 355 nm and duration time of 15 ns was used. Doping area was decided by moving the stage on which a sample was mounted during laser irradiation. In this study, full surface area doping was performed as follows; an x-y-translation stage moved in x-direction from edge to edge of the sample then shifted in y-direction and this cycle was repeated in whole sample surface. The reputation frequency, diameter of laser spot on the sample surface (round shape), stage scanning speed and stage shift value in y-direction were adjustable, and fixed as 30 kHz, 50 μm, 10 mm/s and 25 μm, respectively in a typical experimental condition. The overlap rate between pulses could be calculated as 99.3% in x-direction and 50% in y-direction. The laser output power was varied in the range of 0.30 to 0.55 W (corresponding laser energy density per one pulse of 0.51 to 0.93 J/cm^2). As the reference, a conventional solid phase thermal diffusion (TD) was also performed to form the emitter in the condition of at 900 °C, 30 min, in N_2 ambient.

After the formation of n^+ region on front surface as emitter and p^+ region on back surface as BSF, Ag/Ti grid electrode (front) and Al full-surface electrode (rear) were evaporated. Finally, SiN layer as anti-reflecting coating and passivation was deposited on front surface by plasma enhanced chemical vapor deposition (PECVD) with NH_3 plasma pre-treatment at 100 °C [5.19]. Note that this PECVD step was not applied to samples with laser-

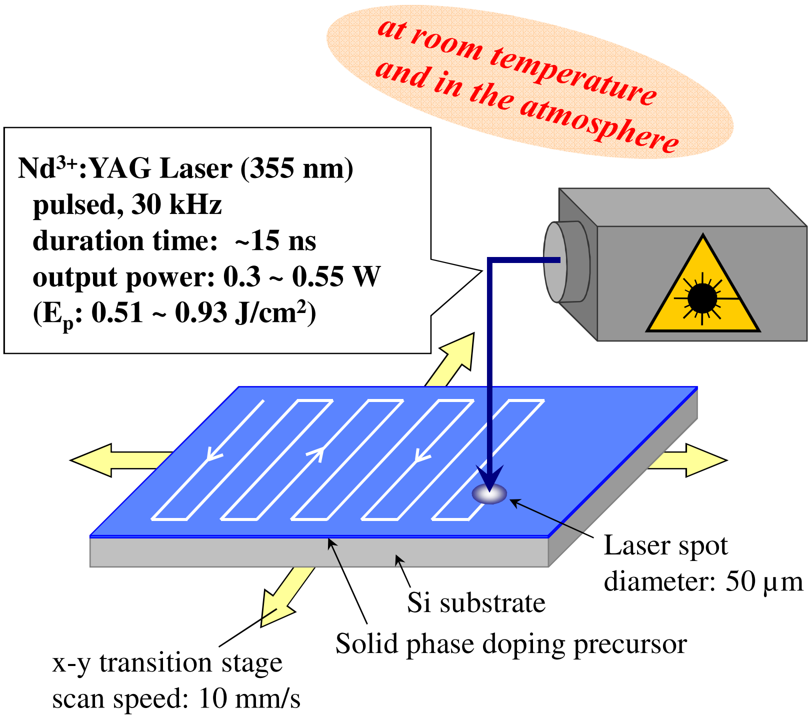

Nd^{3+}:YAG laser

Wavelength: 355 nm
Pulsed, Duration time: ~15 ns
(repetition frequency: variable, normally 30 kHz)

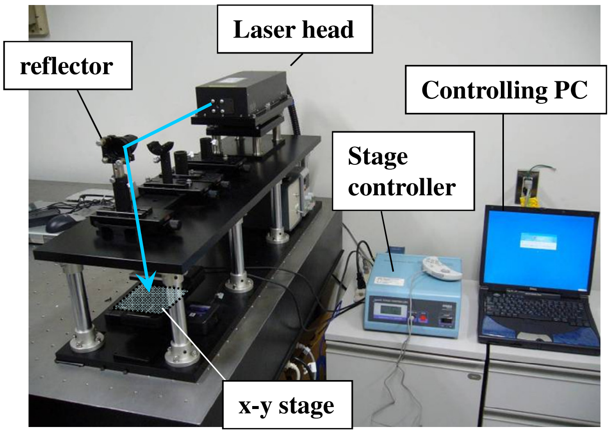

Fig. 5.1: Schematic image of LD technique (upper) and photograph of laser system (down).

doped BSF and any texurization was not applied in this study. It should be emphasized that the highest substrate temperature in this cell fabrication process was 100 °C in the drying step and PECVD.

5.2.3. Doping conditions

As the investigation of doping concentration and depth, the secondary ion mass spectrometry (SIMS) measurement was performed. The profiles of phosphorous and boron atoms doped into p-type silicon substrates with different laser output power were shown in Fig. 5.2 and 5.3, respectively. The highest doping concentration at near silicon surface was around 10^{20}-10^{21} cm^{-3} for phosphorus doping and 10^{19}-10^{20} cm^{-3} for boron doping. Doping depth was controlled by changing the laser output power in the shallower region than 0.3 μm.

The mechanism of LD would be explained as follows [5.20]. Laser irradiation causes the melting of silicon and simultaneously creates dopant atoms by photolysis or pyrolysis of the solid phase doping precursor. Then dopant atoms are incorporated into the molten silicon region by the liquid-phase diffusion during the liquid-phase re-crystallization. At the same time, the activated dopant atoms by the laser would diffuse deeper into silicon substrate. The depth of silicon melting and energy given to dopant atoms strongly depends on the energy density applied at silicon surface, so the doping depth could be controlled by changing laser output power. The difference of phosphorus and boron doping i.e., the concentration or depth would be caused by the difference of conditions of doping precursors because the diffusion coefficient of both atoms in silicon are almost the same. The main difference is the reflectivity of PSG- or BSG-coated silicon samples at 355-nm wavelength, 59.5% in the case of PSG and 10.8% in the case of BSG. However, further investigations will be needed in order to clarify the key factor which determines the doping profiles.

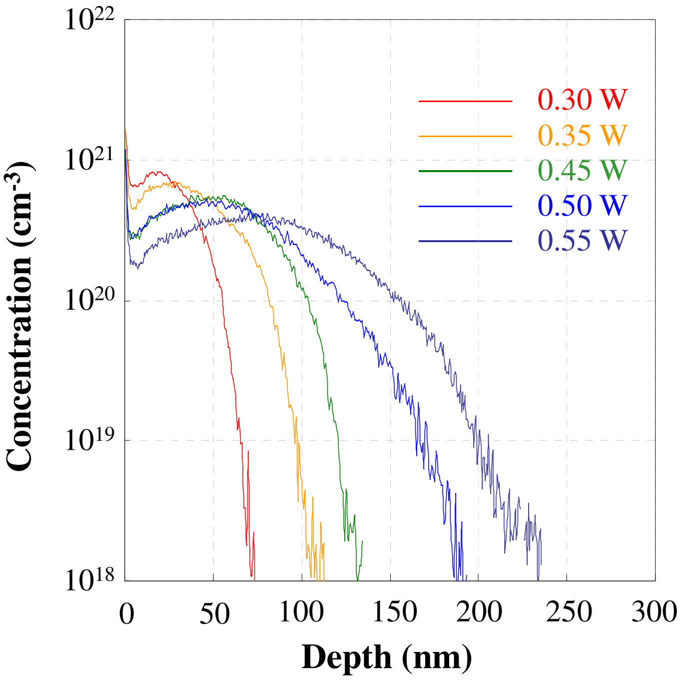

Fig. 5.2: Doping profiles of phosphorus atoms in p-type silicon substrate with different laser output power.

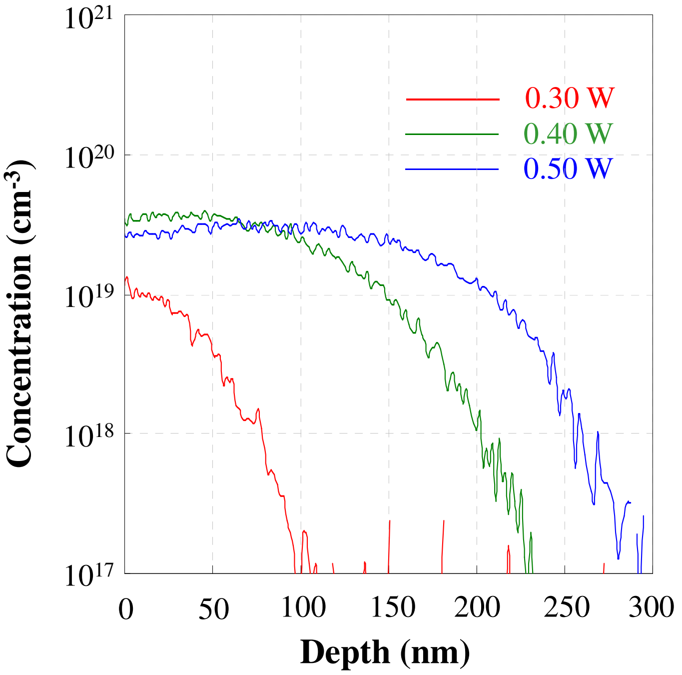

Fig. 5.3: Doping profiles of boron atoms in p-type silicon substrate with different laser output power.

The impurity doping was achieved using an ultraviolet laser at room temperature and in the atmosphere with controlling the doping depth in shallow region, but undesirable atoms such as oxygen and carbon were incorporated at the same time because of the operation under atmosphere. SIMS signals of oxygen and carbon atoms in silicon substrates in phosphorus doping with different laser output power are shown in Fig. 5.4 and 5.5, respectively. For comparison, the data of the conventional thermal diffusion (TD) are also included. The larger number of oxygen and carbon atoms were obtained in LD than TD and the incorporation depth of these atoms followed the laser output power. This is one of the problems of LD in the atmosphere, which should be solved in the future's development.

The symbols in Fig. 5.6 show the measured sheet resistances of the n^+ layers on p-type substrates formed by phosphorus doping by LD with different laser output power. Dashed lines describe the theoretically-calculated sheet resistance of n^+ layer with Gaussian profile as a function of the depth factor with different peak carrier concentration (n_{peak}). In this study, the activation ratio of laser-doped phosphorus atoms was not investigated and thus the exact n_{peak} of laser-doped sample was unknown. However, sheet resistances of laser-doped n^+ layers showed much higher values than the calculations at each depth factor or suitable value for solar cells (lower than 100 Ω/cm^2). This indicated that the actual carrier concentration, in other words, the activation ratio was much lower than assumed, or some additional factors in LD would increase the sheet resistance. The conceivable factors which would increase the sheet resistance were crystalline disorder formation during re-crystallization, doping inhomogeneity and incorporation of oxygen and/or carbon atoms. In further study this high sheet resistance by LD should be improved by dealing with such problems as well as revealing the activation ratio.

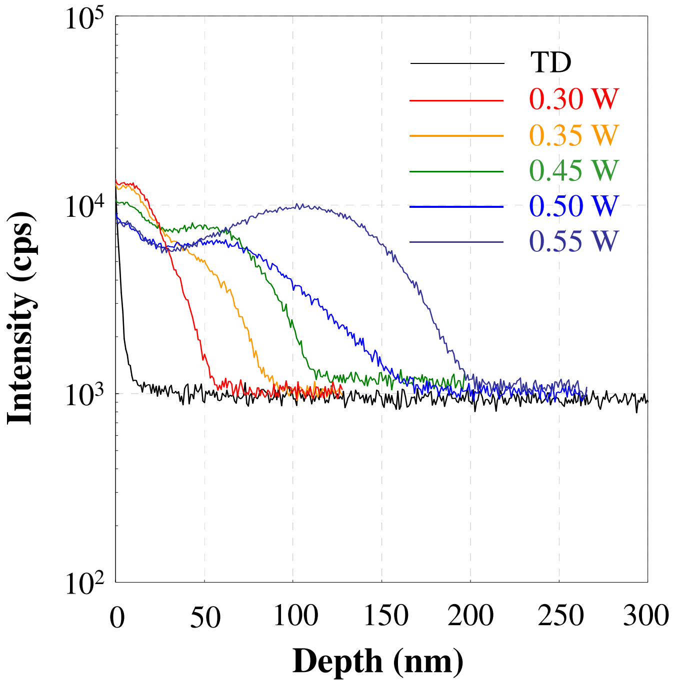

Fig. 5.4: Incorporation profiles of oxygen atoms in p-type silicon substrate with different laser output power in phosphorus doping in comparison with thermal diffusion.

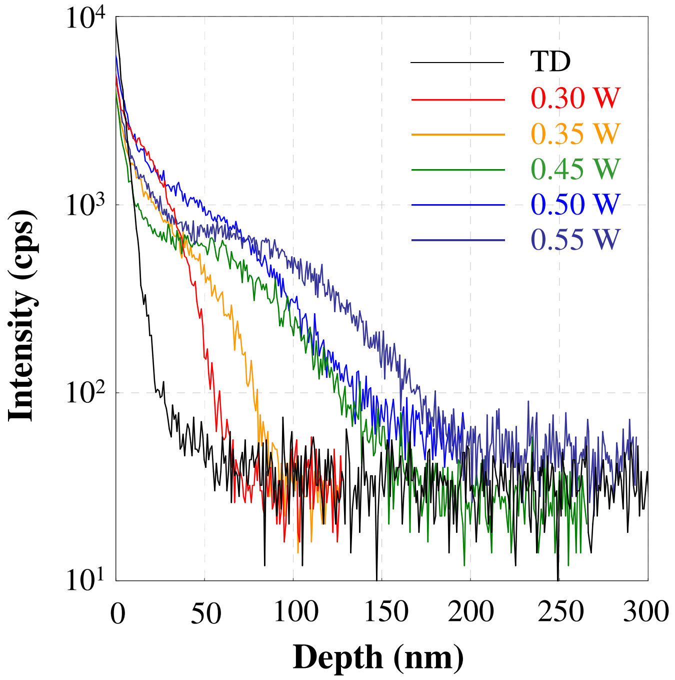

Fig. 5.5: Incorporation profiles of carbon atoms in p-type silicon substrate with different laser output power in phosphorus doping in comparison with thermal diffusion.

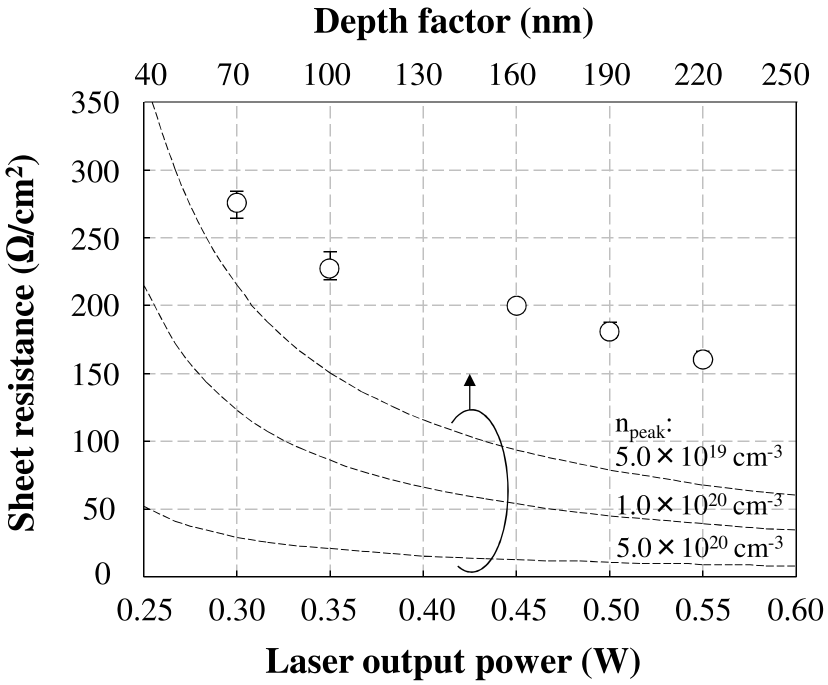

Fig. 5.6: Sheet resistance of the n^+ layer on p-type substrate formed by phosphorus doping by LD as a function of laser output power. Dashed lines describe the theoretically-calculated sheet resistance of n^+ layer with Gaussian profile as a function of the depth factor with different peak carrier concentration (n_{peak}).

5.2.4. Solar cell properties with laser doped-emitter

Figure 5.7 shows the dark current-voltage characteristics of the p-n junctions of p-type silicon solar cells formed by LD technique, compared with p-n junctions formed by TD. As all of the laser-doped samples certainly showed the diode characteristic, the formation of p-n junction by LD at room temperature was confirmed. However, while thermally diffused sample gave the clear 2-step slope (recombination current region and diffusion current region) and enough low reverse current, laser-doped samples showed higher reverse current and recombination current at low forward voltage. In addition, the slope angles of laser-doped samples at high forward voltage were lower than that of TD, indicating higher series resistance. Because the carrier moved horizontal to the junction in emitter layer due to the grid-shaped electrode, this high series resistance could be said to be caused by the high sheet resistance discussed above. Concentrating on laser output power dependency, lines became closer to the case of TD with increasing of laser output power except for the case of 0.55 W. This indicates there should be optimum laser output power for p-n junction formation by LD.

Figure 5.8 shows the average solar cell properties (open circuit voltage: V_{oc}, short circuit current density: J_{sc}, fill factor: *F.F.* and conversion efficiency: *Eff.*) of 6 cells with emitters fabricated by LD as the function of laser output power, as well as that of TD. The red dashed lines in the graphs are the guides to eye. The comparable efficiencies with that of TD were obtained at laser output power of 0.45-0.5 W. J_{sc} at each laser output power was improved rather than TD by the benefit of shallow emitter (TD: 0.5 μm). The remarkable feature is the dependency of V_{oc} on laser output power; marked best results at 0.45-0.5 W and deteriorated both at lower and higher laser output power. This is the same tendency as dark current-voltage curves. At low laser output power, the enough built-in voltage could not be obtained because an emitter was too shallow [5.21]. Too high laser power caused the ablation

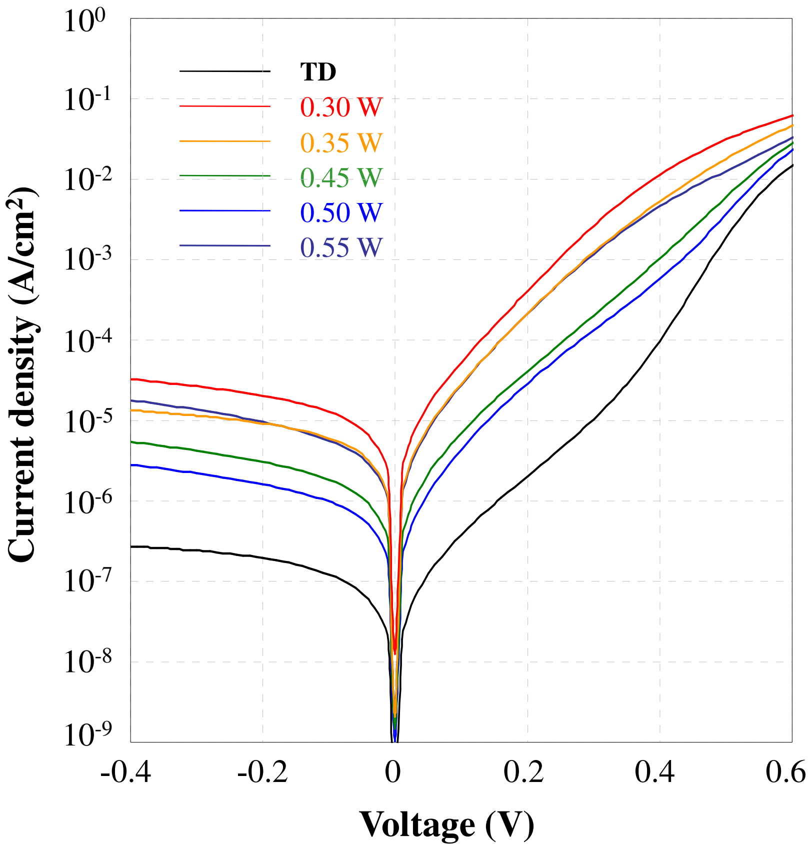

Fig. 5.7: Dark current-voltage characteristics of the p-n junctions of p-type silicon solar cells formed by LD technique, compared with p-n junctions formed by TD.

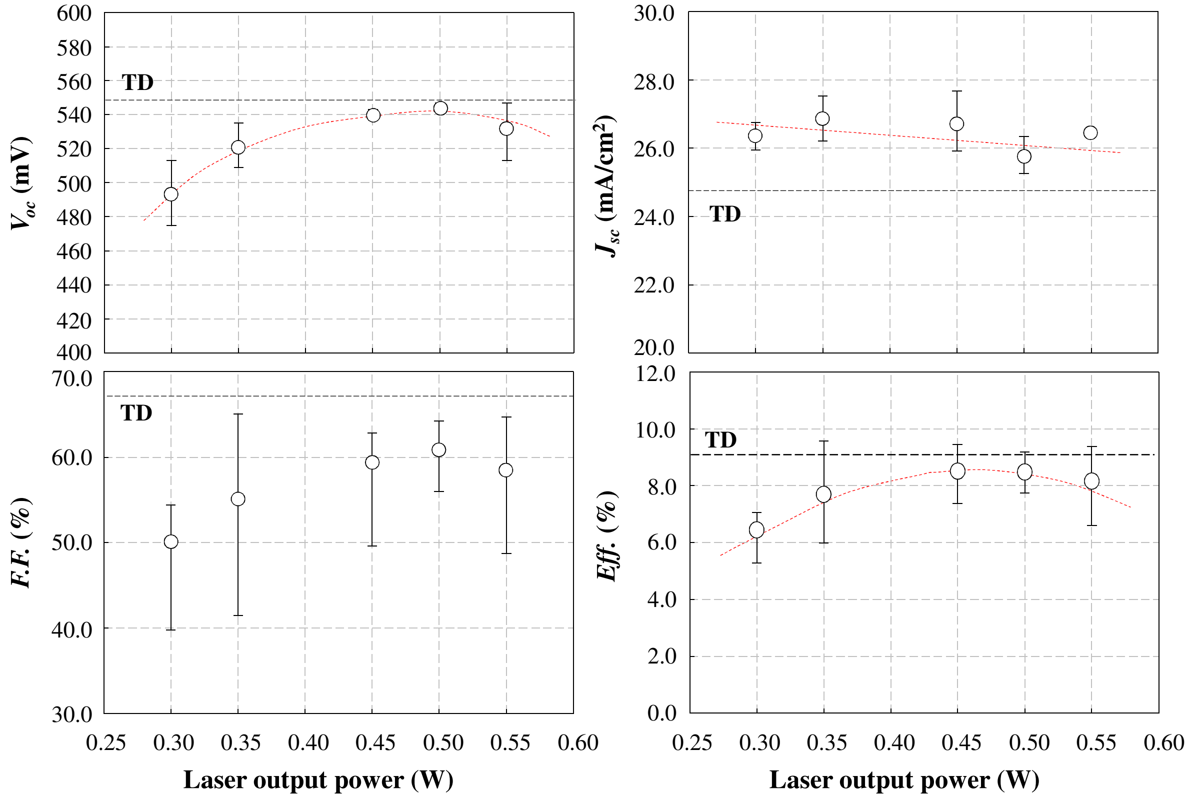

Fig. 5.8: Solar cell properties of cells with emitters fabricated by LD as the function of laser output power, compared with the case of TD. The red dashed lines are the guide for eyes.

of silicon which disturbed the silicon surface and increased the surface recombination, and there were flaws after laser scanning on silicon surface in the case of higher laser power. The feature of *F.F.* followed V_{oc}, but much decreased when compared with TD. The decrease of *F.F.* would be related to the high series resistance indicated in Fig. 5.6 and 5.7. Although this problem of lower *F.F.* should be cleared in future, silicon solar cell with comparable efficiency to conventional method could be obtained in process under 100 °C using LD technique.

Moreover, the electroluminescence (EL) measurement under forward current also gave the proof of high series resistance in emitters fabricated by LD. Figure 5.9 shows EL images of solar cells with emitters fabricated by TD and LD at 0.5 W and their line profiles of EL intensity between indicated points. The images were taken by the cooled (at -55°C) silicon charge-coupled device infrared camera with 2 sec of exposure time, applying a 200-mA/cm^2 forward current. The degree of decrease of EL intensity between grid electrodes was larger in the case of LD than that of TD; decreased about 20-25% like valleys in laser-doped sample while it stayed almost the same in thermal-diffused sample. EL intensity reflects the total number of radiative recombination which is proportional to the total number of minority carriers (electron) in p-type base layer. The total number of electron in base is determined by the injected carrier density from junction and the effective diffusion length of electron and then, EL intensity indicates the emitter or junction condition, assuming there's no distribution of effective diffusion length in monocrystalline materials. The decreased EL intensity between grids showed the less injection of electron to base due to the voltage drop by series resistance. Thus, the higher degree of EL intensity's decreasing between grids in the case of LD than that of TD explained the higher series resistance in emitter by LD [5.22].

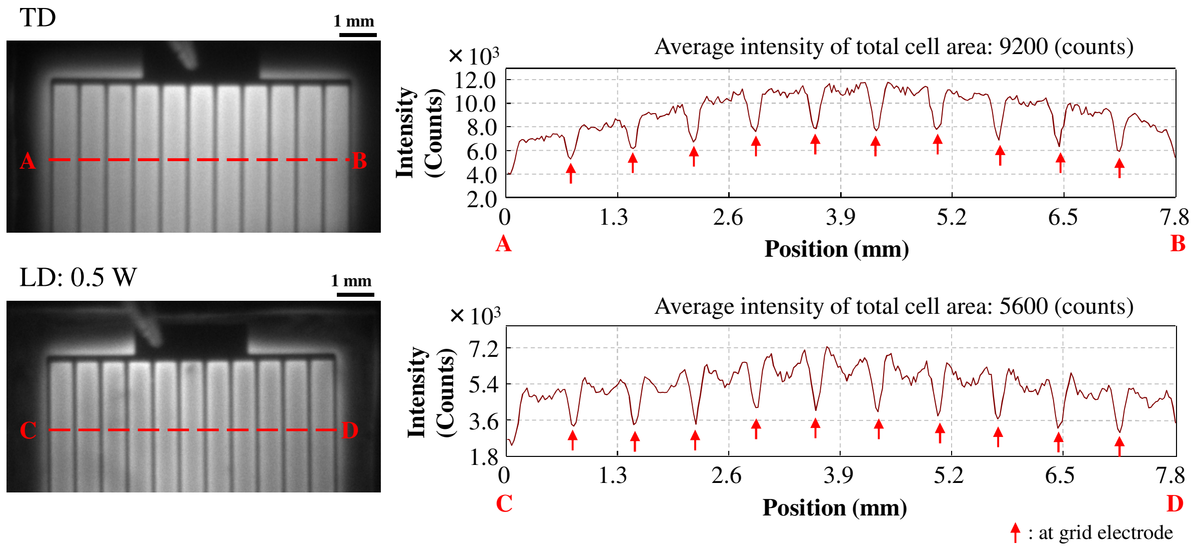

Fig. 5.9: EL results (left: EL images, right: EL intensity line profiles of between indicated points) of solar cells with emitters fabricated by TD and LD at 0.5 W. The images were taken by the cooled (at -55°C) Si CCD camera with 2 sec of exposure time, applying a 200 mA/cm^2 forward current.

5.2.5. Back Surface Field formation

In order to enhance the solar cell properties, boron-BSF layers were formed using LD. As shown in Fig. 5.3, boron atoms could be doped in p-type silicon with the surface concentration of 10^{19}-10^{20} cm^{-3} and depth of 100-300 nm, which was suitable for shallow BSF. Note that the conditions of LD in this section were a little different from former sections; reputation frequency was 34 kHz and overlap rate in y-direction was 80%, and no ARC-SiN layers were deposited. Figure 5.10 shows the illuminated current-voltage characteristics of solar cells with only laser-doped emitter (formed at laser output power of 0.5 W), and with laser-doped emitter (at 0.5 W) and BSF (at 0.35 W). And by forming the very thin and high concentrated BSF by LD, all photovoltaic properties including *F.F.* were improved. The improvement of current density would caused by the driving back effect of carriers by potential barrier at p^+ region, the role of BSF. In addition, *F.F.* would be improved by the contact resistance reduction. And effect of laser-doped BSF was also confirmed in external quantum efficiency measurement shown in Fig. 5.11 (in this case, BSF was formed at laser output power of 0.3 W); the response at rear side (over 900 nm wavelength) was increased.

5.2.6. Laser doping for multicrystalline silicon solar cell

LD was also performed on multicrystalline silicon (mc-Si: 1-4 Ω·cm, 300 μm thickness, p-type, Cast-grown wafer) to form n^+ emitter layer. The condition of LD was the same as BSF formation as mentioned above and laser output power was 0.5 W. Figure 5.12 shows the illuminated current-voltage characteristics of a fabricated mc-Si solar cell with emitters fabricated by LD, without any ARC, passivation, or texturization. Compared with monocrystalline samples, larger decrease of *F.F.* was obtained, showing much larger influence of shut elements.

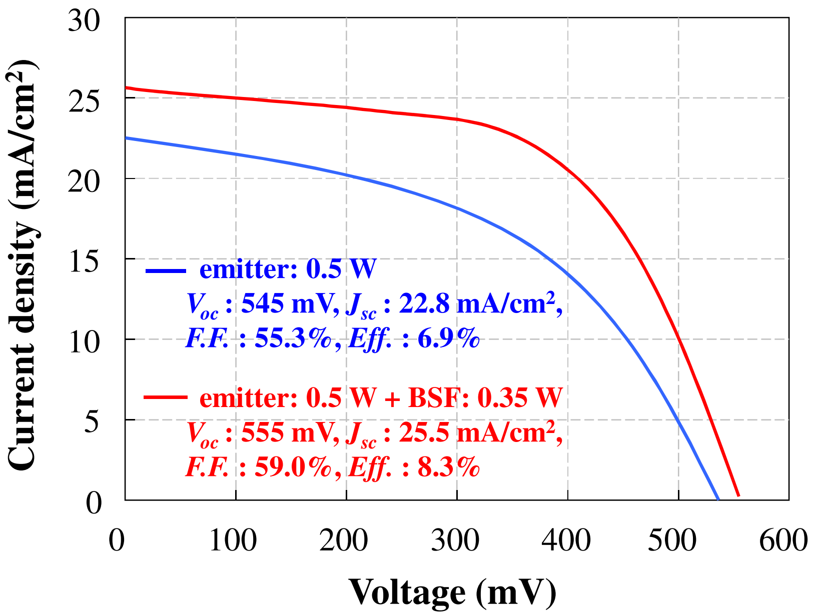

Fig. 5.10: Illuminated current-voltage characteristics of solar cells with only laser-doped emitter formed at laser output power of 0.5 W, and with laser-doped emitter formed at 0.5 W and BSF formed at 0.35 W.

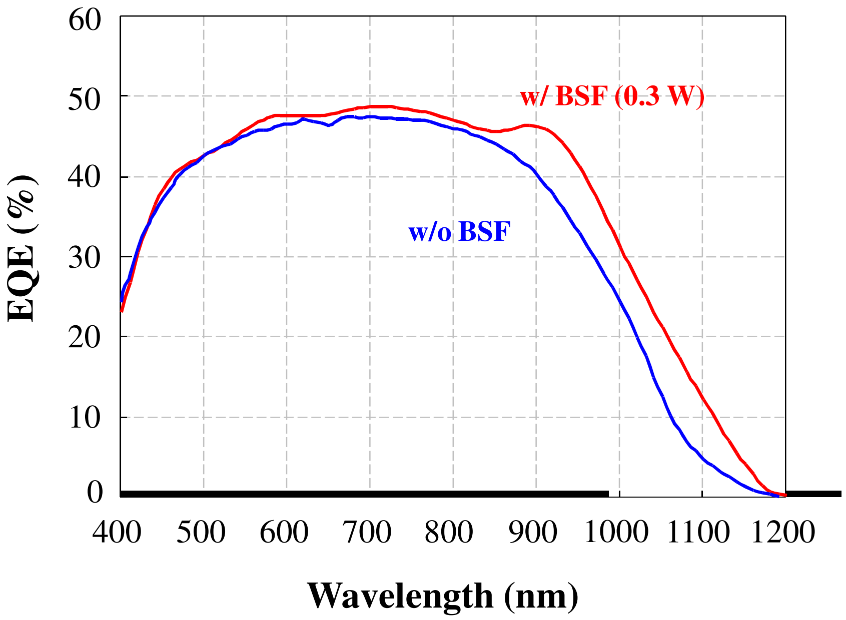

Fig. 5.11: EQE of solar cells with only laser-doped emitter formed at laser output power of 0.5 W, and with laser-doped emitter formed at 0.5 W and BSF formed at 0.3 W.

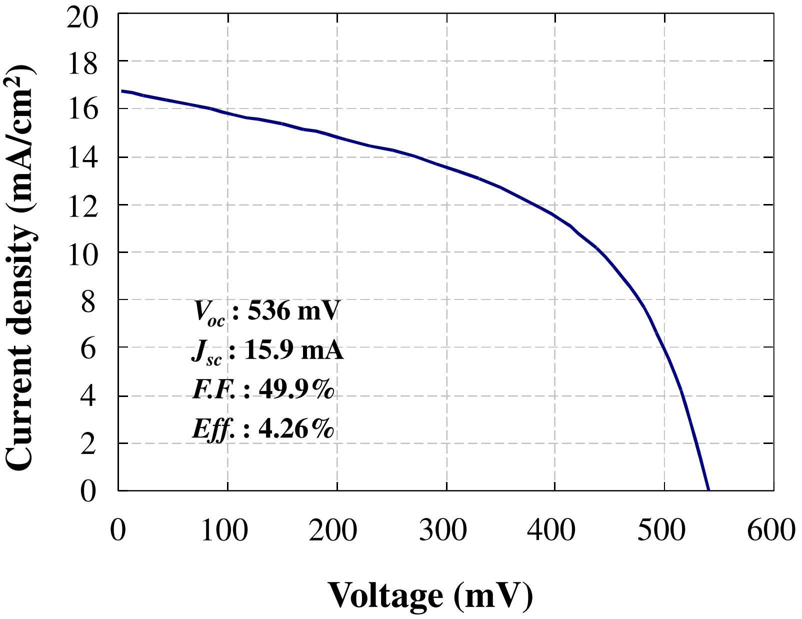

Fig. 5.12: Illuminated current-voltage characteristics of mc-Si solar cells with laser-doped emitter formed at laser output power of 0.5 W.

Figure 5.13 shows the surface images of mc-Si substrate before and after the laser doping. After the laser irradiation, some scars can be seen on the surface as marked by red circles and they became serious near (along) the grain boundaries (GBs). Figure 5.14 shows the Raman scattering spectra of TO-LO-phonon band of the same mc-Si substrates, measured by the 442-nm and 785-nm lasers. The very surface (in the case of 442-nm laser) of laser irradiated sample showed poor crystallinity explained by intensity decrease, position shift from c-Si value (520.5 cm^{-1}) and broadening of the peak, while no significant impacts within material (in the case of 785-nm laser). The mechanism of laser doping is explained as the local melting of silicon by laser irradiation and instantly local re-crystallization combined with the liquid phase diffusion of dopant atoms. The crystallinity after re-crystallization depends on how homogeneous the melting and re-crystallization are. Therefore, if there are some inhomogeneous points on surface like GBs, it would become easier to form badly damaged area easily. In addition, there’s a possibility of segregation of incorporated atoms (P, O, C) at around GBs. These factors would be the reasons of shunt elements.

5.3. Development of poly-Si thin film solar cells on alumina substrates

The LD technique which had very wide utility suitable to poly-Si thin film solar cell fabrication as well as bulk c-Si solar cell process were well-investigated as mentioned above. Using this technique, the interdigitated-type poly-Si thin film solar cells on alumina substrates were fabricated by way of trial.

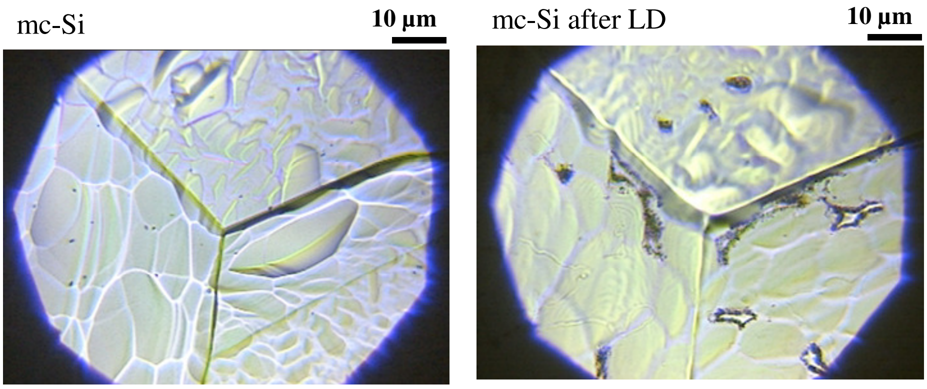

Fig. 5.13: Surface images of mc-Si substrate before and after LD.

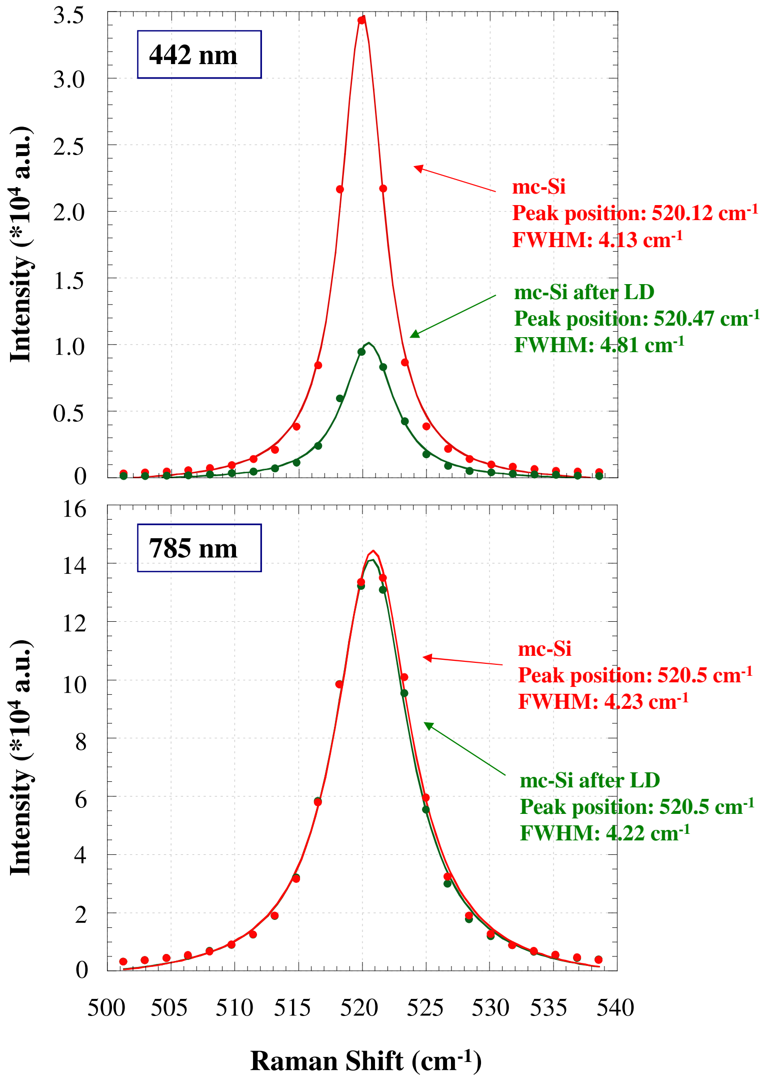

Fig. 5.14: Raman scattering spectra of TO-LO-phonon band of mc-Si before and after LD, measured with the 442-nm and 785-nm lasers.

5.3.1. Device structure of poly-Si thin film solar cells

Three types of device structure are available for poly-Si thin film solar cells considering how to make contacts; a both-side-contact-type, a side-contact-type and an interdigitated-type, as schematically illustrated in Fig. 5.15. Each structure has advantages and disadvantages. In the case of the both-side-contact-type, simple and effective processes of fabrication and integration close to commonly-used ones for the conventional bulk crystalline silicon are available, but substrate selection becomes difficult. In side-contact-type and interdigitated-type, non-conductive materials such as alumina (the most useful candidate of foreign cheap substrate) can be used as substrate, but shading loss by electrodes becomes higher and fabrication process is somehow complicated. For the integration of cells, the interdigitated-type has been proved better [5.23], and many institutes or companies employ this structure [5.24, 5.25]. And LD technique will solve the problem of complicated process of the interdigitated-type which needs several photolithography steps conventionally. Hence in this study, the interdigitated-type structure was applied with photolithography process and LD process.

5.3.2. Fabrication of poly-Si thin film solar cells

The fabrication sequences of poly-Si thin film solar cells on alumina substrates with the p-n junction formed by a conventional thermal diffusion method with photolithography technique and by a new laser doping technique are arranged in Table 5.1 and 5.2, respectively. Both processes consist; 1. substrate preparation, 2. poly-Si deposition, 3. emitter formation (p-n junction formation), 4. contacts formation, and 5. anti-reflection coating (ARC) deposition. The difference is in the emitter formation step, and other steps were performed in the same condition.

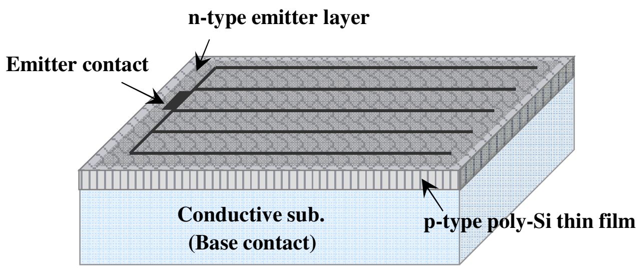

(a) Both-side-contact type

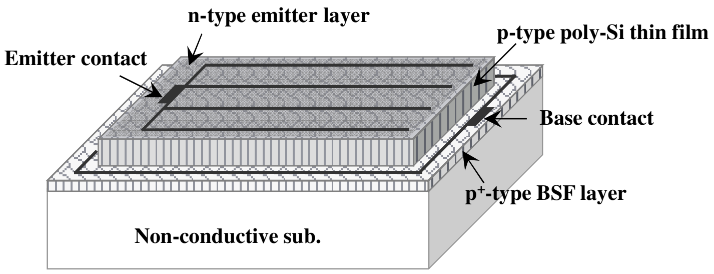

(b) Side-contact type

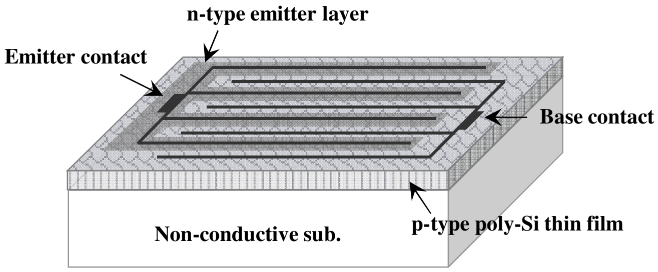

(c) Interdigitated type

Fig. 5.15: Three types of available structure for poly-Si thin film solar cells considering how to make contacts; a both-side-contact-type (upper), a side-contact-type (middle) and an interdigitated-type (down).

Table 5.1: Fabrication process of poly-Si thin film solar cells with thermal diffusion.

Process	Technique	Schematic illustration
Substrate preparation	✓ Ultrasonic cleaning ✓ SiO_x intermediate layer formation by PECVD	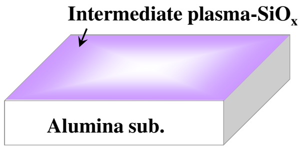
Poly-Si deposition	✓ Thermal APCVD	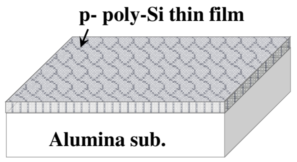
Emitter formation	✓ SiO_x diffusion barrier formation by PECVD ✓ Locally diffusion barrier removal using photolithography	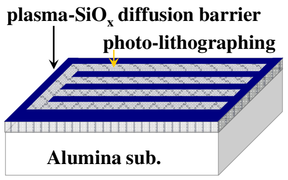
	✓ PSG formation by spin coating an drying	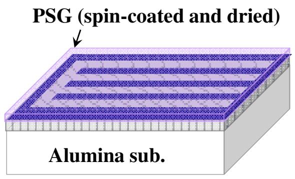
	✓ Solid phase thermal diffusion at 900 °C ✓ PSG and diffusion barrier removal by dipping in HF	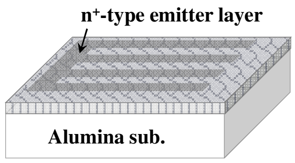
Contacts formation	✓ Evaporation of electrodes (Al)	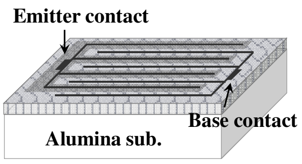
ARC	✓ SiN_x ARC formation by PECVD	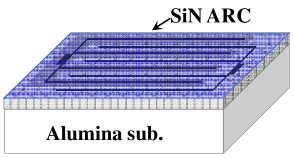

Table 5.2: Fabrication process of poly-Si thin film solar cells with laser doping.

Process	Technique	Schematic illustration
Substrate preparation	✓ Ultrasonic cleaning ✓ SiO_x intermediate layer formation by PECVD	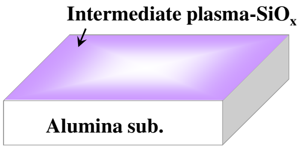
Poly-Si deposition	✓ Thermal APCVD	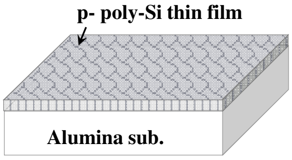
Emitter formation	✓ PSG formation by spin coating an drying ✓ Laser doping using 355-nm pulse laser (local area doping) ✓ PSG removal by dipping in HF	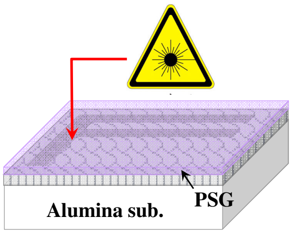
Contacts formation	✓ Evaporation of electrodes (Al)	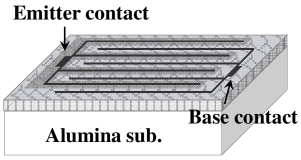
ARC	✓ SiNx ARC formation by PECVD	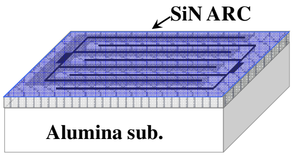

As the substrate preparation, alumina substrates were cleaned by ultrasonic cleaning in acetone liquid in 2 min at room temperature, followed by the intermediate SiO_x layer formation by PECVD in condition shown in Table 2.5. The reference silicon substrates were also prepared with RCA cleaning. On these substrates, p-type poly-Si thin films were deposited by thermal-APCVD at 1100 °C with in-situ grain size controlling by an intermittent source gas supply method. The deposited poly-Si thin film had the thickness of approximately 10 μm and carrier concentration of around 10^{17} cm^{-3}.

The interdigitated-type emitter was formed by a conventional thermal diffusion (TD) method with photolithography technique and by LD. In TD, firstly 500-nm-thick SiO_x layer was formed on the surface of poly-Si thin film by PECVD as the diffusion barrier for P, and subsequently removed at the interdigitate-shaped area for an emitter by using the photolithography technique. Then, the dopant contained liquid was spin-coated and dried on a hotplate at 100 °C to obtain the solid phase doping precursor, and thermally-treated in the furnace at 900 °C, 30 min, in N_2 ambient; so-called solid phase diffusion. In LD, solid phase doping precursor was formed directly on full-surface of poly-Si thin film and laser irradiation was demonstrated locally at the part for an emitter, using a Nd^{3+}:YAG pulsed laser with 355-nm wavelength and duration time of 15 ns at room temperature in the atmosphere. The laser output power, reputation frequency, laser spot diameter, stage scanning speed, x- and y-overlap rate were 0.5 W, 34 kHz, 50 μm, 10 mm/s, 99.3%, and 80%, respectively.

After the emitter formation, the residual PSG and diffusion barrier SiO_x were removed by dipping in HF solution, followed by the both contact formation of Al by vacuum evaporation. And then, the SiN_x layer with thickness of about 70 nm as ARC was formed by PECVD. The overview of a fabricated poly-Si thin film solar cell on alumina substrate is shown in Fig. 5.16.

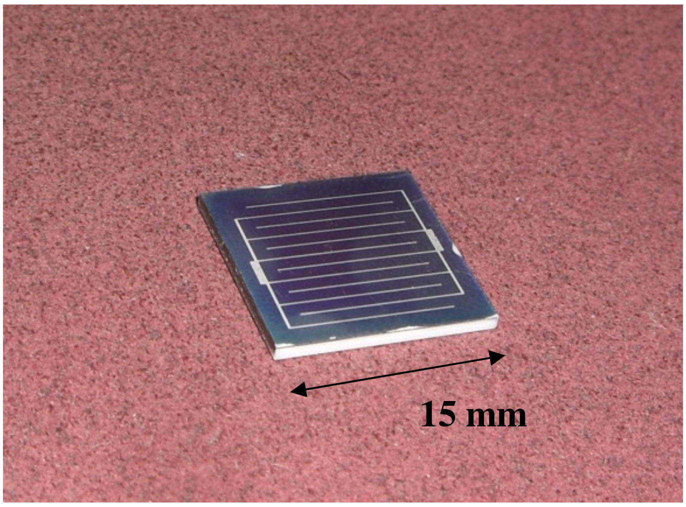

Fig. 5.16: Overview of the fabricated poly-Si thin film solar cell on alumina substrate with the interdigitated structure.

Finally, the fabricated poly-Si thin film solar cells were treated by high-pressure water vapor heat treatment (HWT) developed in Chapter 4 at 1.52 MPa and 300 °C.

5.3.3. Poly-Si thin film solar cell properties

Figure 5.17 shows open circuit voltage of fabricated poly-Si thin film solar cells. First of all, each sample showed certain photo-generated voltage. However, they were still poor properties because the cell fabrication process has not established well.

Poly-Si thin film solar cell on alumina substrates showed reduced voltage than the case of cells on silicon substrates, as expected. This is due to the higher inner compressive stress resulted from the difference of thermal expansion coefficient between silicon and alumina, as discussed in Chapter 3. However, the grain size enlargement from a few μm to 6-10 μm led to the increase of V_{oc} by 20-60 mV. This is the outcome of reduction of recombination by decreasing both GBs and internal stress. Comparing the emitter formation method, the conventional TD still led to the higher value of voltage. There is a possibility that poly-Si thin film is easier to create laser damages than bulk mc-Si thanks to the large amount of GBs. No detail investigation could be done on the interdigitated-type p-n junction, especially formed by LD, and then, more discussion is necessary in further study.

The effect of HWT was clearly shown. V_{oc} was improved by more than 30 mV, much higher than the case of bulk mc-Si. And the spectral response of poly-Si thin film solar cell was much improved by HWT, as shown in Fig. 5.18. Especially in short wavelength region, the drastic increase could be seen, implying the effective defect passivation near p-n junction. So far it is inevitable that the response above 500 nm is poor because of ‘thin film’, more improvements are indispensable in further development such as applying the micro-texturization techniques.

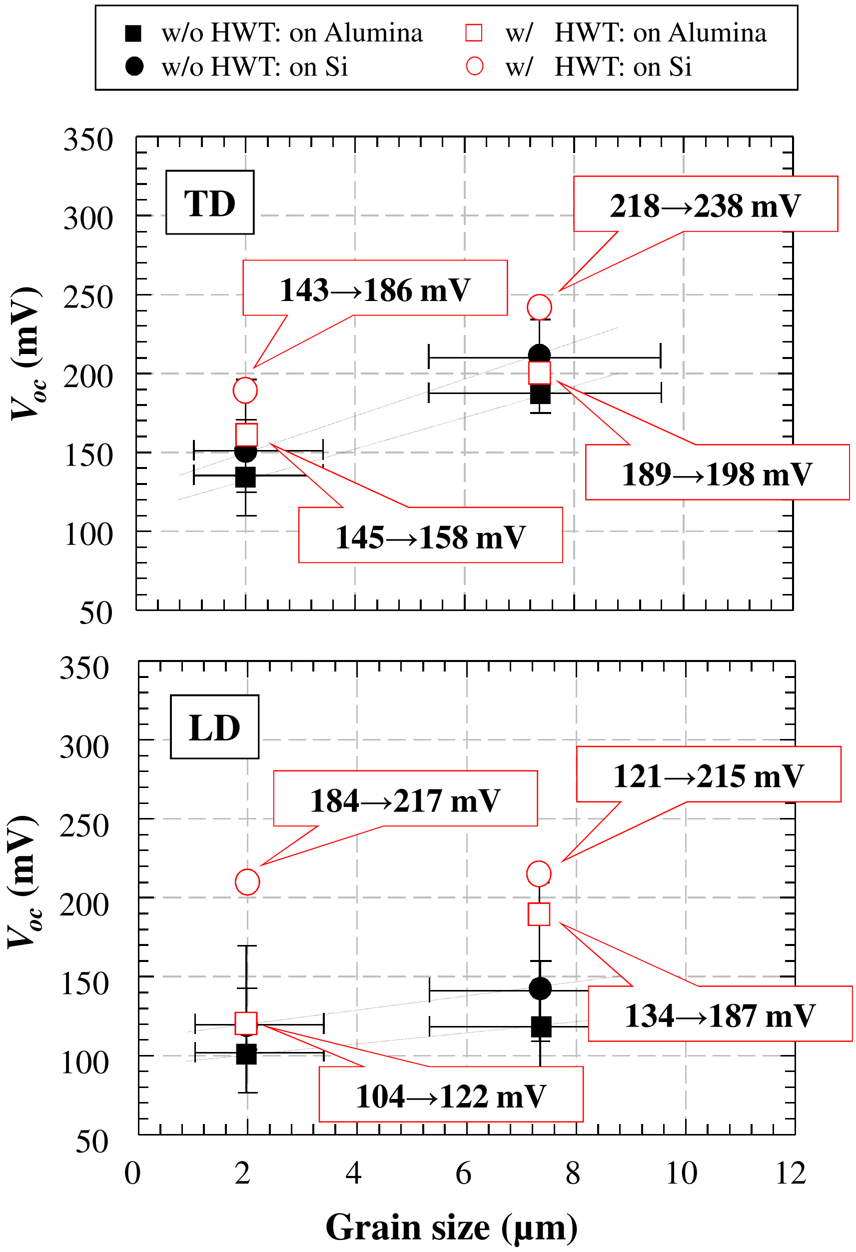

Fig. 5.17: Open circuit voltage of the interdigitated-type poly-Si thin film solar cells on alumina and silicon substrates with different grain size, fabricated by TD and LD, with and without HWT.

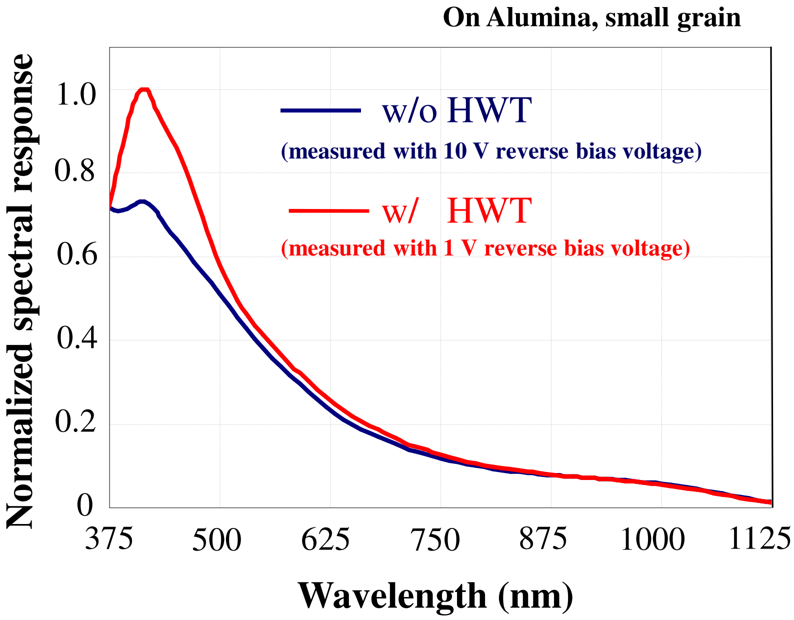

Fig. 5.18: Normalized spectral response of the interdigitated-type small-grained poly-Si thin film solar cells on alumina substrates with and without HWT.

5.4. Summary

In the first part of this Chapter, laser doping technique for crystalline silicon solar cell fabrication was developed and discussed. In this study, a pulsed laser with 355-nm wavelength was used for the doping of both phosphorous and boron atoms into p-type mono- and multi-crystalline silicon with controlling the doping conditions by changing the laser output power. Crystalline silicon solar cells were fabricated at very low temperature below 100 °C. As the result, doping depth was precisely controlled by changing the laser output power in shallow region under 0.3 μm with high doping concentration at near silicon surface of 10^{19}-10^{21} cm^{-3}. Although silicon solar cells with laser doped-emitter had the problem of the high series resistance which deteriorated *F.F.*, comparable values of V_{oc} and J_{sc} to conventional thermal diffusion were obtained. In addition, by forming the very thin and high concentrated BSF by LD, all photovoltaic properties including *F.F.* were improved. By the shallower doping using a short-wavelength laser, the effective formation of emitters and back surface fields was confirmed. Multicrystalline silicon solar cell showed decreased *F.F.* value, which indicates the damage creation at around GBs.

The interdigitated-type poly-Si thin film solar cells on alumina substrates were fabricated by the way of trial, and certain photo-generated voltage was obtained. Poly-Si thin film solar cells on alumina substrates showed lower voltage than that of cells fabricated on silicon, due to the higher inner compressive stress. However, the grain size enlargement led to the increase of V_{oc} by 20-60 mV, because of decreasing both GBs and internal stress. Comparing the emitter formation method, the conventional TD still led the higher value of voltage. The effect of HWT was clearly shown; V_{oc} and the spectral response were improved, implying the effective defect passivation near p-n junction.

References of Chapter 5

[5.1] H. B. Serreze, K. V. Tavi, and C. V. Hari Tao: Appl. Phys. Lett., **32** (1978) p.503.

[5.2] P. H. Holloway: J. Van. Sci. Technol., **21** (1982) p.19.

[5.3] G. Beaucarne, M. Caymax, I. Peytier, and J. Poortmans: Solid State Phenomena, **80-81** (2001) p.269.

[5.4] G. Beaucarne, J. Poortmans, M. Caymax, J. Nijs, and R. Mertens: Solid State Phenomena, **67-68** (1999) p.577.

[5.5] T. Yamazaki: Ph. D. Thesis, Graduate School of Materials Science, Nara Institute of Science and Technology (2005) p.80.

[5.6] E. Schneiderlöchner, R. Preu, R. Lüdemann, and S. W. Glunz: Progr. Photovolt., **10** (2002) p.29.

[5.7] J. Rentsch , F. Bamberg, E. Schneiderlöchner, and R. Preu: Proc. of 20th European Photovoltaic Solar Energy Conference (2005) p.1321.

[5.8] T. M. Bruton, N. B. Mason, S. Roberts, O. Nast-Hartley, S. Gledhill, J. Fernandez, R. Russell, G. Willeke, W. Warta, S. W. Glunz, and O. Schultz: Proc. of 3rd World Conference on Photovoltaic Energy Conversion (2003) p.899.

[5.9] S. Hermann, P. Engelhart, A. Merkle, T. Neubert, T. Brendemühl, R. Meyer, N. P. Harder, and R. Brendel: Proc. of 22nd European Photovoltaic Solar Energy Conference (2007) p.970.

[5.10] T. Sameshima, S. Usui, and M. Sekiya: J. Appl. Phys., **62** (1987) p.711

[5.11] S. Matsumoto, S. Yoshioka, J. Wada, S. Inui, and K. Uwasawa: J. Appl. Phys., **67** (1990) p.7204.

[5.12] M. Ametowobla, A. Esturo-Bretón, J. R. Köhler, and J. H. Werner: Proc. of 31st IEEE

Photovoltaic Specialists Conference (2005) p.1277.

[5.13] C. Carlsson, A. Esturo-Bretón, M. Ametowobla, J. R. Köhler, and J. H. Werner: Proc. of 21st European Photovoltaic Solar Energy Conference (2006) p.938.

[5.14] A. Esturo-Bretón, M. Ametowobla, C. Carlsson, J. R. Köhler, and J. H. Werner: Proc. of 21st European Photovoltaic Solar Energy Conference (2006) p.1247.

[5.15] B. S. Tjahjono, J. H. Guo, Z. Hameiri, L. Mai, A. Sugianto, S. Wang, and S. R. Wenham: Proc. of 22nd European Photovoltaic Solar Energy Conference (2007) p.966.

[5.16] M. Ametowobla, J. R. Köhler, A. Esturo-Bretón, and J.H.Werner: Proc. of 22nd European Photovoltaic Solar Energy Conference (2007) p.1403.

[5.17] C. Carlsson, A. Esturo-Bretón, M. Ametowobla, J. R. Köhler, and J. H. Werner: Proc. of 22nd European Photovoltaic Solar Energy Conference (2007) p.1593.

[5.18] C. Carlsson, J. R. Köhler, and J. H. Werner: Tech. dig. of 17th Int’l Photovoltaic Science and Engineering Conference (2007) p.538.

[5.19] Y. Takahashi, J. Nigo, A. Ogane, Y. Uraoka, and T. Fuyuki: Jpn. J. Appl. Phys., **47** (2008) p.5320.

[5.20] T. Sameshima, and S. Usui: Jpn. J. Appl. Phys., **26** (1987) L1208.

[5.21] S. M. Sze: “Physics of Semiconductor Devices”, Wiley (1981) p.823.

[5.22] K. Bothe, P. Oohl, J. Schmidt, T. Weber, P. Altermatt, B. Fischer, and R. Brendel: Proc. of 21st European Photovoltaic Solar Energy Conference (2006) p.597.

[5.23] I. Gordon, L. Carnel, D. Van Gestel, G. Beaucarne, and J. Poortmans: Thin Solid Films, Vol. **516**, Issue 20 (2008) p.6984.

[5.24] A. Slaoui, E. Pihan, and A. Focsa: Solar Energy Materials and Solar Cells, **90** (2006) p.1542.

[5.25] M. J. Keevers, A. Turner, U. Schubert, P. A. Basore, and M. A. Green: Proc. of 20th European Photovoltaic Solar Energy Conference (2005) p.1305.

Chapter 6

Conclusions

6.1. Summary

Systematic investigation has been carried out for polycrystalline silicon (poly-Si) thin films fabricated by atmospheric pressure chemical vapor deposition on foreign substrates, heading for the photovoltaic applications, concentrating on the improvement of poly-Si thin films' crystallographic and electronic properties with grain size enlargement and defect passivation. The target value was set as $L_g/2S_{GB}$ (L_g: grain size, S_{GB}: surface recombination velocity at grain boundaries (GBs)) of over 5.0×10^{-8} s to be competitive as energy source. The results are summarized as follows.

In Chapter 2, a deposition technique for enlargement of grain size has been investigated. Poly-Si thin films with large grain size have been deposited directly on foreign and cheap alumina substrates by an intermittent source gas supply method. The grain size of poly-Si thin films could be successfully controlled directly in deposition period by the 2-step deposition method with nucleation controlling. The nucleus density could be controlled in the range from 10^6 to 10^{10} cm^{-2} on both silicon and alumina substrates with SiO_x intermediate layers. Then, the grain size could be controlled in the range from a few μm to over 10 μm, the suitable value for solar cell designing. It can be concluded that the deposition of large grain poly-Si thin films fabricated by using the intermittent source gas supply method is applicable effectively to the low-cost processing of poly-Si thin film solar cells.

In Chapter 3, the crystalline quality of poly-Si thin films was investigated, concerning the grain size and substrate type. The crystallinity of poly-Si thin films was improved by grain size enlargement by nucleation control. This was cofirmed by the TO-LO phonon Raman peak and appearance of the TO-BE phonon band in PL spectra. Large grain size could relax the stress caused by grain collisions during the film growth. Hall mobility increased up to 60 cm^2/Vs in poly-Si thin films with grain size of 12 μm without any passivation due to decrease of carrier scattering at grain boundaries. Large compressive stress was found in poly-Si thin films with small grain size on alumina substrates. Crystalline disorder and compressive stress was dramatically reduced with an increase of grain size. Smaller TO-BE PL peak was observed in poly-Si thin films on alumina substrates in spite of the same grain size of poly-Si thin films on oxidized silicon. Tail-to-tail and D1 peaks were substantially shifted to higher energy as the grain size enlargement. Deep tail states were observed in poly-Si thin films on alumina substrates and the deep tail states and/or deteriorated grain lead to poor electronic properties than that on silicon substrates. KFM measurement for microscopic characterization revealed that the value $L_g/2S_{GB}$ equals to 1.42×10^{-10} s, much less than the target of 5.0×10^{-8} s for poly-Si thin films with small grains on silicon substrates. The simple assumption of the difference of grain size brings one order higher value of $L_g/2S_{GB}$ in case of poly-Si thin films with enlarged grain. Additionally, the quality of intra-grain would be improved by grain size enlargement, however it is expected that poly-Si thin films on alumina substrates have poor crystallinity.

In Chapter 4, for a new technique of passivation with advantages of simple, safe, and at low temperatures, high-pressure water vapor heat treatment (HWT) was proposed and demonstrated on both bulk crystalline silicon solar cells with SiO_x or SiN_x passivation layer, and poly-Si thin films. By the treatment at 1.52 MPa and 300 °C, a Si-O-Si bonding network formation, which would terminate the silicon dangling bonds, was confirmed from FT-IR and SIMS measurement. For bulk crystalline silicon solar cells with SiO_x and SiN_x passivation layers, the reduction of recombination centers improved the photovoltaic performances, increasing the conversion efficiency by approximately 1%. From the investigation of EL emission intensity, the passivation effect at defects such as GBs was confirmed as well as the surface passivation. HWT was also effective to poly-Si thin films, and this was confirmed in improvements of crystallinity, Hall mobility and potential barrier height at GBs (ϕ_b). The distributions of ϕ_b, the trap density at GBs (N_T) and S_{GB} were clearly shifted to lower values and the value $L_g/2S_{GB}$ increased to 1.74×10^{-9} s by HWT.

In Chapter 5, the interdigitated-type poly-Si thin film solar cells on alumina substrates were fabricated by the way of trial with using the laser doping (LD) technique. First, LD for bulk crystalline silicon solar cell fabrication was developed with a pulsed laser with 355-nm wavelength and investigated. The doping depth was precisely controlled by changing the laser output power in shallow region under 0.3 μm with high doping concentration at near silicon surface of 10^{19}-10^{21} cm^{-3}. Although silicon solar cells laser-doped emitter had the problem of the high series resistance which deteriorated fill factor (*F.F.*), comparable values of open circuit voltage (V_{oc}) and short circuit current density (J_{sc}) to that of cells fabricated with a conventional thermal diffusion were obtained. And by forming the very thin and high concentrated back surface fielld by LD, all cell properties including *F.F.* were improved. By the shallower doping using a laser with short-wavelength, the effective formation of emitter and BSF was confirmed. However, a multicrystalline silicon solar cell showed decreased *F.F.*, which indicates the damage creation at around GBs. Poly-Si thin film solar cells on alumina substrates showed lower voltage than that of cells fabricated on silicon, due to the higher inner compressive stress. However, the grain size enlargement led to the increase of V_{oc} by 20-60 mV, because of decreasing both GBs and internal stress. Comparing the emitter formation method, the conventional TD still led the higher value of voltage. The effect of HWT was clearly shown; V_{oc} and the spectral response were improved, implying the effective defect passivation near p-n junction.

6.2. Outlooks

For further improvement of poly-Si thin film solar cells with high and stable efficiency by low-cost fabrication, following issues must be cleared.

1. In this work, alumina was applied for the substrate with several reasons. However, the other candidates should be taken into account, comparing with each other. Each candidate has advantages and disadvantages for cell applications, but should be investigated from the point of the quality of poly-Si thin films as in this study.

2. The electronic properties which are related to solar cell properties were estimated with a lot of assumptions in this study. The measurements that can investigate the action of photo-generated carriers directly should be introduced.

3. The more optimization of cell fabrication processing is indispensable. Especially, laser doping technique is still under developing even in bulk crystalline silicon solar cell

fabrication.

4. High-quality passivation methods of defects are indispensable. High-pressure water vapor heat treatment proposed in this study in one answer for easy and low-cost passivation method, however, the effect was not satisfactory established. Some innovative techniques which lead to the excellent passivation are needed.

5. The junction formation is one big issue in poly-Si thin film solar cells. Recently heterojunction by a-Si/c-Si has gathered much attention. Further investigation about junction formation is desirable including laser doping technique.

6. Because of thin silicon material, an effective light trapping structure is necessary. Texturization techniques which are suitable for poly-Si thin film solar cells should be researched such as micro-texturing using plasma-etching method.

Combination of the perceptions obtained in this study and new technologies that solve the problems above will lead to poly-Si thin film solar cells with high-performance, which play an important role in the society.

Appendix: Summary of characterization methods

1. AFM, C-AFM, KFM

The atomic force microscope (AFM) is a very high-resolution type of scanning probe microscope, with demonstrated resolution of fractions of a nanometer. The AFM was invented by Binnig, Quate and Gerber in 1986, and is one of the foremost tools for imaging, measuring and manipulating matter at the nano-scale [A.1]. AFM can provide illustrative topography information about the surface of almost any type of materials within the field view of 100 μm×100 μm down to the atomic resolution. Traditionally, the sample is mounted on a piezoelectric tube that can move the sample in the z direction for maintaining a constant force, and the x and y directions for scanning the sample.

The AFM consists of a micro-scale cantilever with a sharp tip (probe) at its end that is used to scan the specimen surface. The cantilever is typically silicon or silicon nitride with a tip radius of curvature on the order of nanometers. When the tip is brought into proximity of a sample surface, forces between the tip and the sample lead to a deflection of the cantilever according to Hooke's law. Depending on the situation, forces that are measured in AFM include mechanical contact force, Van der Waals forces, capillary forces, chemical bonding, electrostatic forces, magnetic forces, Casimir forces, solvation forces, and so on. Typically, the deflection is measured using a laser spot reflected from the top surface of the cantilever into an array of photodiodes. Other methods that are used include optical interferometry, capacitive sensing or piezoresistive AFM cantilevers.

The AFM can be operated in a number of modes, depending on the application. In general, possible imaging modes are divided into static (also called contact) modes and a variety of dynamic (or non-contact) modes where the cantilever is vibrated.

Combined or current sensing AFM (C-AFM) is suitable for the simultaneous characterization of electronic properties and topography image [A.2]. This combined AFM measurement setup is almost the same as standard AFM system. Cantilever, which must be conductive, is scanning the surface in contact mode, simultaneously detecting the current passing through the sample induced by applied voltage. By this method, topography and local current map can be obtained simultaneously.

Kelvin force microscopy (KFM) is AFM variation, which offers another powerful method for analyzing the surface potential of materials [A.3, A.4]. In KFM measurement, an AC-voltage ($V_{AC}\cdot\sin(\omega\cdot t)$) is applied between the cantilever and the sample, in addition to a DC-bias (V_{DC}). The AC-voltage induces oscillatory electrostatic force (F_{es}),

$$F_{es} = -1/2\cdot(\partial C/\partial z)\cdot V^2, \qquad \text{(A.1)}$$

and the spectral component at the frequency (F_ω) of the AC-voltage results to,

$$F_\omega = (\partial C/\partial z)\cdot(V_{DC} - CP)\cdot V_{AC}\cdot\sin(\omega\cdot t), \qquad \text{(A.2)}$$

where $\partial C/\partial z$ is the capacitance gradient between cantilever and sample and CP is the contact potential, the difference in work function of cantilever and sample. The oscillation is detected using a lock-in amplifier and a controller is used to reduce the amplitude to zero by adjusting V_{AC} to match the *CP*. This V_{DC} value corresponds to the potential difference between the tip and sample surface.

2. EL Imaging

The phenomenon of Electroluminescence (EL) in semiconductor, one form of luminescence following the electric-excitation, is well-investigated from long ago and already applied to device structures such as Light Emitting Diode or EL display. For solar cell characterization, EL Imaging is the very powerful and fast tool providing spatially resolved information about the electrical and optical properties [A.5].

In the case of crystalline silicon solar cells, cell emits infrared light (wavelength: around 1100 to 1200 nm, corresponding to silicon band gap) under forward bias condition, whose intensity reflects the total number of radiative recombination. The total radiative recombination rate is proportional to the total number of minority carriers in active layer, and the total number (N) of minority carrier (electron in p-type or hole in n-type) is determined by the diffusion length (L_n or L_h) and the injected carrier density at the edge of junction ($n_{p(0)}$ or $p_{n(0)}$), expressed as,

$$N = \int_0^{+\infty} n_{p(0)} \exp(-x / L_n) dx = n_{p(0)} L_n \quad \text{(in the case of p-type active layer).} \qquad \text{(A.3)}$$

Then, EL intensity indicates the minority carrier diffusion length at the fixed injection condition. The EL image consist the contrast of intensity, so the darker area corresponds to the shorten diffusion length region by crystalline defects or less injected region by contact breakages. Thus, EL imaging technique can be applied to detect the deteriorated regions in a sample as well as comparison of cell performance among samples very easily and precisely.

3. FT-IR

Infrared spectroscopy (IR spectroscopy) is the subset of spectroscopy that deals with the infrared region of the electromagnetic spectrum. It covers a range of techniques, the most common being a form of absorption spectroscopy. As with all spectroscopic techniques, it can be used to identify compounds or investigate sample composition. Infrared spectroscopy exploits the fact that molecules have specific frequencies at which they rotate or vibrate corresponding to discrete energy levels (vibration modes). These resonant frequencies are determined by the shape of the molecular potential energy surfaces, the masses of the atoms and, by the associated vibronic coupling. In order for a vibration mode in a molecule to be IR active, it must be associated with changes in the permanent dipole. The frequency of the vibrations can be associated with a particular bond type. Simple diatomic molecules have only one bond, which may stretch. More complex molecules have many bonds, and vibrations can be conjugated, leading to infrared absorptions at characteristic frequencies that may be related to chemical groups. For example, the atoms in a CH_2 group, commonly found in organic compounds can vibrate in six different ways; symmetrical and antisymmetrical stretching, scissoring, rocking, wagging and twisting.

The infrared spectrum of a sample is collected by passing a beam of infrared light through the sample. Examination of the transmitted light reveals how much energy was absorbed at each wavelength. This can be done with a monochromatic beam, which changes in wavelength over time, or by using a Fourier transform instrument to measure all wavelengths at once. From this, a transmittance or absorbance spectrum can be produced, showing at which IR wavelengths the sample absorbs. Analysis of these absorption characteristics reveals details about the molecular structure of the sample.

Fourier transform infrared (FT-IR) spectroscopy is a measurement technique for collecting infrared spectra. Instead of recording the amount of energy absorbed when the frequency of the infra-red light is varied (monochromater), the IR light is guided through an interferometer. After passing through the sample, the measured signal is the interferogram. Performing a mathematical Fourier transform on this signal results in a spectrum identical to that from conventional (dispersive) infrared spectroscopy.

4. Hall effect

The basic physical principle underlying the Hall effect is the Lorentz force. When an electron moves along a direction perpendicular to an applied magnetic field, it experiences a force acting normal to both directions and moves in response to this force and the force effected by the internal electric field. For an n-type, the carriers are predominately electrons of bulk density n. When assuming that a constant current I flows along the x-axis from left to right in the presence of a z-directed magnetic field, electrons subject to the Lorentz force initially drift away from the current line toward the negative y-axis, resulting in an excess surface electrical charge on the side of the sample. This charge results in the Hall voltage, a potential drop across the two sides of the sample. This transverse voltage is the Hall voltage V_H and its magnitude is equal to $I \cdot B/q \cdot n \cdot W$, where I is the current, B is the magnetic field, W is the sample thickness, and q is the elementary charge. Thus, by measuring the Hall voltage V_H and from the known values of I, B, and q, one can determine the sheet density n_s of charge carriers in semiconductors by,

$$n_s = I \cdot B / q \cdot V_H \,. \qquad \text{(A.4)}$$

The sheet resistance R_S of the semiconductor can be conveniently determined by use of the van der Pauw resistivity measurement technique. Since sheet resistance involves both sheet density and mobility, one can determine the Hall mobility (μ_H) from the equation,

$$\mu_H = V_H / R_S \cdot I \cdot B = 1/(q \cdot n_S \cdot R_S) \cdot \qquad \text{(A.5)}$$

5. Illuminated current-voltage measurement

The current-voltage measurement under illumination is the most basic and important measurement to characterize the solar cell performance. In the case of the standard sunlight distribution to which the measurements are referenced is AM1.5 (*air mass*) distribution. Recommended illumination sources for testing are natural sunlight (with certain constraints on the presence of clouds, air mass, and the variation of intensity), or an appropriately filtered Xenon lamp whose spectral content is reasonably close to sunlight. The illumination source must give a collimated light of uniform intensity at a measurement plane and be stable during the time of measurement, with the total power of 100 mW/cm^2. A four-point contacting scheme is desirable in which voltage and current leads are kept separated in order to reduce the effect of series resistance.

The relationship between voltage and current of a typical silicon solar cell with p-n homo- junction bases on the ideal diode law,

$$J_d = J_0\{\exp(qV/kT) - 1\}, \qquad \text{(A.6)}$$

where J_d is diode current and J_0 the saturation current density defined as,

$$J_0 = A\left(\frac{qD_n n_i^2}{L_n N_A} + \frac{qD_p n_i^2}{L_p N_D}\right), \qquad \text{(A.7)}$$

where A is the cross-sectional area of the diode (the meaning of other symbols are arranged in List of abbreviations and symbols). When illuminated, the photo-current (J_L) is generated as,

$$J_L = qAG_{av}(L_n + W + L_p)\,, \qquad \text{(A.8)}$$

so the total current (J) as the function of voltage equals to J_d-J_L.

Four parameters are usually used to characterize solar cell outputs. One is the short circuit current density (J_{sc}), ideally equal to J_L. A second parameter is the open circuit voltage (V_{oc}), obtained by setting J=0,

$$V_{oc} = \frac{kT}{q}\ln\left(\frac{J_L}{J_0} + 1\right). \qquad \text{(A.9)}$$

The energy conversion efficiency (η) is then given by,

$$\eta = \frac{P_{\max}}{P_{in}(=100mA/cm^2)} \times 100 = V_{\max} \cdot J_{\max} = V_{oc} \cdot J_{sc} \cdot F.F., \qquad \text{(A.10)}$$

where P_{in} is the total power in the light incident, P_{max} the maximum output power at (V_{max}, J_{max}), and $F.F.$ the fill factor defined as $F.F.=V_{max}\cdot J_{max}/V_{oc}\cdot J_{sc}$.

6. µ-PCD

The measurement of a carrier lifetime is based on the recombination dynamics of excess carriers which are normally generated optically. The detailed analysis of the recombination dynamics is explained by using the continuity equation of the excess minority carriers,

$$\frac{\partial \Delta n}{\partial t} = G_{bulk}(t,x) - U_{bulk}(t,x) + \frac{1}{q}\frac{dJ_n}{dx}, \qquad \text{(A.11)}$$

where G_{bulk} and U_{bulk} are the generation rate and the recombination rate in the bulk, Δn the excess minority carrier density and J_n the electron current density. The combination of the bulk and surface recombination rates into an effective recombination rate (U_{eff}) will define an effective lifetime (τ_{eff}) regardless of the decay time of the illumination source,

$$\tau_{eff} = \frac{\Delta n_{av}}{G_{av}(t) - \partial \Delta n_{av}(t)/\partial t}, \qquad \text{(A.12)}$$

where n_{av} is the average excess carrier density and G_{av} the average generation rate, both calculated over the whole wafer thickness. In the case of the sharp pulse of illumination that is rapidly turned off and subsequent determination of the excess carrier density without illumination, the transient condition, equation (A.12) can be simplified to,

$$\tau_{eff} = \frac{\Delta n_{av}}{\partial \Delta n_{av}(t)/\partial t}, \qquad \text{(A.13)}$$

which is only valid when carrier lifetime is significantly higher than the decay time of the illumination source.

The microwave-detected Photo Conductance Decay (µ-PCD) technique is a pure transient technique; the effective carrier lifetime being determined form asymptotic decay of the average excess carrier density following a pulse-like excitation normally by a diode laser. This decay is monitored via the changes in the sample photo-conductance which in turn is measured via changes in its microwave reflectance since the microwave reflectance is a highly non-liner function of free carrier density [A.6, A.7]. The time dependence of the excess photo-conductance ($\Delta\sigma(t)$) of the sample has the relationship with $\Delta n_{av}(t)$ as,

$$\Delta n_{av}(t) = \Delta\sigma(t) / q \cdot (\mu_n + \mu_p) \cdot W \ , \qquad \text{(A.14)}$$

where W is the sample thickness and μ_n and μ_p are the electron and hole mobility. As μ_n and μ_p are themselves functions of the carrier density, the determination of Δn_{av} requires an iterative procedure on the basis of a carrier-density-dependent mobility model [A.8]. The use of a laser for the excitation enables the mapping of lifetimes with high resolution.

7. PL

Photoluminescence (PL) is a process in which a chemical compound absorbs photons (electromagnetic radiation), thus being excited to a higher electronic energy state, and then, radiates photons out, returning to a lower energy state. Quantum mechanically, this can be described as an excitation to a higher energy state and then a return to a lower energy state accompanied by the emission of a photon. This is one of many forms of luminescence (light emission) and is distinguished by photo-excitation (excitation by photons). The period between the absorption and emission is typically extremely short, in the order of 10 nanoseconds. The sample illuminated by certain wavelength light emits the luminescence related with phonon, band-to-band, tail-to-tail and defects recombination process. PL has been employed for characterization of crystalline silicon for a long time [A.9- A.11]. PL spectra are sensitive to crystalline quality, density of dislocations and thermal oxygen, carrier concentration and also the external stress.

8. Raman spectroscopy

Raman spectroscopy is a spectroscopy technique used in condensed matter physics and chemistry to study vibrational, rotational and other low-frequency modes in a system. The sample is illuminated by the laser light with a certain frequency, which undergoes an inelastic scattering generating phonons. The amount of energy loss is then reflected in the shift of frequency, which is characteristic of the studied material, its structure and chemical bonds.

For silicon material, the Raman scattering spectroscopy is widely used for characterization of structure. The ratio of crystalline-phase peak (TO-LO phonon band, 520.5 cm^{-1}) and amorphous-phase peak (480 cm^{-1}) determines the crystal volume fraction [A.12]. Moreover, Raman spectra contain information about crystalline disorder and stress. FWHM of Raman spectra and band shape are closely related to the crystalline order. The presence of crystalline disorder produces a decrease of the phonon lifetime, which broads the crystalline-phase peak. And the frequency of phonon band depends on the masses and positions of atoms, the inter-atomic forces and the bond lengths. Any effects altering these features will produce a change in the frequency of the band, therefore for instance, tensile stress will determine an increase in lattice spacing and, hence, a decrease in the wavenumber of vibrational mode, and in the case of compressive strain, the decrease of lattice parameter yields a corresponding increase of the vibrational frequency. If the deformation of the structure follows an elastic behavior, the shift will vary linearly with the magnitude of the stress, and as the result, the position of the Raman spectra of crystalline silicon is quite sensitive to the presence of stress. It is well known that sharp Lorentzian band at 520.5 cm^{-1} of the first order Raman spectra of crystalline silicon is quite sensitive to the presence of stress. For a biaxial stress in elastic regime, the stress σ_{in} in silicon can be obtained from,

$$\sigma_{in} = -250 \times \Delta, \qquad \text{(A.15)}$$

where Δ is the Raman shift wavenumber expressed in cm^{-1}[A.13, A.14].

9. SEM

The scanning electron microscope (SEM) is a type of electron microscope that images the sample surface by scanning it with a high-energy beam of electrons in a raster scan pattern. The electrons interact with the atoms that make up the sample producing signals that contain information about the sample's surface topography, composition and other properties such as electrical conductivity. The types of signals produced by SEM include secondary electrons, back scattered electrons (BSE), characteristic x-rays, light (cathode-luminescence), specimen current, and transmitted electrons. These types of signal all require specialized detectors for their detection that are not usually all present on a single machine.

The signals result from interactions of the electron beam with atoms at or near the surface of the sample. In the most common detection mode, secondary electron imaging, the SEM can produce very high-resolution images of a sample surface, revealing details about 1 to 5 nm in size. Due to the way these images are created, SEM micrographs have a very large depth of field yielding a characteristic three-dimensional appearance useful for understanding the surface structure of a sample. A wide range of magnifications is possible, from about ×25 (about equivalent to that of a powerful hand-lens) to about ×250,000, about 250 times the magnification limit of the best light microscopes.

10. SIMS

Secondary ion mass spectrometry (SIMS) is a technique to analyze the composition of solid materials by sputtering the surface of the specimen with a focused primary ion beam and collecting and analyzing ejected secondary ions. These secondary ions are measured with a mass spectrometer to determine the elemental, isotopic, or molecular composition of the surface. SIMS is the most sensitive surface analysis technique, being able to detect elements present in the parts per billion range. Typically, a secondary ion mass spectrometer consists of primary ion gun generating the primary ion beam, primary ion column, accelerating and focusing the beam onto the sample, high vacuum sample chamber holding the sample, the secondary ion extraction lens, and mass analyzer separating the secondary ions according to their mass.

There are three basic types of ion guns. In one, ions of gaseous elements are usually generated with Duo-plasmatrons or by electron ionization for instance oxygen (O^-, O_2^+). A second source type, the surface ionization source, generates Cs^+ primary ions. A third source type, the liquid metal ion source, operates with metals or metallic alloys, which are liquid at room temperature or slightly above. The choice of the ion species and ion gun respectively depends on the required current (pulsed or continuous), the required beam dimensions of the primary ion beam and on the sample which is to be analyzed. Oxygen primary ions are often used to investigate electropositive elements due to an increase of the generation probability of positive secondary ions, while cesium primary ions often are used when electronegative elements are being investigated.

Dependent on the SIMS type, there are three basic analyzers available: sector, quadrupole, and time-of-flight. A sector field mass spectrometer uses a combination of an electrostatic analyzer and a magnetic analyzer to separate the secondary ions by their mass to charge ratio. A quadrupole mass analyzer separates the masses by resonant electric fields, which allow only the selected masses to pass through. The time of flight mass analyzer separates the ions in a field-free drift path according to their kinetic energy. It requires pulsed secondary ion generation using either a pulsed primary ion gun or a pulsed secondary ion extraction. It is the only analyzer type able to detect all generated secondary ions simultaneously, and is the standard analyzer for static SIMS instruments.

11. SR, QE

It is very important for solar cells to evaluate how much response can be obtain to illuminated light with certain wavelength. The rate of obtained short circuit current (I_{sc}) to monochromatic light with fixed power ($P_{in}(\lambda)$) is called Spectral Response (SR), and the rate of the number of outputted carriers to the number of illuminated photons is defined as Quantum Efficiency (QE). SR and QE as the function of wavelength (λ) are expressed as,

$$SR(\lambda) = \frac{I_{sc}(\lambda)}{P_{in}(\lambda)}, \qquad \text{(A.16)}$$

$$QE(\lambda) = \frac{hc}{q\lambda}\frac{I_{sc}(\lambda)}{P_{in}(\lambda)} \times 100 = \frac{hc}{q\lambda} SR(\lambda) \times 100, \qquad \text{(A.17)}$$

where *h* is plunk constant, *c* the light speed.

The QE mentioned above is so-called External Quantum Efficiency (*EQE*), in which the photon un-input into solar cell because of surface reflectance is not considered. In order to obtain the information of photon-electron interaction inside the device, Internal Quantum Efficiency (*IQE*) is defined with subtracting the surface reflectance (*R*) as,

$$IQE(\lambda) = \frac{QE(\lambda)}{1-R} = \frac{hc}{q\lambda}\frac{I_{sc}(\lambda)}{(1-R)P_{in}(\lambda)}. \qquad \text{(A.18)}$$

12. XRD

X-ray diffraction (XRD) finds the geometry or shape of a molecule using X-rays. X-ray diffraction techniques are based on the elastic scattering of X-rays from structures that have long range order. The most comprehensive description of scattering from crystals is given by the dynamical theory of diffraction. In polycrystalline samples, the crystallographic structure, crystallite size (grain size), and preferred orientation can be characterized. It is commonly used to identify unknown substances, by comparing diffraction data against a database maintained by the International Centre for Diffraction Data. It may also be used to characterize heterogeneous solid mixtures to determine relative abundance of crystalline compounds and, when coupled with lattice refinement techniques, such as Rietveld refinement, can provide structural information on unknown materials. XRD is also a common method for determining strains in crystalline materials. An effect of the finite crystallite sizes is seen as a broadening of the peaks in an X-ray diffraction. Thin film diffraction and grazing incidence X-ray diffraction may be used to characterize the crystallographic structure and preferred orientation of substrate-anchored thin films.

The sample is exposed to the incident X-ray beam under the angle. If the Bragg's law is fulfilled (match of structural plane distance and angle with the X-ray wavelength), an elastically scattered (diffracted) beam with high intensity can be collected under the same reflection angle. During the measurement, a selected range of angles is scanned and the intensity of the diffracted beam is recorded providing an XRD pattern. The positions of the peaks in the XRD pattern are typical of each crystalline material. Polycrystalline materials provide pattern with peaks of different intensity.

References of Appendix

[A.1] G. Binnig, C. F. Quate, and Ch. Gerber: Phys. Rev. Lett., **56** (1986) p. 930.

[A.2] B. Rezek, J. Stuchlík, A. Fejfar, and J. Kočka: Appl. Phys. Lett., **74** (1999) p.1475.

[A.3] M. Nonnenmacher, M. P. O'Boyle, and H. K. Wickramasinghe: Appl. Phys. Lett., **58** (1991) p.2921.

[A.4] J. M. R. Weaver, and D. W. Abraham: J. Van. Sci. Technol., **B 9** (1991) p.1559.

[A.5] T. Fuyuki, H. Kondo, Y. Kaji, A. Ogane, and Y. Takahashi: J. Appl. Phys., **101** (2007) 023711.

[A.6] M. Schöfthaler, and Ralf Brendel: J. Appl. Phys., **77** (7) (1995) p.3162.

[A.7] U. Creutzburg: Ph. D. Thesis, Dissertation, Universität Bremen (1991).

[A.8] F. Dannhäuser: Solid-State Electron, **15** (12) (1972) p.1371.

[A.9] M. Tajima: Appl. Phys. Lett., **53** (1988) p.959.

[A.10] M. Tajima, P. Stallhofer, and D. Huber: Jpn. J. Appl. Phys., **2** (1983) L586.

[A.11] M. Tajima, S. Kishino, M. Kanamori, and T. Iizuka: J. Appl. Phys., **51** (1986) p.2247.

[A.12] M. Ledinský, J. Stuchlík, T. Mates, A. Fejfar and J. Kočka: J. Non-Crystal. Solids, **352** (2006) p.1209.

[A.13] N. H. Nickel, P. Lengsfeld and I. Sieber: Phys. Rev., **B 61** (2000) 1558.

[A.14] E. Annastassakis: in Physical Problems in Microelectronics, Proc. of the 4th Int'l School ISPPM, edited by J. Kassavod (1985) p.128.

List of publications

Academic journals

[1] "Crystallographic properties of grain size-controlled polycrystalline silicon thin films deposited on alumina substrate"
Akiyoshi Ogane, Shinya Honda, Yukiharu Uraoka, Takashi Fuyuki, Antonín Fejfar, and Jan Kočka
Journal of Crystal Growth, **311**, Issue 3 (2009) p.789-793.

[2] "High-pressure water vapor heat treatment for enhancement of SiO_x or SiN_x passivation layers of silicon solar cells"
Akiyoshi Ogane, Athapol Kitiyanan, Yukiharu Uraoka, and Takashi Fuyuki
Japanese Journal of Applied Physics, in-press.

[3] "Laser doping technique using ultraviolet laser for shallow doping in crystalline silicon solar cell fabrication"
Akiyoshi Ogane, Kenji Hirata, Koyo Horiuchi, Yoshiyuki Nishihara, Yu Takahashi, Athapol Kitiyanan, Yukiharu Uraoka, and Takashi Fuyuki
Submitted to Japanese Journal of Applied Physics.

International conferences

[1] "Large grain poly-Si thin films on ceramic substrate deposited by intermittent source

gas supply”

Akiyoshi Ogane, Tsutomu Yamazaki, Yukiharu Uraoka, and Takashi Fuyuki

Proceedings of 20th European Photovoltaic Solar Energy Conference and Exhibition (Barcelona, Spain, 2005) p.1028.

[2] “Crystallographic properties of large grain poly-Si thin films on deposited by intermittent source gas supply”

Akiyoshi Ogane, Yu Takahashi, Yukiharu Uraoka, and Takashi Fuyuki

Technical Digest of 15th International Photovoltaic Science and Engineering Conference (Shanghai, China, 2005) p.806.

[3] “Fine-grained polycrystalline silicon thin film solar cells fabricated by APCVD with in-situ hydrogen annealing”

Akiyoshi Ogane, Yu Takahashi, Yukiharu Uraoka, and Takashi Fuyuki

Proceedings of 21st European Photovoltaic Solar Energy Conference and Exhibition (Dresden, Germany, 2006) p.1133.

[4] “High pressure water vapor heat treatment as the novel passivation method toward mono- and multicrystalline silicon solar cells”

Akiyoshi Ogane, Jin Nigo, Yuki Kishiyama, Yu Takahashi, Athapol Kitiyanan, Yukiharu Uraoka, and Takashi Fuyuki

Proceedings of 22nd European Photovoltaic Solar Energy Conference and Exhibition (Milan, Italy, 2007) p.1419.

[5] "High pressure water vapor heat treatment for the passivation of polycrystalline silicon thin film solar cells"

Akiyoshi Ogane, Yu Takahashi, Athapol Kitiyanan, Yukiharu Uraoka, and Takashi Fiyuki

Technical Digest of 17th International Photovoltaic Science and Engineering Conference (Fukuoka, Japan, 2007) p.702.

[6] "Feasible control of laser doping profiles in silicon solar cell processing using multiple excitation wavelengths"

Akiyoshi Ogane, Kenji Hirata, Koyo Horiuchi, Athapol Kitiyanan, Yukiharu Uraoka, and Takashi Fuyuki

Proceedings of 33rd IEEE Photovoltaic Specialists Conference (San Diego, USA, 2008) No.311.

[7] "Crystallographic properties of grain size controlled polycrystalline silicon thin films deposited on alumina substrate"

Akiyoshi Ogane, Shinya Honda, Yukiharu Uraoka, Takashi Fuyuki, Antonín Fejfar, and Jan Kočka

Abstracts of the 4th Asian Conference on Crystal Growth and Crystal Technology (Sendai, Japan, 2008) p.99.

[8] "Application of laser doping technique to bulk and thin film multicrystalline silicon solar cells"

Akiyoshi Ogane, Kenji Hirata, Koyo Horiuchi, Athapol Kitiyanan, Yukiharu Uraoka, and Takashi Fuyuki

Proceedings of 23rd European Photovoltaic Solar Energy Conference and Exhibition (Valencia, Spain, 2008) p.1929.

[9] “Application of laser doping technique to bulk and thin film multicrystalline silicon solar cells”

Akiyoshi Ogane

Annual Report of The Murata Science Foundation, No. **22** (2008) p.662.

Domestic conferences

[1] “Large grain polycrystalline silicon thin film solar cells fabricated by intermittent source gas supply method”

Akiyoshi Ogane, Tsutomu Yamazaki, Yu Takahashi, Yukiharu Uraoka, and Takashi Fuyuki

Abstracts of 1st Next Generation Photovoltaic System Symposium (Tokyo, 2004) p.75, in Japanese.

[2] “Development of large grain polycrystalline silicon thin films deposited by intermittent source gas supply method”

Akiyoshi Ogane, Yu Takahashi, Yukiharu Uraoka, and Takashi Fuyuki

IMR Workshop on ‘Material Approach for High Efficiency Crystalline Silicon Solar Cells’ (Sendai, 2005), only poster presentation.

[3] “Grain size enlargement of polycrystalline silicon thin films by intermittent source gas

supply method and their crystallographic properties"

Akiyoshi Ogane, Yu Takahashi, Yukiharu Uraoka, and Takashi Fuyuki

Abstracts of 2nd Next Generation Photovoltaic System Symposium (Gihu, 2005) p.114, in Japanese.

[4] "Crystallinity modification of polycrystalline silicon thin films on foreign substrates by in-situ H_2 annealing"

Akiyoshi Ogane, Yu Takahashi, Yukiharu Uraoka, and Takashi Fuyuki

Abstracts of 3rd Next Generation Photovoltaic System Symposium (Nara, 2006) p.128, in Japanese.

[5] "High quality polycrystalline silicon thin films deposited by AP-CVD and their photovoltaic applications"

Akiyoshi Ogane, Yu Takahashi, Yukiharu Uraoka, and Takashi Fuyuki

Abstracts of 4th Symposium of Collaboration Research Promotion Center on Super High Efficiency Photovoltaic Conversion (Nagoya, 2006) p.55, in Japanese.

[6] "Development of high pressure water vapor heat treatment as passivation layers enhancement technique for bulk and thin film polycrystalline silicon solar cells at low temperature"

Akiyoshi Ogane, Yuki Kishiyama, Yu Takahashi, Athapol Kitiyanan, Yukiharu Uraoka, and Takashi Fuyuki

Abstracts of 4th Next Generation Photovoltaic System Symposium (Sendai, 2007) p.163, in Japanese.

[7] "Microscopic analysis of polycrystalline silicon thin films using scanning prove microscope"

Akiyoshi Ogane, Athapol Kitiyanan, Yukiharu Uraoka, and Takashi Fuyuki

Abstracts of 5th Next Generation Photovoltaic System Symposium (Miyazaki, 2008) p.141, in Japanese.

Related academic journals

[1] "Annealing in water vapor as a new method for improvement of silicon thin film properties"

Shinay Honda, Antonín Fejfar, Jan Kočka, Tsutomu Yamazaki, Akiyoshi Ogane, Yukiharu Uraoka, and Takashi Fuyuki

J. Non-Crystal. Solids, **352**, (2006) p.955.

[2] "Electroreflectance study of silicon nanocrystals fabricated from n-type silicon substrate"

Toshihiko Toyama, Tetsuya Suzuki, Akiyoshi Ogane, Jun Ota, and Hiroaki Okamoto

J. Mater. Sci. Mater. Electron., **18**, Suppl. 1, (2007) p.443.

[3] "Analytic findings in the electroluminescence characterization of crystalline silicon solar cells"

Takashi Fuyuki, Hayato Kondo, Yasue Kaji, Akiyoshi Ogane, and Yu Takahashi

J. Appl. Phys., **101** (2007) 023711, DOI:10.1063/1.2431075.

[4] "NH_3 plasma interface modification for silicon surface passivation at very low temperature"

Yu Takahashi, Jin Nigo, Akiyoshi Ogane, Yukiharu Uraoka, and Takashi Fuyuki

Jpn. J. Appl. Phys., **47**, No. 7, (2008) p.5320-5323.

[5] "Rear side passivated monocrystalline silicon thin film solar cells with laser fired contact process"

Yu Takahashi, Kenji Hirata, Akiyoshi Ogane, Yukiharu Uraoka, and Takashi Fuyuki

Appl. Phys. Exp., **1**, No. 8 (2008) 085002, DOI: 10.1143/APEX.1.085002.

[6] "Comprehensive study of electroluminescence in multicrystalline silicon solar cells"

Athapol Kitiyanan, Akiyoshi Ogane, Ayumi Tani, Tomoaki Hatayama, Hiroshi Yano, Yukiharu Uraoka, and Takashi Fuyuki

J. Appl. Phys., in-press.

Related international conferences

[1] "Annealing in water vapor as a new method for improvement of silicon thin film properties"

Shinya Honda, Antonín Fejfar, Jan Kočka, TsutomuYamazaki, Akiyoshi Ogane, Yukiharu Uraoka, and Takashi Fuyuki

Proceedings of 21st International Conference on Amorphous and Nanocrystalline Semiconductor (Lisbon, Portugal, 2005).

[2] "Characterization of polycrystalline silicon solar cells by electroluminescence"

Yasue Kaji, Yu Takahashi, Akiyoshi Ogane, Yukiharu Uraoka, and Takashi Fuyuki
Technical Digest of 15th International Photovoltaic Science and Engineering Conference (Shanghai, China, 2005) p.153.

[3] "Analysis of thin monocrystalline silicon solar cells by photographic survey"
Yu Takahashi, Yasue Kaji, Akiyoshi Ogane, Yukiharu Uraoka, and Takashi Fuyuki
Technical Digest of 15th International Photovoltaic Science and Engineering Conference (Shanghai, China, 2005) p.192.

[4] "Analytic findings in the photographic characterization of crystalline Si solar cells using electroluminescence"
Takashi Fuyuki, Yasue Kaji, Akiyoshi Ogane, and Yu Takahashi
Proceedings of 4th World Conference on Photovoltaic Energy Conversion (Hawaii, USA, 2006) p.905.

[5] ""Luminoscopy"- Novel tool for the diagnosis of crystalline silicon solar cells and modules utilizing electroluminescence"
Yu Takahashi, Yasue Kaji, Akiyoshi Ogane, Yukiharu Uraoka, and Takashi Fuyuki
Proceedings of 4th World Conference on Photovoltaic Energy Conversion (Hawaii, USA, 2006) p.924.

[6] "Effective interface modification by NH_3 plasma for silicon surface passivation at very low temperature"
Jin Nigo, Yu Takahashi, Akiyoshi Ogane, Yoshiyuki Nishihara, Yukiharu Uraoka, and

Takashi Fuyuki

Proceedings of 21st European Photovoltaic Solar Energy Conference and Exhibition (Dresden, Germany, 2006) p.934.

[7] “Selected junction formation in back contact thin silicon solar cells at very low temperature by laser doping”

Yoshiyuki Nishihara, Yu Takahashi, Akiyoshi Ogane, Jin Nigo, Yukiharu Uraoka, and Takashi Fuyuki

Proceedings of 21st European Photovoltaic Solar Energy Conference and Exhibition (Dresden, Germany, 2006) p.941.

[8] “Quantitative imaging of excess carrier density in crystalline silicon cells by Luminoscopy”

Takashi Fuyuki, Yu Takahashi, Jin Nigo, Yoshiyuki Nishihara, Yasue Kaji, Akiyoshi Ogane, and Athapol Kitiyanan

Proceedings of 21st European Photovoltaic Solar Energy Conference and Exhibition (Dresden, Germany, 2006) p.1381.

[9] “Analysis of polycrystalline silicon thin films with different grain sizes”

Shinya Honda, Jiří. Oswald, Karel Knížek, Karel Melichar, Tomáš Mates, Martin Ledinský, Antonín Fejfar, Jan Kočka, Akiyoshi Ogane, Yukiharu Uraoka, and Takashi Fuyuki

Proceedings of 21st European Photovoltaic Solar Energy Conference and Exhibition (Dresden, Germany, 2006) p.1396.

[10] "Selective imaging of defects and faults in Si substrates by electroluminescence differentiated in temperature"
Athapol Kitiyanan, Yu Takahashi, Akiyoshi Ogane, Takashi Fuyuki, and Karsten Bothe
Proceedings of 22nd European Photovoltaic Solar Energy Conference and Exhibition, (Milan, Italy, 2007) p.1387.

[11] "Profile controlled laser doping for n-type silicon solar cells"
Koyo Horiuchi, Yoshiyuki Nishihara, Akiyoshi Ogane, Yu Takahashi, Athapol Kitiyanan, Yukiharu Uraoka, and Takashi Fuyuki
Proceedings of 22nd European Photovoltaic Solar Energy Conference and Exhibition, (Milan, Italy, 2007) p.1423.

[12] "Anneal and deposition temperature-dependent passivation effect of SiN laer with interface modification by NH_3 plasma"
Yu Takahashi, Jin Nigo, Yuki Kishiyama, Akiyoshi Ogane, Yukiharu Uraoka, and Takashi Fuyuki
Proceedings of 22nd European Photovoltaic Solar Energy Conference and Exhibition, (Milan, Italy, 2007) p.1644.

[13] "Rear surface SiN passivated monocrystalline silicon thin film solar cells with laser fired process"
Yu Takahashi, Akiyoshi Ogane, Koyo Horiuchi, Yuki Kishiyama, Athapol Kitiyanan,

Yukiharu Uraoka, and Takashi Fuyuki

Technical Digest of 17th International Photovoltaic Science and Engineering Conference (Fukuoka, Japan, 2007) p.253.

[14] "Fabrication of silicon solar cells with back surface field by laser doping technique"

Koyo Horiuchi, Yu Takahashi, Akiyoshi Ogane, Athapol Kitiyanan, Yukiharu Uraoka, and Takashi Fuyuki

Technical Digest of 17th International Photovoltaic Science and Engineering Conference (Fukuoka, Japan, 2007) p.542.

[15] "Detection of crack location in multicrystalline silicon solar cells by electroluminescence image subtraction technique"

Athapol Kitiyanan, Karsten Bothe, Yu Takahashi, Akiyoshi Ogane, and Takashi Fuyuki

Technical Digest of 17th International Photovoltaic Science and Engineering Conference (Fukuoka, Japan, 2007) p.706.

[16] "Electroluminescence analysis of crystalline silicon solar cells"

Athapol Kitiyanan, Karsten Bothe, Yu Takahashi, Akiyoshi Ogane, and Takashi Fuyuki

Abstracts of 2nd International Workshop on Science and Technology of Crystalline Silicon Solar Cells (Xiamen, China, 2007) p.18.

[17] "Investigation of intrinsic deficiency in crystalline Si solar cell by electroluminescence

image under reverse bias condition"

Athapol Kitiyanan, Yu Takahashi, Akiyoshi Ogane, and Takashi Fuyuki

Abstracts of the 4th Asian Conference on Crystal Growth and Crystal Technology (Sendai, Japan, 2008) p.105.

[18] "Complementary analysis of crystalline defects in Si solar cells by electroluminescence imaging combining forward and reverse bias condition"

Athapol Kitiyanan, Yu Takahashi, Akiyoshi Ogane, Ayumi Kawakita, Tomoaki Hatayama, Hiroshi Yano, Yukiharu Uraoka, and Takashi Fuyuki

Proceedings of 23rd European Photovoltaic Solar Energy Conference and Exhibition, (Valencia, Spain, 2008) p.1503.

[19] "Novel silicon solar cell process by laser doping technique"

Kenji Hirata, Akiyoshi Ogane, Takashi Saitoh, Athapol Kitiyanan, Yukiharu Uraoka, and Takashi Fuyuki

will be presented at The 5th International Congress on Laser Advanced Materials, (Kobe, Japan, 2009).

Related domestic conferences

[1] "Development of monocrystalline silicon thin film solar cells with sub-micron surface texturing"

Yu Takahashi, Akiyoshi Ogane, Yukie Yamamoto, Tsutomu Yamazaki, Hiroshi Yano, Tomoaki Hatayama, Yukiharu Uraoka, and Takashi Fuyuki

Abstracts of 1st Next Generation Photovoltaic System Symposium (Tokyo, 2004) p.79, in Japanese.

[2] "Analysis of rear side surface recombination of thin monocrystalline silicon solar cells using electroluminescence imaging"
Yu Takahashi, Yasue Kaji, Akiyoshi Ogane, Yukiharu Uraoka, and Takashi Fuyuki
IMR Workshop on 'Material Approach for High Efficiency Crystalline Silicon Solar Cells' (Sendai, 2005), only poster presentation.

[3] "Rear side passivation effect of 120-μm thick monocrystalline silicon solar cells characterized by electroluminescence"
Yu Takahashi, Yasue Kaji, Akiyoshi Ogane, Yukiharu Uraoka, and Takashi Fuyuki
Abstracts of 2nd Next Generation Photovoltaic System Symposium (Gihu, 2005) p.139, in Japanese.

[4] "Electroluminescence photographing for rapid diagnostic tool for crystalline silicon solar cells and modules production"
Athapol Kitiyanan, Hiroshi Ueno, Yu Takahashi, Akiyoshi Ogane, Yukiharu Uraoka, and Takashi Fuyuki
Abstracts of 3rd Next Generation Photovoltaic System Symposium (Nara, 2006) p.144.

[5] "Surface texture formation of silicon solar cells using laser ablation"
Yoshiyuki Nishihara, Akiyoshi Ogane, Jin Nigo, Yu Takahashi, Yukiharu Uraoka, and Takashi Fuyuki
Abstracts of 3rd Next Generation Photovoltaic System Symposium (Nara, 2006) p.148,

in Japanese.

[6] "SiN passivation of monocrystalline silicon solar cells with interface modification by NH_3 plasma treatment at low temperature"
Jin Nigo, Yu Takahashi, Akiyoshi Ogane, Yoshiyuki Nishihara, Yukiharu Uraoka, and Takashi Fuyuki
Abstracts of 4th Symposium of Collaboration Research Promotion Center on Super High Efficiency Photovoltaic Conversion (Nagoya, 2006) p.57, in Japanese.

[7] "Selective emitter formation of back-contact type silicon solar cells using laser doping method"
Yoshiyuki Nishihara, Yu Takahashi, Akiyoshi Ogane, Jin Nigo, Yukiharu Uraoka, and Takashi Fuyuki
Abstracts of 4th Symposium of Collaboration Research Promotion Center on Super High Efficiency Photovoltaic Conversion (Nagoya, 2006) p.59, in Japanese.

[8] "Development of rear surface passivated 15-μm thick monocrystalline silicon thin film solar cells with laser fired contact process"
Yu Takahashi, Akiyoshi Ogane, Koyo Horiuchi, Yuki Kishiyama, Athapol Kitiyanan, Yukiharu Uraoka, and Takashi Fuyuki
Abstracts of 4th Next Generation Photovoltaic System Symposium (Sendai, 2007) p.27, in Japanese.

[9] "Categorization of defects and faults in crystalline silicon solar cells by

electroluminescence photographing at different temperature”

Athapol Kitiyana, Karsten Bothe, Yu Takahashi, Akiyoshi Ogane, and Takashi Fuyuki

Abstracts of 4th Next Generation Photovoltaic System Symposium (Sendai, 2007) p.131.

[10] “Development of silicon solar cell fabrication process using laser doping”

Koyo Horiuchi, Yu Takahashi, Akiyoshi Ogane, Athapol Kitiyanan, Yukiharu Uraoka, and Takashi Fuyuki

Abstracts of 4th Next Generation Photovoltaic System Symposium (Sendai, 2007) p.151, in Japanese.

[11] “Electroluminescence characterization of SiN passivated silicon solar cells with interface modification by NH_3 plasma treatment”

Yuki Kishiyama, Akiyoshi Ogane, Yu Takahashi, Athapol Kitiyanan, Yukiharu Uraoka, and Takashi Fuyuki

Abstracts of 4th Next Generation Photovoltaic System Symposium (Sendai, 2007) p.167, in Japanese.

[12] “Interface modification by NH_3 plasma in SiN_x passivation for solar cell”

Yuki Kishiyama, Yu Takahashi, Akiyoshi Ogane, Athapol Kitiyanan, Yukiharu Uraoka, and Takashi Fuyuki

IEICE Technical Committee on Silicon Device and Materials (SDM) (Ikoma, 2007) p.43, in Japanese.

[13] “Development of laser doping for silicon solar cells”

Kenji Hirata, Koyo Horiuchi, Akiyoshi Ogane, Yu Takahashi, Yukiharu Uraoka, and Takashi Fuyuki

Abstracts of the 55th Spring Meeting of the Japan Society of Applied Physics and Related Societies (Funabashi, 2008) p.1530, in Japanense.

[14] “Development of laser doping process using Green laser for silicon solar cell fabrication”

Kenji Hirata, Akiyoshi Ogane, Athapol Kitiyanan, Yukiharu Uraoka, and Takashi Fuyuki

Abstracts of 5th Next Generation Photovoltaic System Symposium (Miyazaki, 2008) p.137, in Japanese.

[15] “The study of defects in crystalline Si solar cells by electroluminescence imaging under reverse bias condition”

Athapol Kitiyanan, Marie Buffière, Ayumi Kawakita, Akiyoshi Ogane, Kenji Hirata, and Takashi Fuyuki

Abstracts of 5th Next Generation Photovoltaic System Symposium (Miyazaki, 2008) p.145.

[16] “Development of laser doping in the fabrication of crystalline Si solar cells”

Takashi Fuyuki, and Akiyoshi Ogane

Abstracts of 71st Meeting of Japan Laser Processing Society (Tokyo, 2008) p.55, in Japanese.

[17] "Laser doping technique using continuous wave Nd:YVO_4 laser for silicon solar cell fabrication"

Takashi Saitoh, Kenji Hirata, Akiyoshi Ogane, Yukiharu Uraoka, and Takashi Fuyuki

will be presented in the 56th Spring Meeting of the Japan Society of Applied Physics and Related Societies (Tsukuba, 2009), in Japanese.

[18] "Spectral analysis of electroluminescence evaluation for multicrystalline silicon solar cells"

Emi Sugimura, Athapol Kitiyanan, Kenji Hirata, Akiyoshi Ogane, Ayumi Tani, and Takashi Fuyuki

will be presented in the 56th Spring Meeting of the Japan Society of Applied Physics and Related Societies (Tsukuba, 2009), in Japanese.

About the author

Personal data

Name: Akiyoshi Ogane

Data of birth: 8th August in 1980, Kasaoka city in Okayama pref., Japan

Nationality: Japan

E-mail: o-akiyos@ms.naist.jp

Education

2000-2004 Bachelor course study at Department of Electronics and Materials Physics, School of Engineering Science, Osaka University

Bachelor thesis on ***Electroreflectance Study of n-type Porous Silicon***

2004-2006 Master course study at Graduate School of Materials Science, Nara Institute of Science and Technology (NAIST)

Master thesis on ***Analysis and Modification of Polycrystalline Silicon Thin Films' Crystallographic Properties Deposited by Intermittent Source Gas Supply***

2006-2009 Doctor course study at Graduate School of Materials Science, NAIST

Ph. D. thesis on ***Polycrystalline Silicon Thin Films with Improved Crystallographic and Electronic Properties for Photovoltaic Applications***

Oversea study at Department of Thin films, Institute of Physics, Academy of Science of the Czech Republic in Prague (Jan.-Feb. in 2008)

Research interests

- Structural and electronic properties of polycrystalline silicon thin films for solar cell applications
- Technologies for the improvement of photovoltaic properties of silicon solar cells
- Theoretical analysis of silicon semiconductor devices, especially solar cells

Language

Japanese, English

Financial support acquirement

- Exemption from returning of scholarship during master course from Japan Student Services Organization (2006)
- International research activity support by Foundation for Nara Institute of Science and Technology (2006)
- International research activity support by Kansai Research Foundation for Technology Promotion (2007)
- Competitive research support by Graduate school GP program (2007)
- International research activity support by The Murata Science Foundation (2008)